Computational Analysis of Motorcoach Rollover for Passenger Safety Assessment

By

Wei Zhou

A Thesis Submitted to the Faculty of Graduate Studies of

The University of Manitoba

In partial fulfillment of the requirement of the degree of

MASTER OF SCIENCE

Department of Mechanical Engineering

University of Manitoba

Winnipeg, Manitoba

Dedication

I would like to show my heartiest gratitude to my parents for the sacrifices and supports they made for me during my studying.

This thesis has contained works from the following papers:

Zhou W, Kuznetcov A, Telichev I, Wu C. "Deformable-Rigid Switch in Computational Simulation of Bus Rollover Test." Proceedings: 24th International Congress of Theoretical and Applied Mechanics 2016.

Zhou W, Kuznetcov A, Wu C, Telichev I. "A Comparative Numerical Study of Motorcoach Rollover Resistance under ECE R66 and Proposed NHTSA Regulation Conditions." Under Review

Zhou, W, Wu C, Telichev I. "Application of the U* Index Theory for Load Transfer Analysis of Vehicle Structure Subjected to Elastic-Plastic Deformation." Under Review

Abstract

Under increasing public concern for the passenger safety in large passenger vehicles, legislative regulations are enforced and continuously updated. Recently, a new federal regulation was proposed in North America to enhance the safety level of the motorcoach passengers under the rollover, based on regulation No.66 of the Economic Commission for Europe, but with more severe loading conditions in the form of full passenger mass ballasted to all seats. The studies in this thesis use the explicit finite element method (implemented in LS-DYNA) and the load transfer index U* to model and analyze the motorcoach rollover event in order to evaluate the structural performance and passenger safety in accordance with related legislative regulations. A modified version of complete finite element model of a typical motorcoach is developed and validated using data from the component test and the complete vehicle rollover test. The rollover tests are numerically replicated for loading conditions corresponding to the vehicle with zero and full passenger mass respectively. The comparative study is performed on the structural resistance to deformation and energy absorption capability. The original concept of U* index is applied for analysis of key structural components experiencing the elastic-plastic deformation to determine the load path and examine the load transfer efficiency.

Obtained coach rollover simulation results indicate that test condition of the proposed regulation leads to a 150% increase in penetration distance to the surviving space of the passenger compartment compared to the ECE R66 condition. The key structural members, which absorb the most energy in the rollover impact, are identified, and the need for the higher rollover resistance of the coach for its compliance with the newly proposed regulation is demonstrated. Obtained load transfer analysis results show the effectiveness of the application of the U* approach in detecting the change of load path within the structural elements experiencing plastic deformation. It shows that the U* approach can be used in combination with FEM as an effective tool for the vehicle crashworthiness analysis. Overall, results of this study can provide a data basis for the automotive manufacturers to evaluate and improve the rollover resistance of motorcoaches.

Acknowledgement

I would like to give my gratitude to my advisor, Dr. Christine Q. Wu, for her support in my studies. Her rich expertise and vision in the academic and industrial field, and her approachable personality have inspired and encouraged me to work on this research.

Also, I would like to give my gratitude to my co-advisor, Dr. Igor Telichev for his guidance for my project and thesis work. I would like to express my appreciation for his help and comments for my studies and this thesis would not be possible without his supervision.

I would also like to thank my colleagues Dr. Anton Kuznetcov, Dr. Qingguo Wang, Mr. Hamid Giahi and Dr. Khashayar Pejhan for their help and useful discussions in the thesis work. Also, I'd like to thank Ms.Tamrin Tanha and Mr.Md Nuruzzaman for sharing the raw material test data with our project team. And I'd also like to thank Dr. Yunhua Luo and Dr. Ehab El-Salakawy for serving as committee members for my graduate program.

Last but not least, I would like to thank my families and friends for their significant support.

This research was enabled in part by support provided by Westgrid (www.westgrid.ca) and Compute Canada (www.computecanada.ca).

Table of Contents

List of Figures

List of Tables

Abbreviations

ECE R66	Regulation No.66 of Economic Commission for Europe
NHTSA	National Highway Traffic Safety Administration, USA
FMVSS	American Federal Motor Vehicle Safety Standards
FEA	Finite Element Analysis
FEM	Finite Element Method
GVWR	Gross Vehicle Weighting Rating
MPP	Massively Parallel Processing
APDL	ANSYS Parametric Design Language

1. INTRODUCTION

1.1. Problem Statement

1.1.1. Background and Motivation

Each traveler is concerned by road safety problems, and vehicle manufacturers together with legislative authorities play an essential role in minimizing the probability of passenger injuries. In the United States in 2014, the National Highway Traffic Safety Administration (NHTSA) reported that 32,675 people were killed in motor vehicle traffic crashes [1]. In Canada in 2015, Transport Canada reported that the number of motor vehicle fatalities was 1,858 with 10,280 seriously injured [2].

Rollover is among the accidents associated with the highest possibility of fatalities. Data for fatal crashes in the United States report that from 2001 to 2010, rollover and roadside events accounted for 74% of all motorcoach fatalities [3]. In Canada, it is reported that among 21 collisions of intercity buses from 1990 to 2001, there were 7 (33%) rollover events accounted for the majority of severe and fatal injuries [4].

Passive safety technology is studied extensively by researchers and engineers to address the passenger safety issues. Vehicle passive safety systems involve all structural parts that could deform to absorb and dissipate kinetic energy in a crash accident and occupant restraint components such as airbags and seatbelts [5]. The ability of the vehicle structure to contribute to occupant protection in the crash event is defined as crashworthiness and it plays an important role in the overall vehicle safety. For example, the crush box is designed to absorb a large

amount of kinetic energy in the vehicle frontal collision. Another critically important aspect of the collision safety is structural integrity, which is the ability of a structural component to withstand the impact load in the collision without failure.

In rollover accidents, the vehicle structure absorbs the kinetic energy of the colliding objects and irreversibly converts it to the strain energy by the deformation and failures such as buckling and fracture. The sufficient energy absorption is required to reduce the acceleration affecting the passengers during a collision. Unlike the frontal collision scenario, the problem arises [5] for the rollover events owing to the absence of the dedicated energy absorption components or structures. The vehicle lateral body and roof are mainly made of thin panels and beams, which provide insufficient energy absorption by the plastic deformation.

From the 1970s researchers suggested that space needs to be preserved in passengers and driver's compartment for better survival possibility in the vehicle crash accident, which is known as the "surviving space" or "residual space" [6]. During the crash test, the passenger compartment must remain nearly non-deformed and non-intruded by other structural components. However, in the real-life rollover accidents, it is usually encountered in the most of the cases that the damaged vehicle has the large deformation, which directly contributes to the fatality rate of passengers.

The superstructure of a motorcoach is the load bearing components of vehicle bodywork as defined by the manufacturer. Consequently, for the passenger protection in the rollover accidents, the superstructure should provide both the required surviving space and sufficient energy absorbing capability. These requirements are contradictive, since the preservation of the surviving space is achieved by minimization of the superstructure' deformations, while energy absorption is usually associated with large deformations.

Thus legislated standards are enacted worldwide in terms of both surviving space and energy absorption to ensure that vehicle products meet the required safety level. One such regulation is the Regulation No.66 of Economic Commission for Europe (ECE R66) [7]. The approval procedure in [7] is based on a rollover test of a complete vehicle. By testing the strength of the superstructure, the main requirement is the preservation of the designated surviving space in the passenger compartment. No parts of the vehicle outside the surviving space at the start of the test shall intrude into the surviving space during the test.

In order to better design for the crashworthiness of the passenger vehicle and assess the structural ability to resist the deformation in the rollover events, it is also necessary to study the application of load transfer analysis in the vehicle crashworthiness problem together with the traditional stress analysis method. It studies the load carry capability of the vehicle structure. The vehicle primary structure should not fail under the normal service condition and behave in a predictable and controllable manner in the accidents. In the viewpoint of the vehicle designer, this requires that the designed vehicle body should achieve a sufficient level of stiffness.

In the modern vehicle industry, the development has shown that the lightweight and low energy-consumption design is pursued by consumers and vehicle manufacturers. Taking into account the needs of both environment and passenger safety, it is necessary to make the vehicle's primary structure more efficient to transfer the load. To this end, it is essential to visualize and determine the load paths within the vehicle's primary structure. With this knowledge of how the load is transferred, the structural performance can be better predicted and improved in the design stage.

1.1.2. Problem Definition

To evaluate the rollover performance of the motorcoach and the passenger safety, the effective simulation methodologies capable of assessing the motorcoach compliance with the latest legislative regulation and the advanced instruments are on demand by the manufacturers and engineers. These approaches can also be effectively applied to the design of the passenger vehicle in terms of the crashworthiness problem.

The current federal regulations related to the rollover protection in the USA are Federal Motor Vehicle Safety Standard (FMVSS) 208 “Occupant crash protection”, FMVSS 216 “Roof crush resistance”, and FMVSS 220 “School bus rollover protection” [8]. They use the static loading method to assess the roof strength of buses. Concerning the lack of the specific regulation for the passenger safety of motorcoaches and other heavy buses in North America, the federal government agency is currently working on updating the current regulation in order to enhance motorcoach safety. New considerations of the test conditions and new requirements will be implemented in the proposal of the new regulation for motorcoach rollover protection. In response to the regulation change, the thesis work will concentrate on the study of the following problems.

Firstly, In consideration of the new requirements owing to the regulatory change, the studies of the modeling approach in order to evaluate the structural performance and the passenger safety in compliance to the latest regulation requirement are thus needed. Secondly, as the design needs to make a compromise between the surviving space preservation for passenger safety and the energy absorption capability of the vehicle structure, the alteration of the design requirement also needs to be studied for rollover in accordance with the existing rollover regulation of ECE R66

and the new regulation. At last, the demonstration of the applicability of load transfer analysis to the vehicle crashworthiness problem is also essential.

1.1.3. Proposed Solution

With the fast development of computing technology, vehicle industry benefits greatly from Computer Aided Design (CAD) and Computer Aided Engineering (CAE), which lead to faster product development, lower cost, and better quality. Computational modeling and simulation are highly valued by engineers and researchers in vehicle industries. The possibility to perform the numerical simulation allows to analyze the different engineering solutions in the very early design stage and evaluate the structural performance under different types of impact events in the design development phase [5].

This study aims to use the numerical simulation to analyze the structural performance of a typical motorcoach in the rollover event and evaluate the compliance of passenger safety to related legislative regulations. Finite element method and U* approach are to be employed together to model and analyze the motorcoach rollover event along with the load transfer analysis of key components identified by FEM.

Experimental methods will also be employed in the thesis work. To obtain the correct material properties and to validate the modeling technique, the material tensile test and the component bending test are to be conducted. The physical rollover test data of the complete motorcoach will be used to validate the simulation result. The workflow of the thesis can be summarized in Figure 1-1.

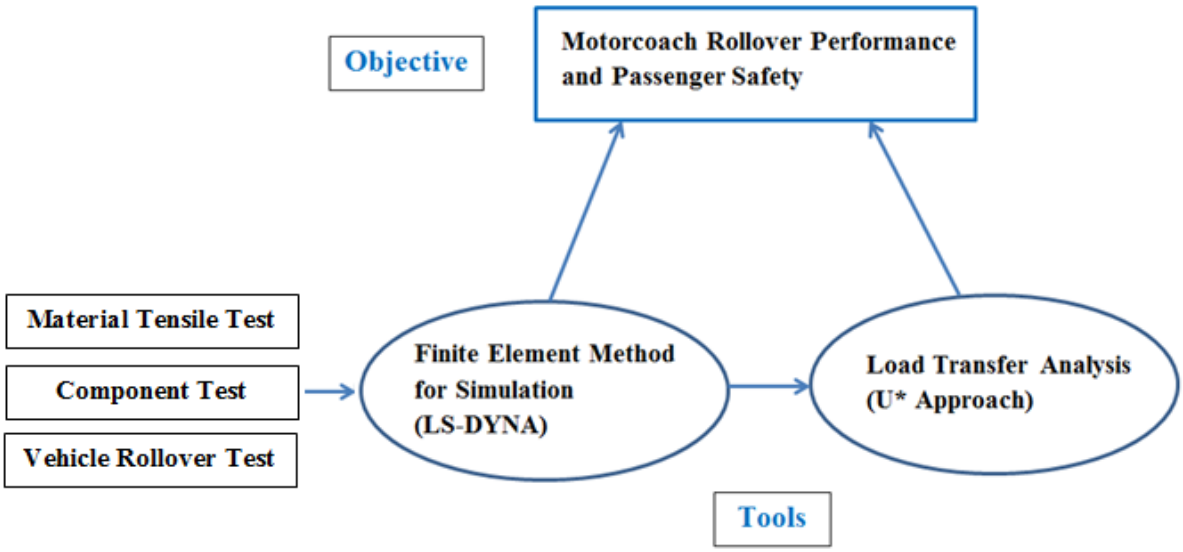

Figure 1-1 Workflow outline of the thesis

1.2. Thesis Formalization

1.2.1. Aim of the Thesis

The objectives of this study can be categorized as two-fold. As different regulations require different test conditions, the main task is to evaluate the structural performance and passenger safety of a typical coach under different regulations using the finite element method. This thesis also aims to apply the load transfer analysis on the vehicle structure. The method of load transfer index U* is chosen as the tool. Through the application of the original concept of U* index on structures experiencing the elastic-plastic deformation, the demonstration in this work will potentially provide a new perspective on the vehicle design against collision problems. These objectives include the following tasks:

1) To perform the coach rollover simulation with a validated model using data from the component test and complete vehicle rollover test;

2) To compare the deformation and energy absorption distribution among structural members under different test conditions in compliance with regulations;

3) To address differences in design criteria to develop a sufficiently resistant vehicle framework for rollover events under the different regulations;

4) To demonstrate the applicability of U* approach to the load transfer analysis of the vehicle structures.

1.2.2. Core Concepts within the Thesis

The following core concepts are used in the context of the thesis:

(a). Motorcoach:

Motorcoach [3] refers to a bus characterized by an elevated passenger deck located over a baggage compartment, excluding the public transit bus and the school bus.

(b). Superstructure

Superstructure [7] of the vehicle refers to the load-bearing components of the bodywork as defined by the manufacturer. It includes those coherent structural components which contribute to the strength and energy absorbing capability of the bodywork and preserve the surviving space in the rollover test.

(c). Crashworthiness

Crashworthiness is the ability of the vehicle structure to contribute to occupant protection in the crash event to reduce the number of fatal and serious injuries.

(d). Load transfer analysis

Load transfer analysis assesses the efficiency and rationality of structures in transferring loads from the loading to the supporting end. It is used as the complementary methodology together with the traditional stress analysis for assessing the vehicle performance in the thesis.

1.2.3. Thesis Organization

The remaining parts of the thesis are outlined as following:

In Chapter 2, firstly, the literature review is provided on rollover regulations and related tests requirements. Limitations of the existing regulation ECE R66 and the new regulation proposal are discussed respectively. This chapter also includes the review of the development of the computational analysis methods for vehicle rollover simulation. The concepts of load transfer analysis, U* index theory and its applications are discussed.

In Chapter 3, the modeling approach and the simulation results of a motorcoach rollover are presented in details. The validation of the finite element model is also presented based on a quasi-static component test for a representative member of the vehicle frame and results of a complete vehicle rollover test under ECE R66 conditions. Based on the validated coach model, a comparative study is presented to evaluate the structural performance of a motorcoach and the passenger safety under a new proposed regulation and the existing regulation ECE R66 using explicit FEA simulation LS-DYNA®.

In Chapter 4, the load transfer analysis using the U* index on the vehicle structure subjected to elastic-plastic deformation is presented. Firstly, the theory preliminaries are reviewed. The numerical procedure is given as the following. Using the U* concept, effects of the material nonlinearity on the load path and the stiffness distribution were analyzed for the representative example structures. The first two examples of the plate demonstrate the load path changes when

the structure starts to deform plastically. In the last example, the U^*_{sum} contour obtained for a vehicle pillar structure demonstrates that the local structural stiffness is changed by the development of the plastic region.

In Chapter 5, the conclusions and contributions of the thesis work are summarized. The limitations of studies are discussed, and the recommendations on the future work are provided.

2. LITERATURE REVIEW

2.1. Rollover Regulations and Tests

2.1.1. Rollover test by Regulation 66 of ECE

The Regulation No.66 of Economic Commission for Europe (ECE R66) is one of the most widely used international regulations related for rollover protection. A rollover test on a full vehicle is the basic method to get the certification of ECE R66 for the compliance with the required safety level. An illustration of ECE R66 full vehicle rollover test is shown in Figure 2-1. The test vehicle is placed on a tilting platform, which is inclined to reach unstable equilibrium position with a minimum rotational velocity. The vehicle is then tipped over with the minimum rotational velocity until it falls freely into a ditch, which has a horizontal, dry and smooth concrete ground surface with a nominal depth of 800 mm.

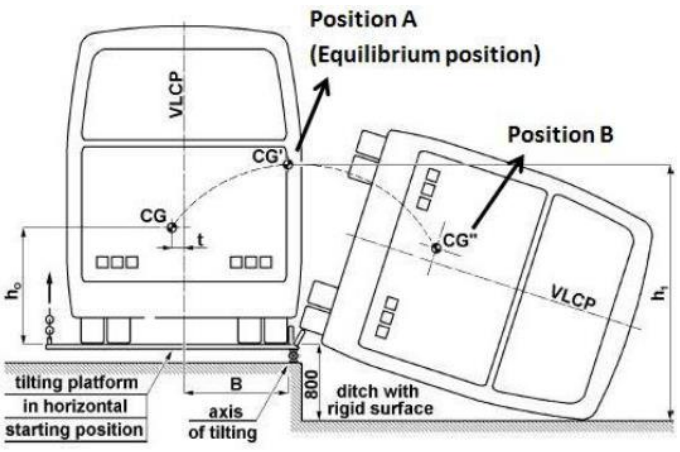

Figure 2-1 Illustration of ECE R66 rollover test [7]

In the latest version, v.2006 [7], including the rollover test as the basic approval method, 4 other methods based on test, calculation or simulations are also included in the regulation. The 4 equivalent methods include:

(1). Rollover test using body sections;

The manufacturer can choose the body section to be tested on the tilting platform instead of the complete vehicle. The center of gravity of the tested body section must be measured and it needs to be the same with the complete vehicle. The structural feature of the body section also needs to be same with the superstructure in regard to the shape, geometry, material and joints. The vehicle is considered to pass the test if all the body sections pass the test. If one of them fails, the vehicle type shall not be approved.

(2). Quasi-static loading test of body sections;

In this equivalent method, the quasi-static loading is applied in the way to be evenly distributed on the cantrail of the vehicle through a rigid beam to simulate the ground in a rollover test, shown in Figure 2-2. The load direction angle α needs to be calculated to match the impact load direction in the rollover test on the tilting platform with 800 mm height.

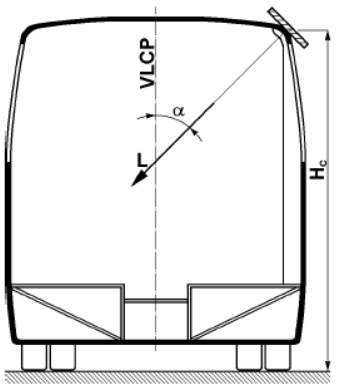

Figure 2-2 Quasi-static loading test of body sections

(3). Quasi-static calculations based on the results of component tests;

This equivalent method needs to identify all the deformable plastic zones and plastic hinges on the vehicle superstructure. The characteristic curves of the plastic zones and plastic hinges need to be obtained by component tests beforehand. The algorithm and computer programs are able to do quasi-static calculations of the model.

(4). Computer simulation of rollover test on a complete vehicle.

Several requirements for this equivalent method include: The simulation must give conservative results. The total mass and CG position of the model must be identical with the real vehicle. The mass distribution in the model corresponds to the real vehicle. The simulation shall run till max deformation is reached. Non-physical energy shall not exceed 5% of total energy.

The original ECE R66 was developed by the European Union in the late seventies to overcome the deficiencies of the vehicle superstructure under rollover impact events. Despite the fact that ECE R66 has been enforced in many countries, during these years, its limitations have also been studied and the new version is discussed by researchers. The recent publications of the research on ECE R66 have shown two main concerns regarding the limitations of ECE R66.

Firstly, the loading condition in ECE R66 depends on whether the seatbelts are installed in the test vehicle. For a coach without seatbelts installed, the unladen curb mass should be used. For a coach equipped with seatbelts, the total effective vehicle mass should be reproduced in the test, meaning a ballast of half of a passenger mass should be mounted to each seat [7]. With the introduction of mandatory seatbelt wearing in coaches in Europe in 2006, the influence of the passenger on the vehicle needs to be considered [9]. However, for ECE R66, the influence of passenger's mass on the deformation of the vehicle has often been neglected in physical tests for

old coaches not equipped with seatbelts. Due to the variance of the restraints of safety belts, related studies on the influence of the effective mass from passengers coupled to the vehicle structure have been conducted by researchers. The researcher in [10] calculates the passenger mass factor via the displacement using a validated bay section model. It is found that 18% of the unrestraint passenger's mass and 93% of the passenger on the 3-point seatbelt are effectively coupled to the vehicle structure in the rollover test. The study in [11] suggests that depending on the restraint system in the vehicle, the energy absorption of the coach could increase up to 60% due to the passenger's mass. The simulation work in [12] shows that the surviving space is severely penetrated in the rollover test with the additional passenger on the coach, and the energy absorption is 37% higher.

The second limitation of ECE R66 is that, in many studies for the compliance to ECE R66, the bay sections have been used in the physical rollover tests and simulations to minimize the associated costs and computational resources. As studies show, the mass of the bay section should be adjusted to obtain a deformation comparable with that of the complete vehicle [10] [13] [14]. The choice of the bay section from the complete vehicle is subjected to engineers' judgment and experiences, and no recommendations are provided in the regulation [7]. Thus the degree of representativeness of complete vehicle structural performance using the bay section still lacks detailed investigations.

2.1.2. Newly Proposed Regulation by NHTSA

In North America, up until recently, there were no regulations concerning the rollover performance for motorcoaches. The existing regulations most closely associated with the rollover protection are FMVSS 220 for school buses and FMVSS 216 for small passenger vehicles, which assess the roof strength of a vehicle under quasi-static loading. Compared with the

regulation using the dynamic test procedure like the ECE R66, existing American regulations are considered as the less effective representation of real situations. Liang et al [15] compared the difference between FMVSS 220 and ECE R66 using numerical simulations, and has shown that the penetration to the passenger compartment is more likely to be underestimated under American regulation test condition.

Taking account of recent severe motorcoach crashes and absence of a dedicated procedure to evaluate the rollover resistance of motorcoaches, National Highway Traffic Safety Agency (NHTSA, USA) has proposed a new regulation aiming to improve vehicle roof resistance to prevent serious occupant injury in rollover crashes [16] in 2014. The proposal will be applied to all new over-the-road buses and other types of buses with Gross Vehicle Weighting Rating (GVWR) greater than 25,000 lbs.

The proposed regulation is based on the complete vehicle rollover test from ECE R66 and the following performance requirements are specified by the proposal [16]:

(1) (Surviving space): Intrusion into the surviving space, demarcated in the vehicle interior, by any part of the bus outside the surviving space is prohibited;

(2) (Seats and parcel racks): Each anchorage of the seats and interior overhead luggage racks and compartments shall not completely separate from its mounting structure;

(3) (Emergency exits): Emergency exits must remain shut during the test and roof and rear emergency exits must be operable in the manner required under FMVSS No. 217 after the test;

(4) (Side window glazing): Each side window glazing opposite the impacted side of the vehicle must remain attached to its mounting such that there is no opening that will allow the passage of a 102 mm diameter sphere.

However, based on the aforementioned shortcomings and limitations of the ECE R66 and additional investigations conducted by NHTSA to determine whether ECE R66 could be applied to the larger and heavier buses sold in the US, the following additional considerations are included in the proposed regulation:

1) A mass of 68 kg shall be ballasted in each designated seating positions in the test, regardless of the ballasting method;

2) Approval of compliance using the equivalent methods of ECE R66 via body sections and quasi-static calculations shall not be given, as the representativeness is suspicious;

3) Complete vehicle rollover test based on the computer simulation shall not be used to get compliance as it is not sufficiently objective.

2.2. Vehicle Rollover Simulation Studies

The passenger safety is one of the top considerations in the vehicle design. Though the vehicle is often equipped with various passive safety devices, the vehicle structure during its failure can be dangerous to the passengers, especially in terms of the rollover impact situation. It is shown that the fatality rate will be 13 times larger when the surviving space is intruded in the rollover events [17]. Consequently, researchers have studied the passive safety of the vehicle structure in the various impact events for decades and developed the methods and tools to evaluate the vehicle structural performance and passenger safety.

As the full scale vehicle physical test is of high cost and also difficult to collect sufficient impact data, researchers have conducted studies on the numerical simulation methods and the virtual testing tools. The numerical model is considered to be an effective and efficient tool enabling extensive investigations once the model is built and validated [18]. The numerical

simulation can also be used as one of the methods to certify the vehicle in compliance with the regulation [7]. As a consequence, in the recent decade various simulation tools for numerical modeling of the vehicle impact events have been developed by the researchers.

(1). From the 1970s, researchers have been attempting to use the numerical simulation method for modeling the vehicle rollover events with a goal to understand the vehicle crash structural performance such as the collapse behavior and look for the efficient method to improve the crashworthiness. As one of the earliest research work shown in [19] in 1979, the computational modeling began to be used as the tool to study vehicle rollover accidents. Based on the studies of the vehicle dynamics in accidents, the numerical modeling was conducted and it showed that most actual rolls occurred with the lateral vehicle motion [19]. A vehicle dynamics program was developed to simulate the free body roll motion. As for the impact simulation, to obtain the deformation history of the vehicle, the structural collapse finite element program was developed. Due to the limited computational resources at the time in 1970s, only the deformation of the bus cross section rings was simulated.

Another example of using the computer simulation method to model the bus rollover accident was shown in [20] to improve its crashworthiness and the stability. To reduce the computational cost, the bus cage model was constructed with beam elements, and the modal analysis was used to identify the dynamic characteristics.

(2). With the increasing computation capabilities and advancement of the dynamic FE code for vehicle crashworthiness application, the numerical simulation has been more widely used to build more complex models. It has been seen that the computational crash analysis is the method to help to fully understand the failure mechanisms with sequential, complex and progressive failure [18]. In 1990s the research in using the computational analysis as an effective tool for

future development was not limited to universities but included the vehicle manufactures and supervising government agencies. E.g., since the 1990s Ford Motor Company has been using the crash simulation code DYNA3D as a key tool for the virtual vehicle collision test [21]. In the NHTSA's initiative Partnership for New Generation Vehicles (PNGV) [22], NHTSA decided to develop detailed FE models of representative vehicles from the highway fleet in the USA using the LS-DYNA program. The paper [23] presented the full-scale detailed FE model of Chevrolet C-2500 pickup truck developed in NHTSA National Crash Analysis Center using LS-DYNA. The above model was validated by comparing the results with the pendulum tests on the pickup suspension and the full-scale crash test.

(3). Later on, taking advantage of the available growing computation resources, the numerical simulations using explicit finite element method were conducted by researchers to evaluate the vehicle crashworthiness in compliance with legislative regulations such as ECE R66. This type of research became particularly active in the recent decade. The work in [9] presents the virtual testing approach using FE modeling based on the thin-walled frame structure to approve the coach rollover performance in accordance with ECE R66 in UK. The work in [24] presents the virtual test of the bus for its ECE R66 compliance using the FE model in OASYS-Primer and the solver OASYS-LSDYNA. The research examined the structural performance of the modified bus superstructure to improve the design in terms of load resistance. In [15], the authors conducted the comparative analysis of the bus rollover distortion configuration of the superstructure under ECE R66 and FMVSS 220 using the LS-DYNA code. Another example in [25] shows that the virtual simulation and evaluation is the key tool in the development of vehicle rollover test devices. The comparison between the FEA simulations of rollover test using the test devices of Jordan Rollover System (JRS) with the over-the-ground rollover test was

conducted, and the simulation results showed that the JRS testing approach was able to closely replicate the equivalent over-the-road rollover event.

(4). Nowadays, the design-related research based on the regulation requirements is becoming a common topic within the vehicle crashworthiness community. The numerical simulation is able to evaluate the structural performance in a wide range of impact scenarios and it is used effectively for studying the design criteria, the design improvement and optimization. For example, the problem of the design criteria of the highly resistant and lightweight vehicle bodywork was studied by the researchers in IDIADA (Institute for Applied Automotive Research, Spain) in 1997 [26]. The explicit FEA method is adopted to study the structural resistance during a rollover for motorcoaches. The beam bending collapse behavior was simulated using the FEA code ABAQUS accompanied by the experimental data. The study suggested that the pillars and roof should be continuous in the structure and have similar resistances so that energy could be absorbed uniformly.

Multiple researchers have studied the energy absorbing capability of the vehicle implementing the crashworthiness design principle. One example of the study is shown in [27] where the elastic-plastic FE model (developed in ANSYS) based on the quasi-static loading test of the body sections was used to identify the essential structural components governing the energy absorbing capability. Parts of the bus structure contributing to the rollover strength can thus be identified.

The preferential method of the structural optimization for the bus rollover crashworthiness design following ECE R66 is presented in [6]. The optimization was conducted using the successive response surface method (SRSM) by LS-OPT and the FE code LS-DYNA with respect to the energy absorption. The results showed that the displacement of the optimized bus structure in the rollover event was largely decreased.

(5). With the recent development and updates of the rollover legislated regulation, studies pertaining to the influence of new requirements to the design have become the particularly important topic. Due to the more severe loading conditions of newly proposed NHTSA regulation, previous design criteria (suggested to meet the ECE R66 requirements [24] [26]) may not be sufficiently applicable to the design under new regulations. For example, the research on effect of the seat structure, passenger weight, and luggage weight on the rollover crashworthiness of the motorcoach was presented in [12]. An investigation of different scenarios was conducted using explicit FEA implemented in LS-DYNA software, and the obtained results on bending deformation and energy absorption were compared. The component tests of a side-body breast knot and a roof edge knot were used to verify the calculation. This research concluded that the used computational model produced comparable results with experimental measurements, and can also be effective for assessment other types of buses and coaches. Another example in [10] also used the FE model built using LS-DYNA and the physical test to study the influence of passenger mass on structural deformation of the bus body section in a rollover event. The obtained data on the addition of the load to the bus structure owing to the passenger mass will be used for the possible modernization and updating of the regulation.

2.3. Load Transfer Analysis and Index U*

The ability of the coach to meet the regulations depends not only on energy absorbing capabilities of its components but also on the load carrying capacities [9]. To maintain the surviving space as required, the high load carrying capacities are essential. Compared with the traditional stress analysis, load transfer analysis provides insights into the stiffness distribution among structural members and the ability of the structure to resist deformation.

Load transfer analysis provides the way for the vehicle design engineers to determine and analyze the load path in the vehicle primary structure. Load transfer analysis assesses the efficiency and rationality of structures in transferring loads from the loading to the supporting end. The methodology for load transfer analysis has been studied since mid-90s [28] [29] [30] [31] [32]. Though the concept of load path had been widely used, a simple descriptive definition was firstly given as "the trajectory taken by a unit of applied load in a prescribed direction within a structure beginning at a point of application and ending at an equilibrating reaction" by Kelly and Elsley (1995) [28], where the principal stress and their directions are used as the indicators of the load distribution. Detailed procedure was later given in [29]. Another method to obtain load path using fluid flow analogy was proposed in [30] where the load path is described as the trajectory along which the constant force is transferred. Method of obtaining load path based on a new concept of transferred and potential transferred force instead of the "stress flow" was presented in [31].

As for the vehicle structures, the complexity of the components geometry has limited the application of the above methods of load transfer analysis. The load transfer index U* was firstly proposed as a method to express the course of the load transfer in the passenger car structure in Japan in 1995 [33]. The index U* is calculated as a non-dimensional value using strain energies. Based on this new index, the procedure of load path analysis was later presented in [34], where the load path is obtained by connecting the ridgeline of the U* contour. The complete implementation of U* using the matrix of internal stiffness was later proposed in [35]. It shows that the U* is an index of the degree of connection between an arbitrary point in the structure and the loading point [35]. The load path is defined as the stiffness line which has the minimum decay rate of U* values. Compared with the stress trajectory based method, the U* index theory

is more effective to express and evaluate the load path in complex structures, since the problem of stress concentration can be avoided [34]. Inspection load method in [36] was then proposed based on the internal stiffness expression of U* for efficient calculation. Experiments have been carried out to prove that U* theory is the true indicator of load transfer in the structure [37]. The U* index method is also used as a new tool to evaluate the design in terms of the load transfer efficiency. Design criteria related to the U* index were introduced in [34] to achieve an efficient and desirable structural design. To better use U* to assist in the design, a new derived index U^*_{sum} was proposed in [38], [39] to evaluate the load transfer efficiency. As the sum of U* values of the loading force and the reaction force, the value of $U^*_{sum}$is used as an indicator of the load path distribution in the structure and as a measure of the effectiveness of the structural design. The index U^*_{sum}enables the evaluation of the load dispersion state within the structure.

Vehicle industry has benefited from the designs employing the index U* method for load transfer analysis on account of its effectiveness. Stiffness problems on the heavy-duty truck cabin in [34] were solved by investigating the load path using U*. Weight efficiency design using U^*_{sum} was presented in [39] for automobile bodies. Design evaluations on the vehicle component using both the U* method and stress analysis were presented in [40]. Work in [41] shows that U* and U^*_{sum} can be used effectively on the parcel rack strut to achieve a modified design of better overall stiffness and reduced weight. Example of structural sheet steel joints in [42] shows U* can be used practically to obtain a design of joints of efficient load transfer. Researchers have also applied the U* method in vehicle crash applications to improve the structural performance. The initial phase of the frontal collision for a truck cab was analyzed using U* in [43]. A dynamic U* analysis for side impact of the passenger car was introduced by considering the inertial force in the U* calculation [44], and the overall rigidity of the

compartment is improved effectively. To accommodate U* theory in more applications, researchers have worked to extend U* theory in complex conditions such as the multiple loading [45], in composites and in nonlinear elastic structures [46]. Up to date there was no research done allowing application of index U* approach to the load transfer analysis of the plastically deformed structures. In order to implement the load transfer analysis approach to the vehicle crashworthiness design the extension of index U* approach to plastic domain is needed.

2.4. Summary

1. Addressing severe consequences of motorcoach crashes and absence of a dedicated procedure to evaluate the rollover resistance of motorcoaches, National Highway Traffic Safety Agency has proposed a new regulation aiming to increase the rollover structural integrity for buses in North America. To implement the legislative regulation change and reduce the high costs associated with the full scale physical test, the numerical simulation tools for the virtual testing of the coach structural performance are needed by the vehicle industry.

2. To avoid the potential subjectivity and questionable representativeness of using body sections, the numerical analysis should include simulation of the complete vehicle with full passenger mass.

3. Nowadays the explicit finite element method is a “working horse” being used to conduct the specialized structural analysis approaches in the viewpoint of the crashworthiness of vehicle.

4. Load transfer analysis provides the way for the vehicle design engineers to determine and analyze the load path in the vehicle primary structure. In order to implement the load transfer analysis approach to the vehicle crashworthiness design, the extension of index U* approach to plastic domain is needed.

3. FINITE ELEMENT MODELING OF MOTORCOACH ROLLOVER

3.1. Explicit Analysis and Used Software

3.1.1. Explicit Analysis

The finite element analysis can be conducted using the implicit approach or the explicit approach. As it is shown in the literature review the explicit approach is the primary technique for analysis of the dynamic response of a structure subjected to the impact and rapidly changing time-dependent loads. Different with the implicit approach, in the case of explicit finite element solution, the equations become uncoupled, and they can be solved directly, i.e. explicitly without iteration for nonlinear problems. A lumped mass matrix M is required for simple inversion, and no inversion of the stiffness matrix K is needed.

The explicit scheme is shown as the following [47]. In the explicit method, during a time step Δt, the acceleration and velocity are assumed constant. The information at time t is used to determine the values at time $t+\Delta t$. The time step Δt needs to be small enough to maintain the stability of computation. The formulations are presented as following:

$$\mathbf{M}\mathbf{a}_\mathbf{n} + \mathbf{C}\mathbf{v}_\mathbf{n} + \mathbf{K}\mathbf{d}_\mathbf{n} = \mathbf{F}_\mathbf{n}^{\mathbf{ext}} \tag{1}$$

$$\mathbf{M}\mathbf{a}_\mathbf{n} = \mathbf{F}_\mathbf{n}^{\mathbf{ext}} - \mathbf{F}_\mathbf{n}^{\mathbf{int}} \tag{2}$$

$$\mathbf{M}\mathbf{a}_\mathbf{n} = \mathbf{F}_\mathbf{n}^{\mathbf{res}} \tag{3}$$

Where **M** is the mass matrix; **C** is the damping matrix; **K** is the stiffness matrix; $\mathbf{a}_\mathbf{n}, \mathbf{v}_\mathbf{n}, \mathbf{d}_\mathbf{n}$ are vectors of acceleration, velocity and displacement, respectively; $\mathbf{F}_\mathbf{n}^{\mathbf{ext}}$ is the external loading vector; $\mathbf{F}_\mathbf{n}^{\mathbf{int}}$ is the internal force vector; and $\mathbf{F}_\mathbf{n}^{\mathbf{res}}$ is the residual load vector. The residual load

vector $\mathbf{F_n^{res}}$ is also the net nodal force vector, which includes the contributions from external loads such as the body force, pressure and contacts, element stress, damping, bulk viscosity, and hourglass control.

Thus, the acceleration is determined by inverting the mass matrix and multiplying it by the residual load vector. The velocity and displacement are calculated using numerical integration in time.

$$\mathbf{a_n} = \mathbf{M^{-1}F_n^{res}} \tag{4}$$

The loop in the calculation of the explicit solution is shown in the diagram [48] shown in Figure 3-1.

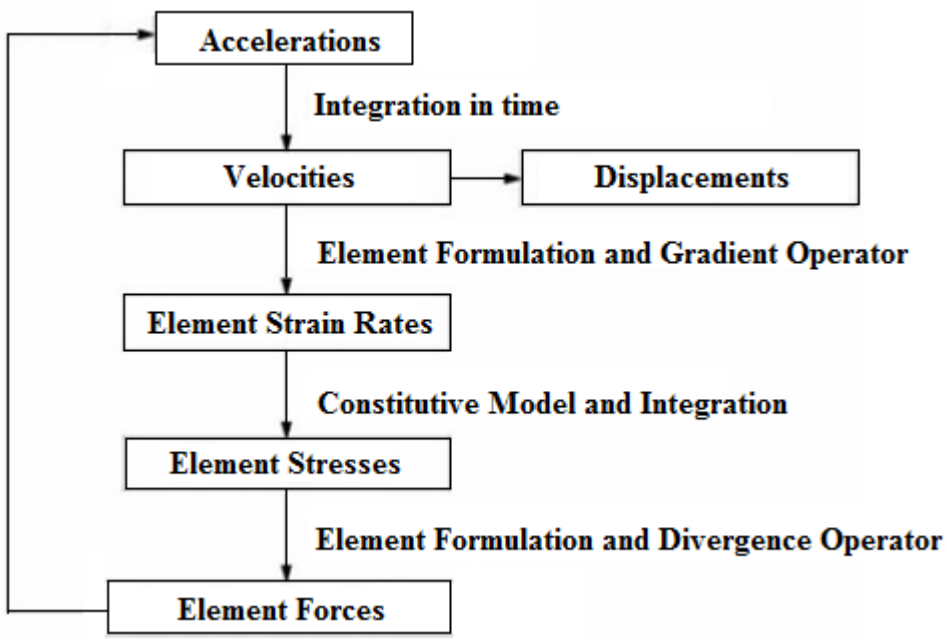

Figure 3-1 Calculation diagram of the explicit method

In summary, compared with the implicit approach, the explicit solution has the following advantages:

(a). The explicit solution handles nonlinearities with relative ease as compared to the implicit analysis. All types of nonlinearities are included in the internal force vector in the explicit solution, as shown in the explicit scheme. The calculation of the internal forces is the major cost. Thus the explicit solution can solve efficiently the problem of various types of contacts, material nonlinearity, and rigid body motion, etc.

(b). For the nonlinear implicit solution [49], each step requires a series of iterations to establish an equilibrium within a certain tolerance, while in the explicit solution, no iteration is needed as the nodal accelerations are solved directly.

(c). The implicit solution requires the inversion of the stiffness matrix over the course of a time step. For a large deformation problem such as the vehicle impact analysis, the stiffness matrix could include millions of degrees of freedom. The matrix inversion operation is computationally expensive, especially for large models. The explicit solution doesn't require the matrix decomposition. The explicit solution only requires the simple inversion of a diagonal mass matrix. Thus it allows solving the large deformation problem more efficiently.

(d). There is also the disadvantage of the explicit solution. The time step for the explicit solution must be smaller than the time required for the stress wave to cross the smallest element in the mesh, which is known as Courant-Friedrichs-Levy (CFL) condition. This time step is usually around 100 – 1000 times smaller than that used in the implicit method.

The vehicle impact event is associated with the physical phenomena of short-duration, highly nonlinear behaviors of the material, large deformation of the structure, and the rigid body motion. For the rollover impact, the large deformation of the superstructure and the plastic hinges formed on the structural beams are the key features for the simulation. These aspects make the traditional

Finite Element Analysis with the implicit approach impossible to solve. Consequently, the explicit FEA tool will have to be employed in this study.

3.1.2. Bus Rollover Simulation and Software Choice

From the literature review, several popular commercial programs for the nonlinear FEA solution in the application of the vehicle impact simulation include LS-DYNA (LSTC, US), PAM-CRASH (ESI, France), MSC.Dytran (MSC, US), MADYMO (TNO, Netherlands), RADIOSS (Altair Engineering, US), and ABAQUS/Explicit (Dassault Systemes, France) [50].

In order to select the best FEA program for the coach rollover simulation, several criteria are considered, which include (1) the expertise in the vehicle crash application, (2) the accuracy and the reliability, (3) the parallel processing capability, and (4) the availability of technical support and resources.

With the consideration of the coach rollover simulation needs and the explicit solver capabilities of the related commercial programs in vehicle crash simulations, the explicit nonlinear finite element dynamic code, LS-DYNA®, developed by Livermore Software Technology Corp (LSTC), was selected to perform the complete coach rollover simulation. The version R7.1.1 is used [51].

The application examples of LS-DYNA as the FEA tool for the rollover crashworthiness can be found in the study of rollover performance of an intercity coach [12] and transit buses [52] [53], the improvement of bus design in rollover [54], and the virtual rollover testing in compliance of ECE R66 [24].

LS-DYNA is a multifunctional explicit and implicit FE program to simulate and analyze highly nonlinear physical phenomena pertaining to real-world problems. Usually, these events

are subjected to large deformations within the short time duration, e.g. the crashworthiness and explosion simulations. The features of LS-DYNA include the advanced contact algorithms, the large library of constitutive models and element types, and the special implementation for the automobile industry. The diagram of typical work steps using LS-DYNA is shown in Figure 3-2.

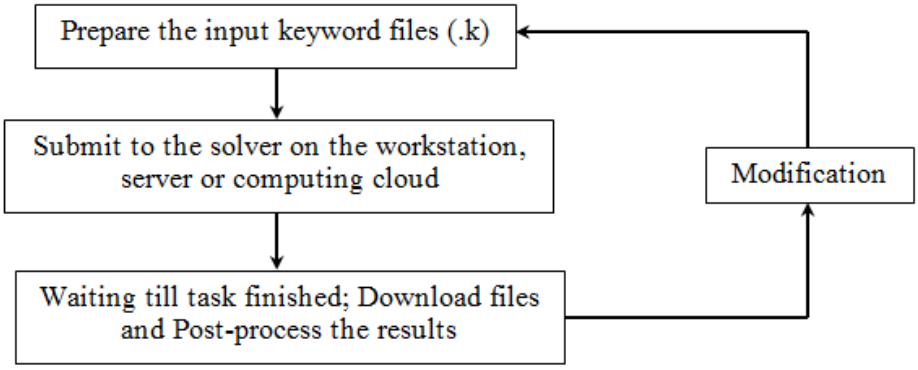

Figure 3-2 Diagram of work steps using LS-DYNA for simulation

The pre/post-processing is accomplished in LS-PrePost (LSPP), also developed by LSTC Company. As an interactive tool for the pre/post-processing, LSPP is designed to have the full LS-DYNA keyword support, the LS-DYNA model visualization, the capability to create and edit the LS-DYNA model, the advanced post-processing, and the importing and exporting data in many common formats [55]. The contour and time histories plotting and simulation animation can be efficiently conducted using LSPP for the complete coach rollover model.

3.2. Modeling Approach and Model Description

The finite element model of a complete motorcoach used for the vehicle rollover simulation is shown in Figure 3-3. The assembly consists of the superstructure, parcel racks, the seat structure, the window glasses and skins, the passenger and baggage floor, the suspension and wheel assemblies, and the simplified models for the engine and transmission.

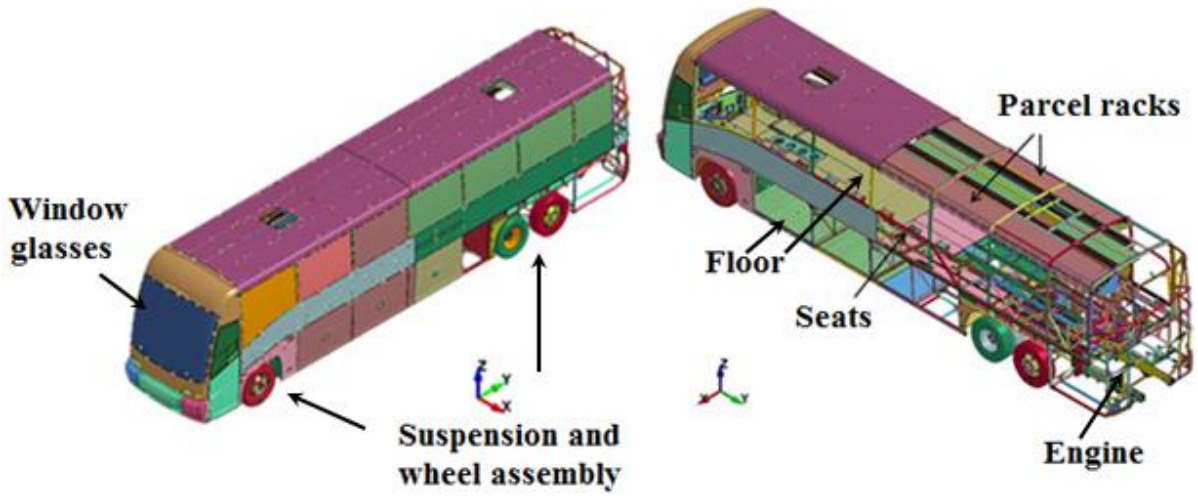

Figure 3-3 Full scale motorcoach model

3.2.1. Modelling Approach

From the requirements of the newly proposed regulation by NHTSA and the literature review of the simulation methods for the bus rollover problem presented in Chapter 2, it is seen that the modelling of the complete vehicle becomes a mandatory part of the modern design procedure. In order to analyze the behaviour of the coach structure and its compliance with the ECE R66 and new regulation, the whole process of the rollover from the very beginning when vehicle falls off the platform to the moment of reaching the maximum deformation should be simulated.

The new regulation also requires examining the structural integrity of the components of the parcel rack assembly and the seats in the rollover test in case they break and penetrate the surviving space. To obtain the accurate simulation results these essential components are included in the complete coach model. They are connected with the superstructure in the modelling using contacts and constraints.

With the above considerations, the details of the coach framework model are shown in Figure 3-4. The components of the parcel racks, window glasses, and skins are hidden for a clear

illustration. As shown in Figure 3-4, the superstructure includes the vertical pillars, cantrails, waistrails, roof beams, seat beams, beams in the frontal end and rear end. The component of the parcel rack model is shown in Figure 3-5.

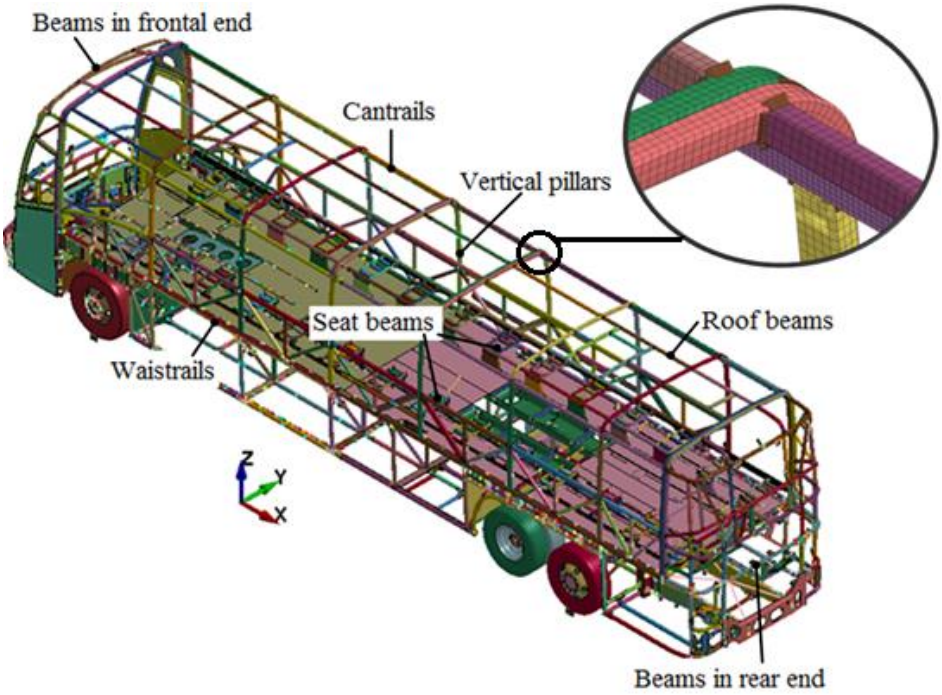

Figure 3-4 Coach framework model

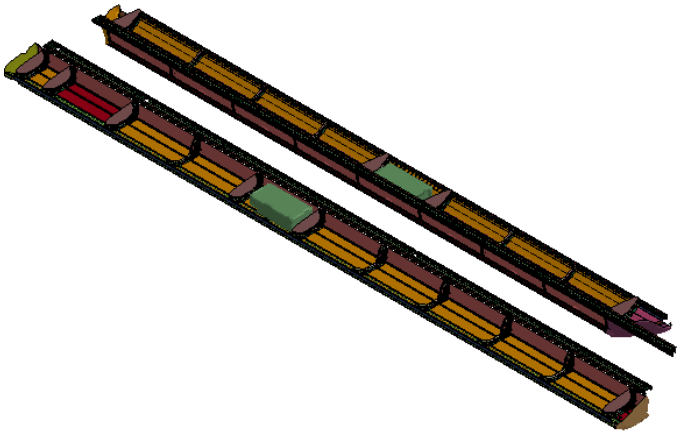

Figure 3-5 Parcel rack model in the coach

The total length of the coach is around 13.8 m, thus the scale of the model is one of the critical question to be addressed. The superstructure of the coach physically is composed of the thin-walled beams. In the rollover event the vehicle structure dissipates the kinetic energy via mechanisms of deformation, buckling and fracture. It produces the essential distortions of geometry and forms the plastic hinges surrounded by the extended zones of plastic deformation. In order to simulate the phenomena, the beam joints in the structure need to be modeled using shell elements. Though the simplification of beams as the beam elements has higher computation efficiency, it is not reasonable as the beam element is unable to simulate the production of plastic hinges. This scale of the modeling is shown in Figure 3-4 by one example of the roof beam joints with welds. This small feature is regarded as very important for the rollover simulation. As shown in Figure 3-4, these beam joints in the coach superstructure are modeled using shell elements with no less than 5 elements across the length of the beams. As a trade-off between the accuracy and cost, this mesh density has been shown to be sufficient to capture the bucking behavior [8].

The model scale of the seat and the parcel rack are shown in Figure 3-6 and Figure 3-7. As the seats and parcel racks are not designed to bear the load directly, their contributions to the resistance to the coach global deformation are much less important than the beams in the superstructure. Though these two components can have many geometrical details, the mesh density in the model is not as fine as for the coach beams. Shown in Figure 3-6, the seat beams only have 2 or 4 elements across the width. The parcel rack struts are designed to be strengthened by stiffeners. They are also modeled using shell elements, shown in Figure 3-7. These stiffeners have the feature of the narrow width, and they have at least 2 elements across the width. With this level of details modeled, they are the smallest part in the coach model.

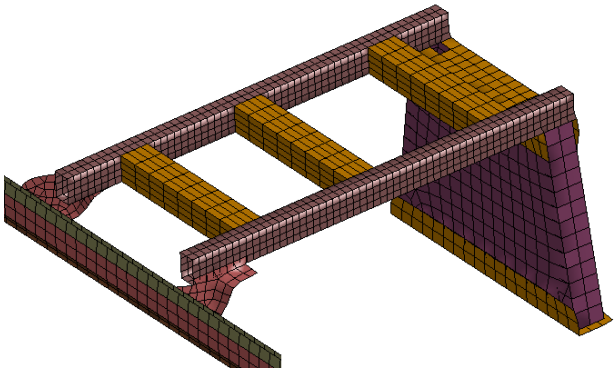

Figure 3-6 Model scale of the seat

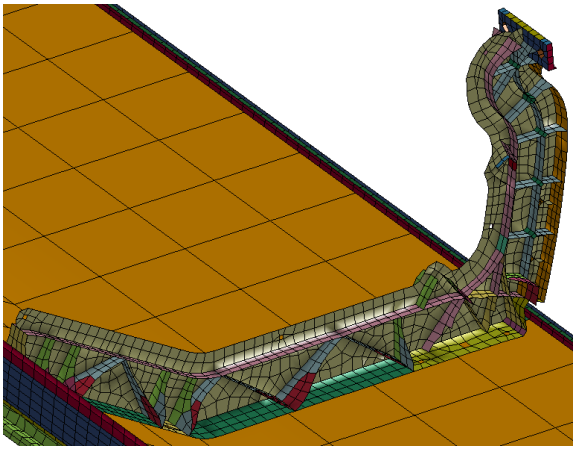

Figure 3-7 Model scale of the parcel rack

With the consideration of the large dimension of the coach and significant number of the geometrical features in the structural components contributing to the global deformation in the rollover, it is not reasonable to have more detailed modeling due to the rapid increasing of computation cost when the density of mesh gets finer. Since the performed simulations demonstrated that the selected mesh density in the current model is able to capture the failure phenomena in the rollover, there is no need to achieve the higher mesh resolution in the model.

Additionally, with the consideration of structural deformation in the rollover event, parts with negligible deformation will be modeled as the rigid body in order to save the computational time.

The rigid parts in the coach model are shown in Figure 3-8. They are mainly the suspension system and the brackets on the seats. Other parts in the coach model will be deformable.

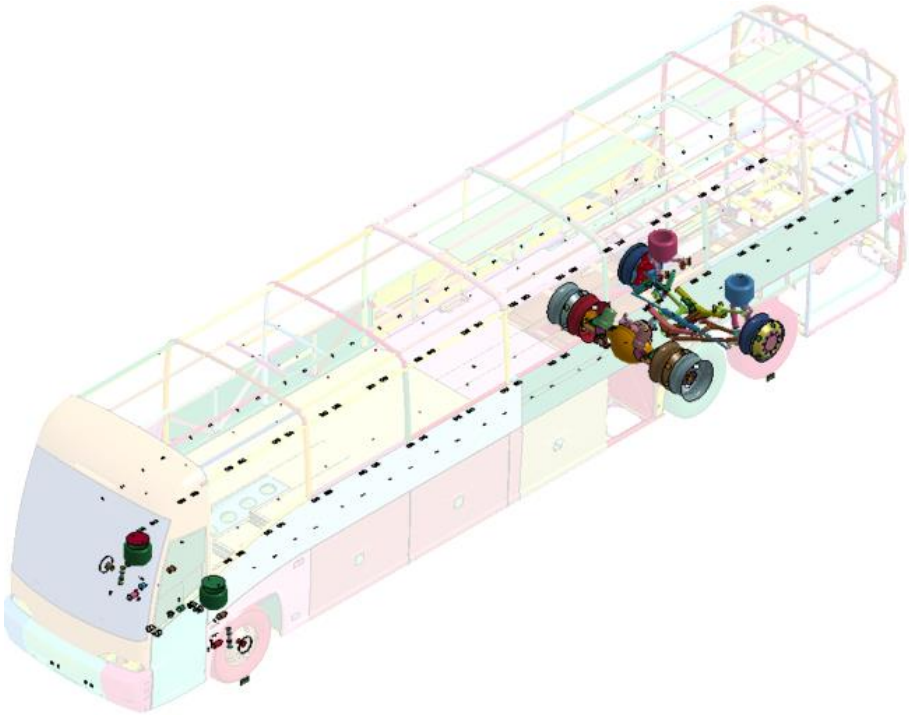

Figure 3-8 Rigid parts in the coach

3.2.2. Input Data and Problem Analysis

The development of the full scale motorcoach FE model is divided into different stages. The model is developed based on the modeling work of *Eicher Engineering Solutions, Inc.* It was initially developed by Eicher for the purpose of evaluating the parcel rack design in the frontal collision events [56]. The Eicher model gives the detailed modeling of coach geometries, contacts and constraints between parts, especially in the frontal part. The University of Manitoba collision project group decided to use it as the base model, and sought the possibility to modify it and adapt it to the rollover simulation.

As shown by the initial run using the Eicher model, the simulation results demonstrated that the model had the problem of the unrealistic deformation, the overlarge artificial energy, and the deviated total energy. It indicated that the Eicher model was far from producing any useful information. The possible reasons for that include the following:

(a). Rigid parts;

As the Eicher model was used for the frontal collision purpose, its modeling approach treats the rear lower structural frame as the rigid bodies, since they will not experience large deformation in the frontal collision. However, this consideration is not acceptable for the rollover conditions due to significance of the rear frame deformation.

(b). Missing geometry;

After checking the Eicher model, it is found that some essential structural geometry in the rear part is missing, such as one transverse beam and the engine cradle. They are considered to make a contribution to resisting the deformation in the rollover. Their absence is thus incorrect.

(c). Unverified material properties;

It is found that the frame material property has a rather low yielding strength, lower than the common structural steel found from literature and the industry specification. It will directly lead to a larger deformation in the rollover simulation. It indicates that the material properties need to be verified with an additional material tensile test. The material properties of other key components also need to be verified.

(d). Boundary conditions.

The Eicher model check also shows that the rollover boundary condition does not comply with the ECE R66 regulation specifications.

3.2.3. Model Modification

To use the Eicher model for the rollover simulation, the heavy modification work has been done by the author, with the objective of achieving rollover simulation results which can be correlated with the physical test results on a similar coach from the database of National Highway Traffic Safety Administration (NHTSA) and show the reasonable deformation and energy verification.

The modification work has been carried out for more than 2 years. LS-PrePost was used as the pre- and post-processing tool for the modification work. Considerable changes were introduced to the boundary conditions, material properties, geometrical modeling of the key structural components, contacts and constraints, mass distributions, and the mesh. Among others, the following major modifications were made, shown in Table 3-1.

Table 3-1 Major modification on the Eicher model

Category	**Details**
(a) Boundary conditions	• Platform height is 800mm as in ECE R66, and the Center of Gravity in equilibrium position before the free falling; • Rotational hinge axis is moved to be on the plane of wheel lower tip; • Gravitational force is perpendicular to the ground modeled as a rigid wall; • Friction coefficient 0.7 is chosen between the vehicle and the ground; • The free falling simulation is run at the first step to obtain the correct initial angular velocity for the impact simulation;
(b) Material property	• The stress-strain curve and the yielding strength of the steel for the frame and welds are obtained from material tensile test; • The rear lower frame is changed from rigid parts to deformable parts, and lost connections

	are made up using Constrained Nodal Rigid Bodies or welding; • The material properties of seat structures are modified using data from "Kiel AVANCE 2010 D-coach single pedestal seats";
(c) Geometrical modeling	• Welds for key joints of the coach frame are modified to tie adequate nodes according to the result of the component test validation; • A transverse frame beam connecting two sides at the very lower rear end is introduced to the model; • The floor at the rear part is modeled; • Accelerometers are modeled by *ELEMENT_SEATBELT_ACCELEROMETER at multiple locations according to NHTSA's rollover test data. The minimum sampling frequency (for output) is studied to get a converged measurement;
(d) Contacts and constraints	• Tied contacts type is replaced by *Contact_tied_shell_edge_to_surface_beam_offset due to the negative sliding interface energy; • Tied contact for seat rails are modified to avoid the penetration;
(e) Mass distribution	• Passengers' mass represented by the mass blocks is removed in the coach model; • Engine mass is modeled by a lumped mass element, which is connected with the mount frame by beam elements, and the corresponding mass is subtracted from the coach rear lower frame;
(f) Mesh, Elements	• Full integration formulation is used for elements modeling the strut of the parcel rack to reduce the hourglass deformation.

(a). Boundary conditions

According to the ECE R66 specification, the height of the platform needs to be 800 ± 20 mm. The axis of the tilting platform is located at the side of the lower edge of wheels, shown in Figure

3-9. As the friction between the ground and the coach also absorbs a certain amount of kinetic energy, the friction coefficient needs to be defined from a validation test or the literature. A typical value 0.7 is defined between the steel and concrete [8]. To obtain the correct angular velocity, the rollover simulation starts from the free falling process.

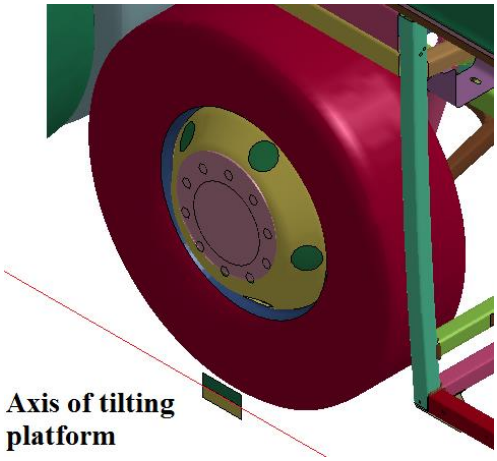

Figure 3-9 Location of axis of tilting platform

(b). Material property

The low yielding strength of the frame material in the original Eicher model leads to the decision that the frame material property needs to be verified. It is decided that the material data from the tensile test of a cut sample of the coach, which will be shown in details in subsection 3.2.5, is used in the simulation, as it represents the real condition. As stated in the initial model problems, the rear lower frame will use the deformable material model because the deformation of the rear lower frame is important in the rollover. Material properties of the seats will be replaced by more detailed material models of the components such as the bracket, beam, leg, and rail to increase the model's representativeness of the current coach in production. The detailed material properties of the seat structure will be shown in subsection 3.2.5.

(c). Geometrical modeling of components

As the plastic hinge developed at the pillar joints is a very important factor for the coach overall structural behavior in the rollover simulation [8], the modeling technique of the welds at key beam connections needs to be validated in accordance with the component bending test of a cross pillar joint sample. This will be shown in details in the subsection 3.4. With the validated behavior of the cross pillar joint by the physical bending test, the coach model will be considered validated at the component level. Missing structural members such as the transverse beam need to be introduced to reduce the excessive deformation of the rear frame. The missing floor is also modeled as it is considered to contribute to the deformation resistance in the coach. To measure the acceleration in the model for the sake of the comparison with the rollover test result of a similar coach, the accelerometer model is introduced in the coach model.

(d). Contacts and constraints

To combat the large negative sliding surface energy in the initial model problems, the tied contact type is studied and compared, and a new tied contact type is used. Another problem for the contact is that the seat rails and the coach frame beams have the noticeable penetration into each other in the initial simulation result. In order to avoid this unrealistic penetration and obtain a correct contact simulation result, the contact thickness in the tied contact parameters is increased to tie more nodes and the choice of the slave part and the master part are adjusted according to the mesh density.

(e). Mass distribution

As the tested coach isn’t ballasted with the passenger mass in the current ECE R66 test, to achieve a comparable rollover simulation results, the passenger mass is removed from the current coach model. Also, in order to obtain a better mass distribution, even when the model is ballasted with passenger mass, the mass will be represented by the mass blocks located above the seats.

For the same reason, the mass of the engine will be represented by a lumped mass element rather than being distributed in the rear coach frame as in the Eicher model. The inertia of the lumped engine mass has a certain influence on the deformation of the rear frame of the coach.

(f). Mesh and elements

During the simulation, it is found that there is evident hourglass deformation of the parcel rack strut, which contributes to the accumulation of the artificial hourglass energy. To deal with this problem, the full integration formulation is used for the shell elements of the strut, which is able to avoid the hourglass deformation occurrence.

3.2.4. Mass Distribution and Centre of Gravity

The modified model was checked for the total mass and the position of the centre of the gravity by comparison with the tilt table test data of a very similar coach provided by the vehicle manufacturer [57]. The results of comparison are shown in

Table 3-2. It demonstrates that there is very small difference between the model and the data, so the mass distribution of this coach is considered accurate to a satisfied extent.

More specifically, the structural curb mass of the complete coach model is measured as 17,616 kg, which includes the structural mass, the fuel and fluids and the driver [7]. Since some of the non-structural components are not represented in the model, to achieve a correct mass distribution, lumped masses are added to the model, with one of 1,637 kg for the engine, and additional points with a total mass of 2,435 kg dispersed on the beams throughout the frame.

Table 3-2 Differences of CG location between model and tilt table test data of a very similar coach

		Model	Tilt table test	Difference	Comments
CG location	Height, mm (Measured as table angle Theta, degree)	42.5	40.73	6.03%	Acceptable
	Length, mm (From frontal axle)	6056	6252	3.1%	Good
	Width, mm (From centerline)	0	0	0%	Very good
	Height from the ground, mm	By calculation using Theta	By calculation using Theta	2.4%	Good
Weight	Total curb weight, kg	17,616	17290	1.89%	Very good

3.2.5. Constitutive Material Models

The material response of the coach FE model is simulated mainly using isotropic piecewise linear plasticity model, with a small number of rigid parts for non-structural elements. The material models used for the coach main frame and the subsystem of seats and parcel racks, which are the main contributors to the coach rollover performance, are listed in Table 3-3.

Table 3-3 Material models of the frame and two key subsystems

Subsystem	Material Model	Locations in coach
Welds	Steel (024 MAT_PIECEWISE_LINEAR_PLASTICITY)	Welds
Frame	Steel (024 MAT_PIECEWISE_LINEAR_PLASTICITY)	Frontal frame and rear frame
Seat Structure	Steel (020 MAT_RIGID)	Seat fasteners
	(020 MAT_RIGID)	Passenger and driver mass blocks
	Steel (024 MAT_PIECEWISE_LINEAR_PLASTICITY)	Bracket seat-to-wall
	Steel (024 MAT_PIECEWISE_LINEAR_PLASTICITY)	Leg and rail floor
	Aluminum, (024 MAT_PIECEWISE_LINEAR_PLASTICITY)	Rail wall
	Steel (024 MAT_PIECEWISE_LINEAR_PLASTICITY)	Beams seat frame
Complete parcel rack	Aluminum (024 MAT_PIECEWISE_LINEAR_PLASTICITY)	Evaporator for Parcel rack
		Parcel rack rails
	Nylon (024 MAT_PIECEWISE_LINEAR_PLASTICITY)	Parcel rack strut and coverings
	054/055 EHANCED_COMPOSTE_DAMAGE	Pultrusions of Parcel rack
	100 SPOTWELD_DAMAGE_FAILURE	Bolts for Parcel rack

Stress-strain curves of the structural stainless steel for the frame beams and welds were obtained by the uniaxial material tensile test per ASTM E8/E8M testing standard on the samples cut from the real vehicle frame, conducted by the University of Manitoba collision project group. Author of the present thesis contributed to the analysis of data. The obtained material properties are presented in Table 3-4:

Table 3-4 Material properties for the frame structural steel

Density (kg/m^3)	Young's modulus (GPa)	Poisson ratio	Yielding strength (MPa)
7850	210	0.3	426.7

The dog-bone specimen and the plastic strain and true stress curve are shown in Figure 3-10. No strain rate effects or failure is considered for the structural steel material in this model. The raw test data and analysis can be found in Appendix A.

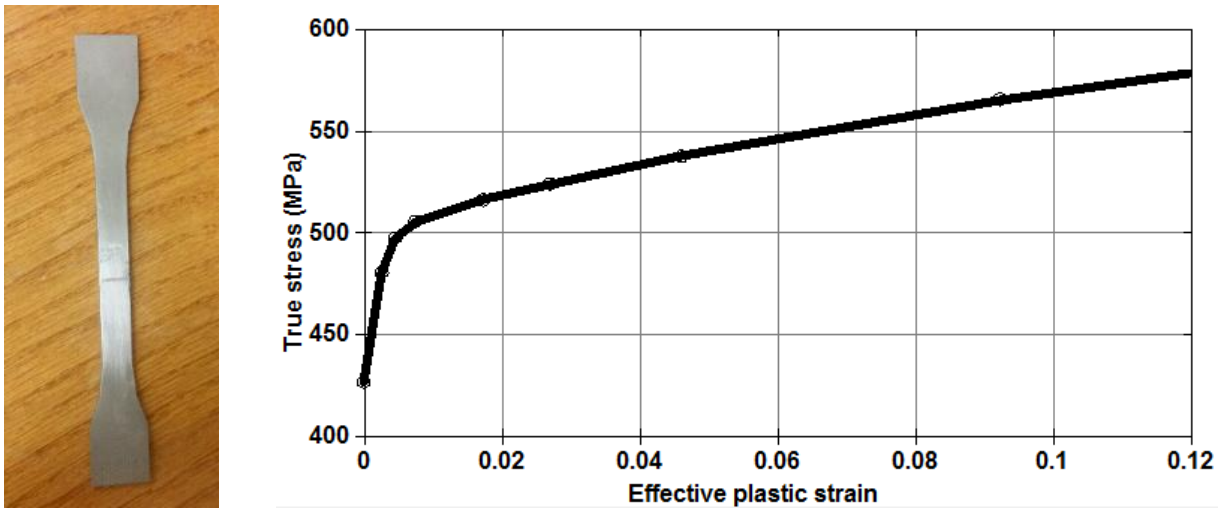

(a) (b)

Figure 3-10 Material properties test and stress-strain curve: (a) Dog-bone specimen; (b) Stress-strain curve of the frame steel

The material properties of the seats differ in different components. The structural components are shown in Figure 3-11 and the material properties are shown in Table 3-5.

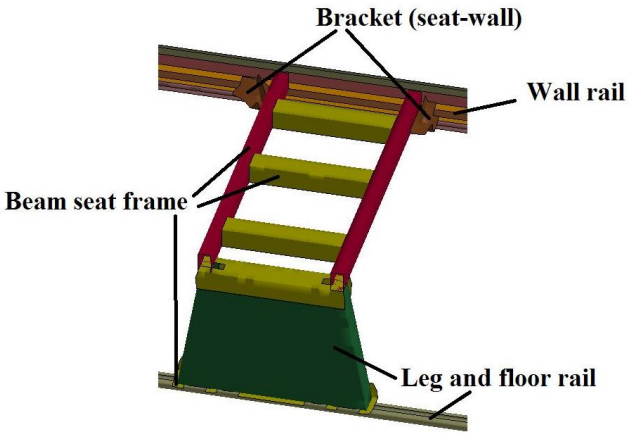

Figure 3-11 Different components of seat structure

Table 3-5 Material properties for seat structure

Components	Young's modulus (GPa)	Poisson ratio	Yielding strength (MPa)
Bracket seat-to-wall (steel_S355)	210	0.3	391
Leg and rail floor (steel_SS304)	195	0.3	258.85
Rail wall (aluminum_AA6060T4)	68.2	0.33	80.58
Beams seat frame (steel_St34)	195	0.3	220

To evaluate the passenger safety in the coach rollover event according to ECE R66, in the modified model the periphery of the surviving space is built using the shell elements with the type of null material (*MAT_NULL) as the surviving space is not an existing component in the coach (Figure 3-12).

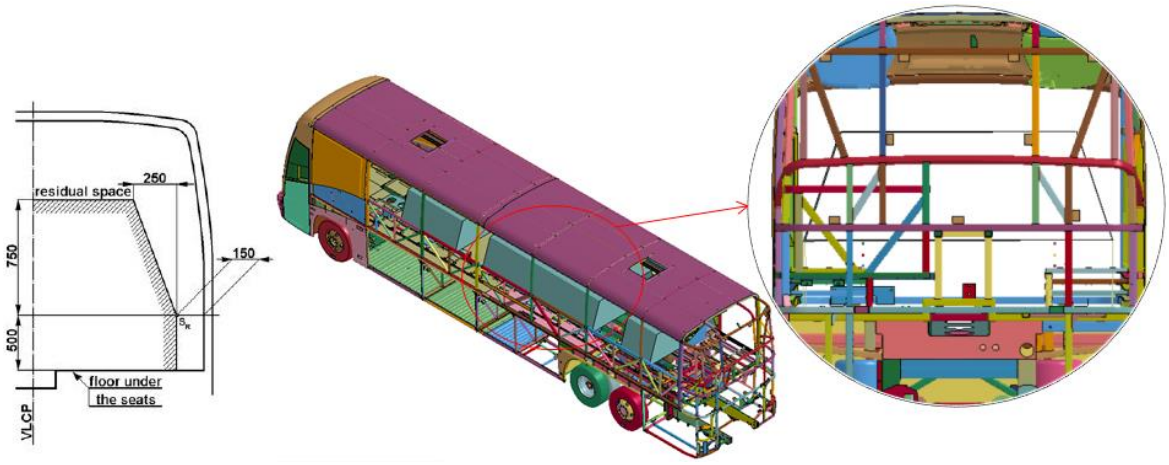

Figure 3-12 Surviving space with the null material

3.2.6. Element Types and Formulations

As the coach structure mainly consists of the thin-walled beams and panels as the frame, shell elements are employed and they dominate in the modified finite element model. This model contains around 4.2 million nodes and 4.7 million elements with approximately 83% of shell elements and 17% of solid elements; the rest are a few beam and discrete elements and mass elements.

The shell element formulation of four-node underintegrated type Belytschko-Tsay with 5 integration points through the thickness is widely used in the finite element model for its advantage of high computational efficiency [58]. It requires 2.5 times less computation time than the fully integrated element formulation (Type 16), and it becomes the default shell element formulation for explicit simulations. The underintegrated shell elements also have the low possibility of the shear locking problem. However, the Belytschko-Tsay elements are prone to the problem of the nonphysical deformation pattern with zero energy deformation modes in the shell elements as the hourglass deformation. LS-DYNA provides the hourglass control with the

introduction of additional stiffness for the elements [51]. Type 1 standard hourglass control with the default coefficient 0.1 is used in the model with the Belytschko-Tsay shell elements.

For the coach frame beams, no less than five elements across the edge of the cross section are used to permit the correct simulation of the buckling behavior of the frame beams, which is critically important to capture the dynamic behavior of the vehicle structure in the rollover.

Solid elements are mainly used in the coach model in the parts of suspension systems. Beam elements are implemented in the model mainly for modelling the air springs and the bolts connecting parcel racks and the coach frame, which are considered to play much less important role in the coach rollover performance. Mass elements are used to tune the mass distribution in the coach.

3.2.7. Contacts and Constraints

The vehicle assembly is built using contacts and multi-point constraints between individual parts. The summary of the contacts defined in the coach model is shown in Table 3-6. Constrained Nodal Rigid Bodies (CNRB) are used in the model to attach most of the small non-structural components to the frame by simply constraining all degrees of freedom. Constraints for the rigid bodies are also defined in the model, mainly for the rigid suspension parts and between the rigid passenger mass blocks and the deformable seat structure. The examples of connections and constraints are shown in Figure 3-13.

Table 3-6 Summary of contacts

Contact type	Details
Automatic_single_surface	Global contact between most of the parts
Automatic_surface_to_surface	Parcel rack to coach side frame
	Parcel rack to coach top frame
	Rear floor to the channel structures beneath the floor
Tied_shell_edge_to_surface_beam_offset	Welds (Slave) tied to the coach frame (Master); welds for main pillars excluded
	Welds (Master) tied to the coach frame (Slave) for main pillar connection
	Seat rails (Master) tied to frame shells (Slave)
	Nodes of parcel rack at the side (Slave) tied to coach top frame (Master) at two sides as the bolts connection
	Nodes of parcel rack near the top center (Slave) tied to coach top frame (Master) at two sides as the bolt connection
	Tied contact within parcel rack components at two sides

The global contact is defined between most of the structural parts to prevent them from penetrating into each other. Other types of contacts are used mainly for the subsystem of parcel racks and seats for the connection within them and the connection with the coach frame. As one of the most important contacts for the coach rollover performance, welds are modeled explicitly

as separate parts with isotropic piecewise linear plasticity model connected to the beams using tied contacts. Shown in Figure 3-13, for the main pillars, adequate numbers of slave nodes on the beam are tied to the welds using the contact type Tied_shell_edge_to_surface_beam_offset [51]. This type of the tied contact is used for the welding modeling because it constrains both the translational and rotational degree of freedoms, and it will not produce large negative sliding surface energy.

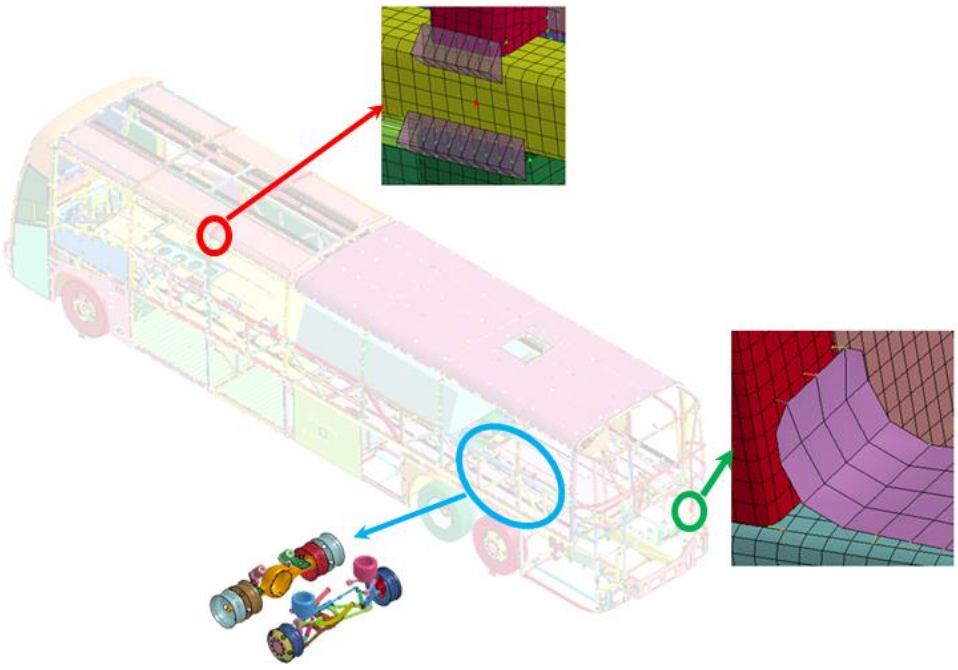

Figure 3-13 Examples of connections and constraints in the coach model: (Red) welds tied to the coach frame for the main pillars with tied nodes highlighted; (Green) CNRB for connecting a bracket to the frame beam; (Blue) Rigid body constraints for the rigid rear suspension parts

3.2.8. Hardware Support

Considering the model size and the nature of the small time step of the explicit FEA solution, the computation cost requirement is very high and it exceeds the hardware capability of any

personal computer or workstation. Supercomputing facility provided by the network of Compute Canada is employed. The simulations are performed using MPP (Massively Parallel Processing) version LS-DYNA on the supercomputing facility GREX, which is part of Compute Canada's Westgrid network. For the simulation of the impact event of 800 ms duration, the simulation takes around 74 hours running on 26 cores. The pre- and post-processing is conducted on the PC using the tool LSPP.

3.3. Boundary Conditions

Replicating the conditions of a physical test, the simulation starts with the equilibrium position shown in Figure 3-14. Initially, the center of the gravity is at its highest position when the wheel lift-off starts. The gravitational load is applied as the external loading using the keyword *LOAD_BODY to add the acceleration in the vertical direction. The interaction between tires and an edge of the platform is represented by a rotary hinge with the axis parallel to the longitudinal axis of the vehicle using the keyword *CONSTRAINED_JOINT_REVOLUTE. The hinge is deactivated by defining the time for the revolute joint failure when the wheels leave the platform.

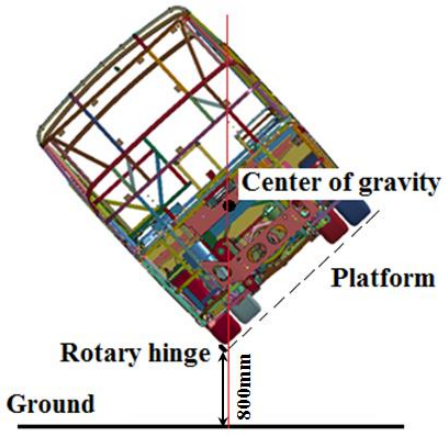

Figure 3-14 Initial condition of rollover simulation

Shown in Figure 3-15, a wheel support on the rigid tilting platform is used to prevent wheels of the tested vehicle from sliding sideways. To simplify the modeling of the tilting platform and the contact between wheels and the support, a hinge is built where the outward surface of wheels touches the wheel support, shown in Figure 3-16. The lower half of the hinge is fixed and the upper half is connected to the wheel using nodal constraints. The revolute joint between the lower and upper half is used as the rotation axis for tilting.

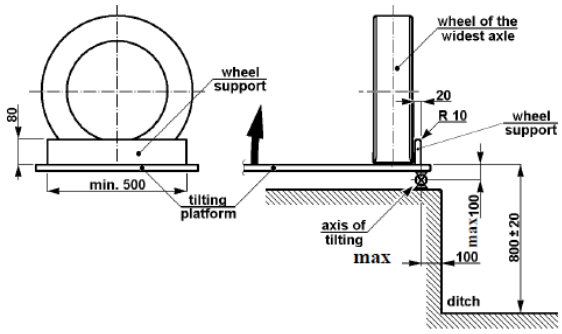

Figure 3-15 Tilting platform and wheel support in ECE R66 [7]

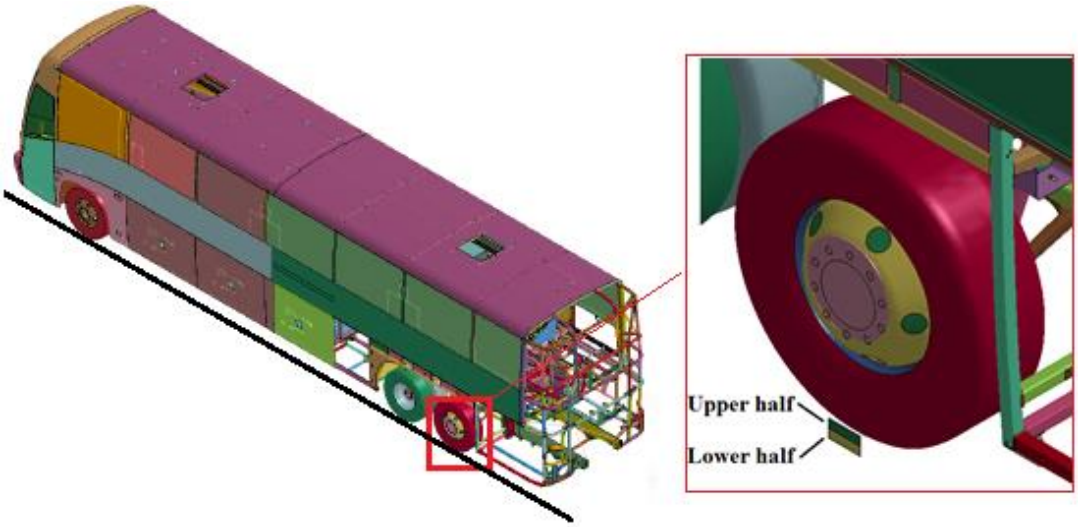

Figure 3-16 Hinge in the model

The contact of the coach model and the ground is implemented in LS-DYNA using a rigid wall with a frictional contact using the keyword *RIGIDWALL_PLANAR, shown as the green

plane in Figure 3-17. All nodes in the coach model will be set as the slave nodes except for nodes for welds. A coulomb friction coefficient 0.7 is defined for the rigid wall as a typical value between the steel and concrete contact [8]. Dissipated energy will be stored as the rigid wall energy (RWEN in *CONTROL_ENERGY = 2).

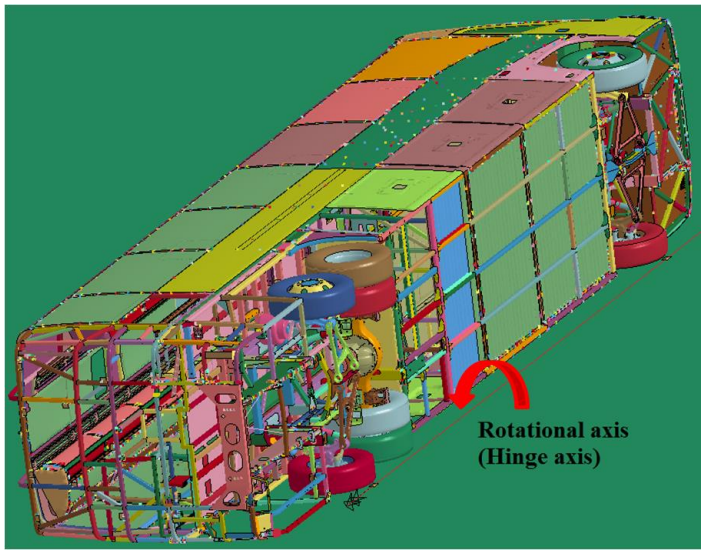

Figure 3-17 Rigid wall modelling for coach impact

For the treatment of the interaction with the rigid wall, in the keyword *CONTROL_CONTACT (entry: RWPNAL = 0.0), rigid bodies interacting with rigid walls are not considered. The constrained method is used by default for the treatment of nodes impacting the rigid wall. The velocity of any penetrating node is reset to zero and the node will be moved on the surface of the wall. The lost kinetic energy will be stored as part of the rigid wall energy.

The rollover simulation is divided into two stages, i.e. free falling simulation and impact simulation. Before the impact to the ground, the coach falls off the platform from the equilibrium position with a fixed rotational axis, shown in Figure 3-18. Since the deformation of the coach structure is negligible at this stage, the simulation is performed for a rigid model, using the technique of deformable-to-rigid switch available in LS-DYNA with the keyword

*DEFORMABLE_TO_RIGID_AUTOMATIC [59] [60]. All parts are switched to the rigid state and be merged as one body at the time 0 s. The rotational velocity at the moment of impact is then recorded. At the next stage, an impact simulation is performed, where the model is treated as the deformable state. The simulation starts at the coach position just before the impact with the applied initial rotational velocity, recorded in the free falling simulation. The keyword *INTIAL_VELOCITY_GENEGRATION is used to define the initial rotation velocity.

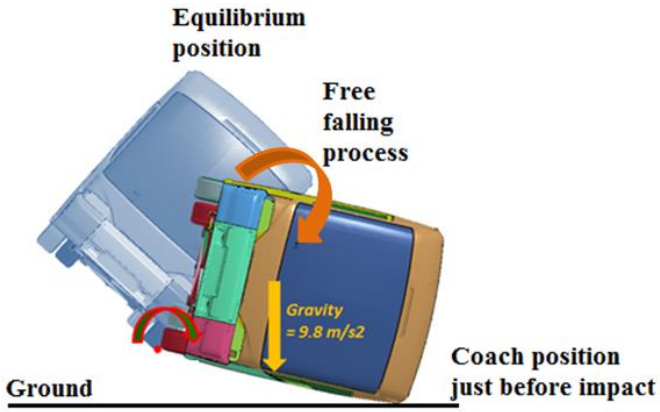

Figure 3-18 Rollover simulation for free falling and impact

3.4. Component Test and Validation

Due to the model complexity and limited amount of information available for model validation from a complete rollover test, the model validation at the component level was carried out. A typical joint between a vertical pillar and a roof beam is utilized as one of the representative members of the coach. One example of the pillar connection with roof beams is shown in Figure 3-19. Such a connection is considered to play an important role in contributing to the structural integrity in the rollover event, as most of the overall deformation for the coach structure is dictated by the plastic hinge developed at the pillar joints. Thus, the validation of a model of the pillar joint will lead to the correct structural behavior of the majority of the coach frame.

Figure 3-19 Example of pillar structure in a typical coach

The quasi-static component bending test on the cross pillar sample was firstly conducted. The significance of the component test is that it provides the way to validate the simulation technique used in the full coach model for the pillar-roof connection, including the material model, mesh density, element type and welding modeling approach. Due to the complexity of the loading and the boundary condition of the cross pillar in the dynamic rollover event, the quasi-static bending test will not produce the same failure mode as in the real rollover event. However, the same loading and boundary condition can be duplicated in the simulation. Based on the comparison of the simulation and component test results, the simulation technique can therefore be validated.

3.4.1 Component Bending Test

The pillar sample was cut from the coach frame directly, made of the stainless steel. The test setup is shown in Figure 3-20 (a). The loading is applied by an MTS loading machine with the displacement-controlled method at the rate of 10 mm per minute. Shown in Figure 3-20 (b), three ends of the pillar were fixed while the lower end was subjected to a quasi-static vertical load

until failure occurred at around 100 mm displacement. It is noted that the three fixed-end connections are strengthened to ensure the failure will happen at other locations of the pillar. The displacement and the force data at the loading point were recorded during the test. More detailed description and discussions about the test setup can be found in [61].

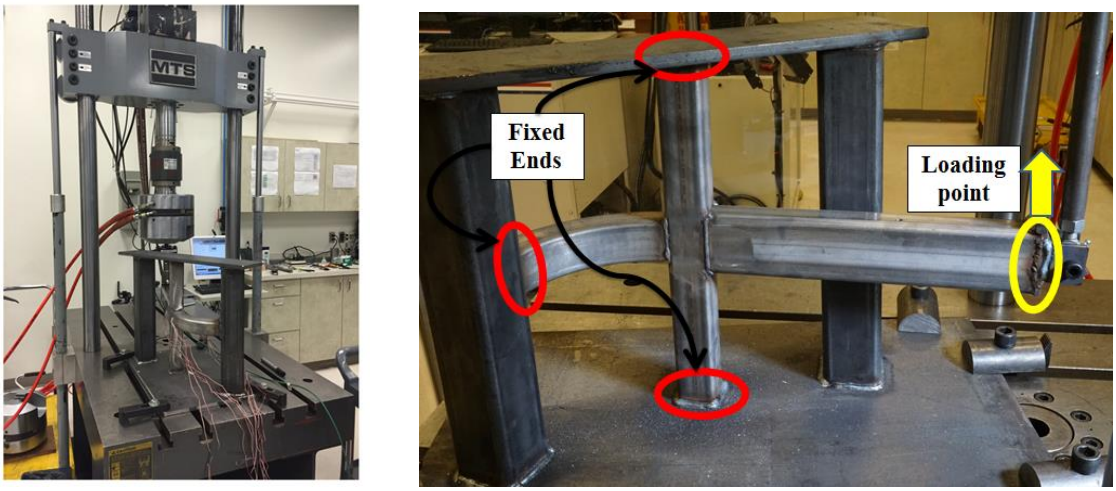

(a) (b)

Figure 3-20 Pillar bending test setup [61] *(permission acquired)*: (a) Loading machine and fixture; (b) Boundary conditions of the pillar before the test

The deformed pillar after the loading is applied is shown in Figure 3-21 (a). At the end of the test, the pillar joint fails due to the buckling and fracture at the welded areas, shown in Figure 3-21 (b) (c) (d). The force-displacement curve for the test is shown in Figure 3-22.

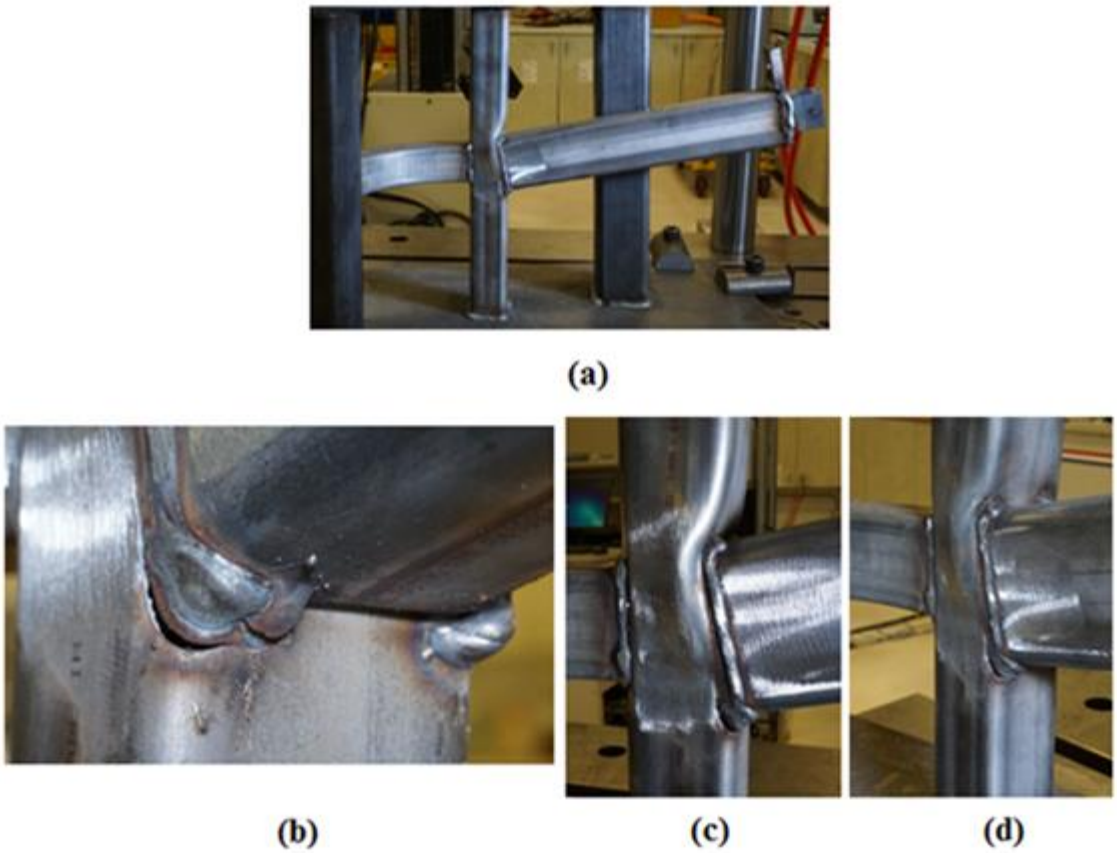

Figure 3-21 Quasi-static component test results of the pillar: (a) Deformed pillar; (b) Fracture at welding; (c) Close view of failure; (d) Another close view of the failure

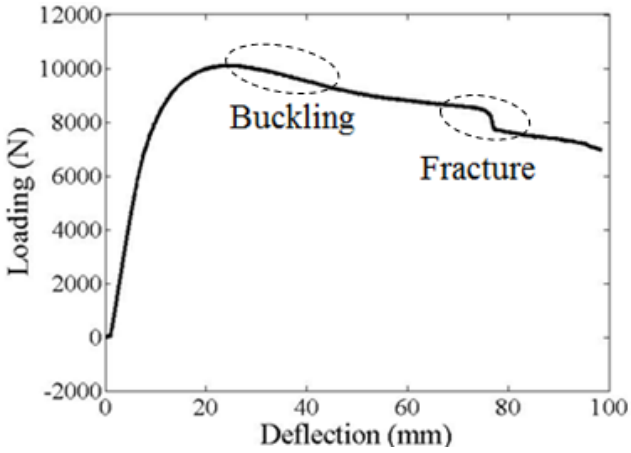

Figure 3-22 Force-displacement curve of the component test

3.4.2 Model Validation

The pillar connection model is directly extracted from the coach main frame model, shown in Figure 3-23, and the same boundary conditions as in the component test are applied. The deformed pillar at the end of the simulation is shown in Figure 3-24 (a), and the comparison of the deformation and force-displacement curves between the simulation and the test is presented in Figure 3-24 (b) (c). Table 3-7 shows data on the quantitative comparison of the force-displacement curves.

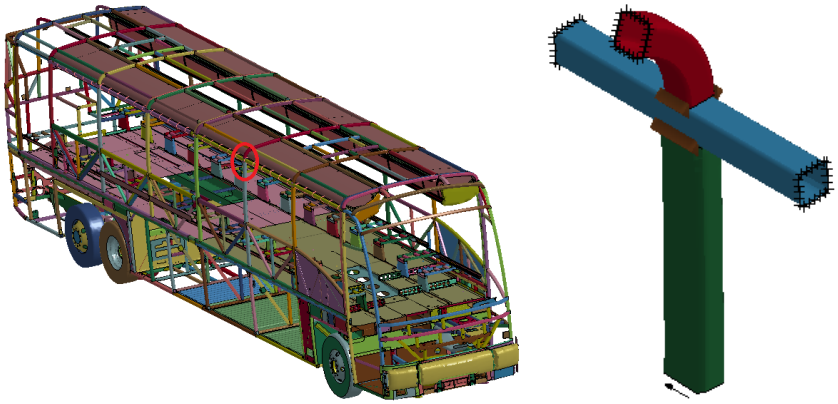

(a) (b)

Figure 3-23 Pillar from the coach model: (a) Location of the pillar in the coach; (b) Pillar model

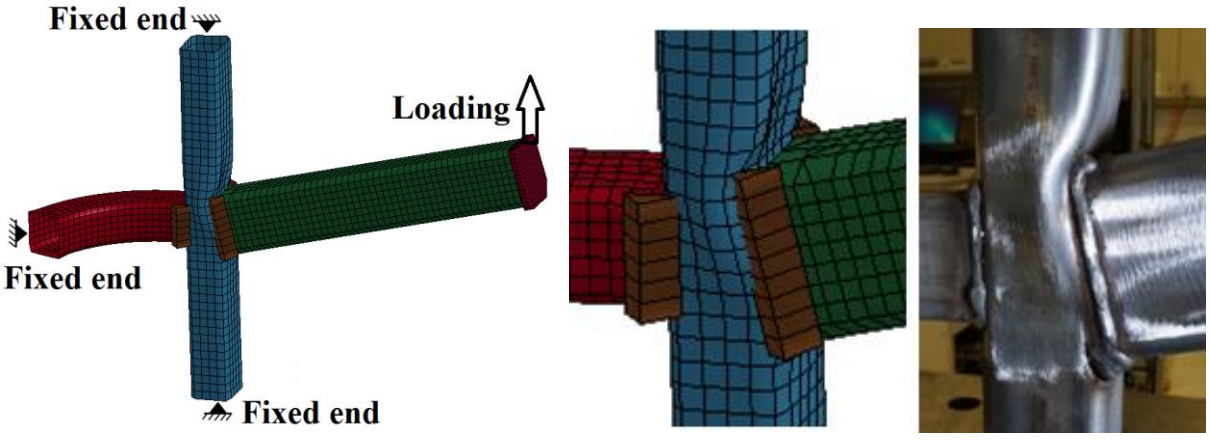

(a) (b)

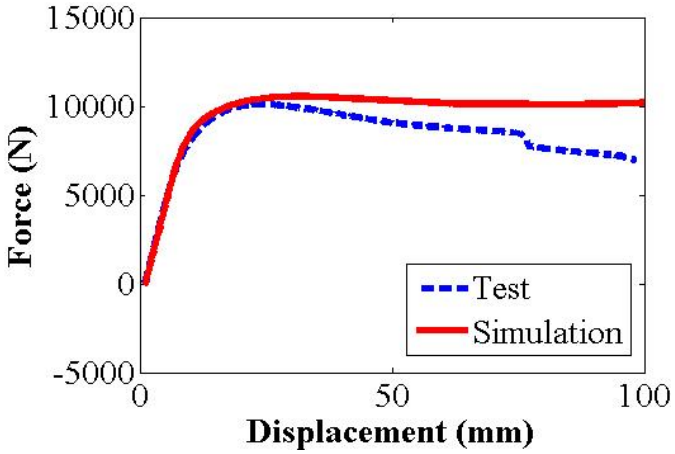

(c)

Figure 3-24 Simulation results of pillar submodel from the coach frame model: (a) Deformation of submodel; (b) Comparison of deformation between the simulation and test; (c) Comparison of f-d curves between the simulation and test

Table 3-7 Quantitative comparison of the force-displacement curves

Metrics	Experiment	Simulation	Difference %
Peak force at buckling, F_{max} (kN)	10.1	10.5	4.0
Stiffness in linear region, K (N/mm)	1122	1080	-3.7
Energy absorbed up at 97mm, E (J)	793	917	15.6

Figure 3-24 (c) shows that the model is capable of reproducing the linear and initial buckling behavior of the pillar. The difference between the slopes in the linear region and maximum values of the two curves are small enough to be both within 4%. There is a noticeable difference in the post-buckling behavior between the model and test, shown in Table 3-7. By refining the mesh and introducing the failure criteria, it is expected that the simulation curve can get closer to the test. As the global deformation of the coach primarily depends on the linear behavior of the

structural members, taking account of the limitations imposed by the scale of the full vehicle model, a good correlation of the connection strength for the pillar submodel has been obtained with the component test result. Consequently, the component submodeling and the simulation technique is considered to be sufficiently validated.

3.5. Free Falling Simulation and Results

The process of the free falling is firstly simulated for the coach rollover. The simulation is performed for a rigid body using the deformable-to-rigid switch technique. Shown in Figure 3-25, the coach starts falling when the wheel lift-off starts at the equilibrium position. The tilt table angle is measured as around 42.5 degrees at this moment.

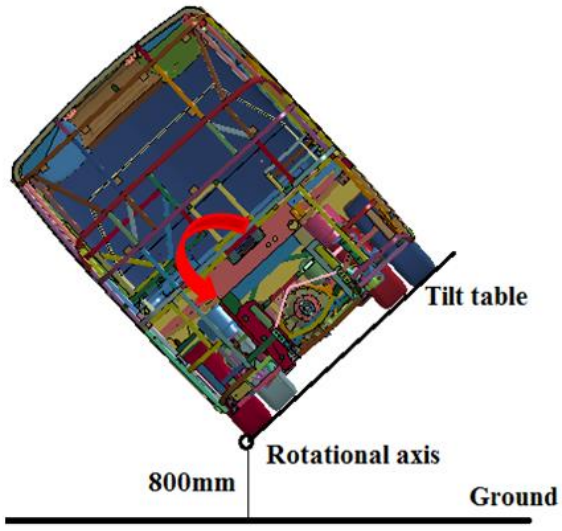

Figure 3-25 Initial state of free falling process of coach rollover

In order to accelerate the simulation, an initial angular velocity is set up for 0.35 rad/s for the free falling simulation, which is considered an acceptable value as the added kinetic energy is negligible when compared with that at the moment of impact.

In the free falling process, the potential energy of the coach is transferred into the kinetic energy. And the total mechanical energy is conserved in this process.

$$mg\Delta H = K_2 - K_1 \quad (5)$$

Where K_1, K_2 are the kinetic energy at the initial moment and impact moment.

Results of the free falling simulation will be used as the boundary condition for the impact simulation. The angular velocity at the moment of impact will be extracted.

3.5.1. Simulation Results

The free falling simulation shows that at the moment when the roof corner impacts with the ground, shown in Figure 3-26, the impact force angle is roughly around 13.6 degrees.

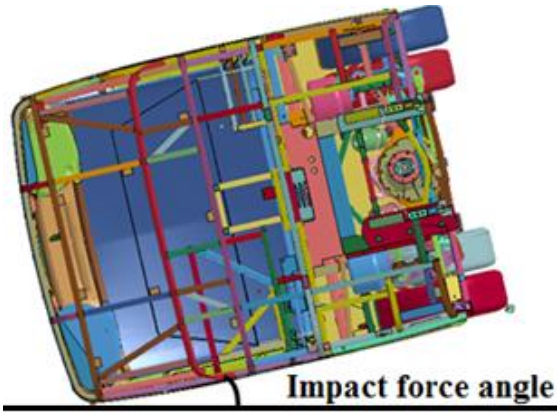

Figure 3-26 Impact force angle

The angular velocity time history in the global coordinate is shown in Figure 3-27. As all nodes in the model give the same angular velocity, the choice of nodes here is arbitrary.

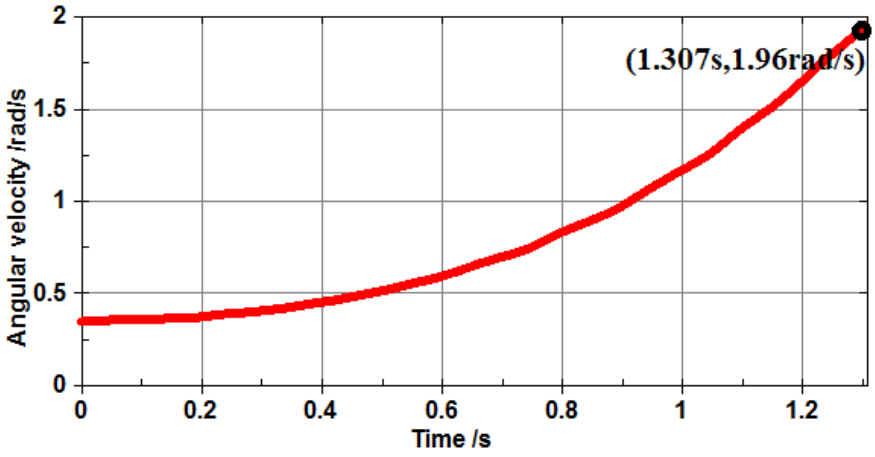

Figure 3-27 Angular velocity time history

At the moment of impact (around 1.30 s), the angular velocity is measured as 1.96 rad/s.

As the total mechanical energy is conserved, from Equation (5), we have:

$$mg\Delta H = \frac{1}{2}J_o(\omega_2^2 - \omega_1^2) \quad (6)$$

Where J_o is the moment of inertia, and the angular velocity at the initial moment and at impact moment are:

$\omega_1 = 0.35\frac{\text{rad}}{\text{s}}$, and $\omega_2 = 1.96\frac{\text{rad}}{\text{s}}$

Consequently, when $\omega_1 = 0$, ω_2 will be around 1.92 rad/s, which is used as the initial angular velocity for the impact simulation.

3.5.2. Energy Verification

The energy time history of the free falling simulation is shown in Figure 3-28. The potential energy, shown in the graph as the external work by gravity, is transformed into the kinetic energy. The total energy is conserved. The added initial kinetic energy due to the initial angular velocity is small enough for only around 3.2% of the kinetic energy at the impact moment.

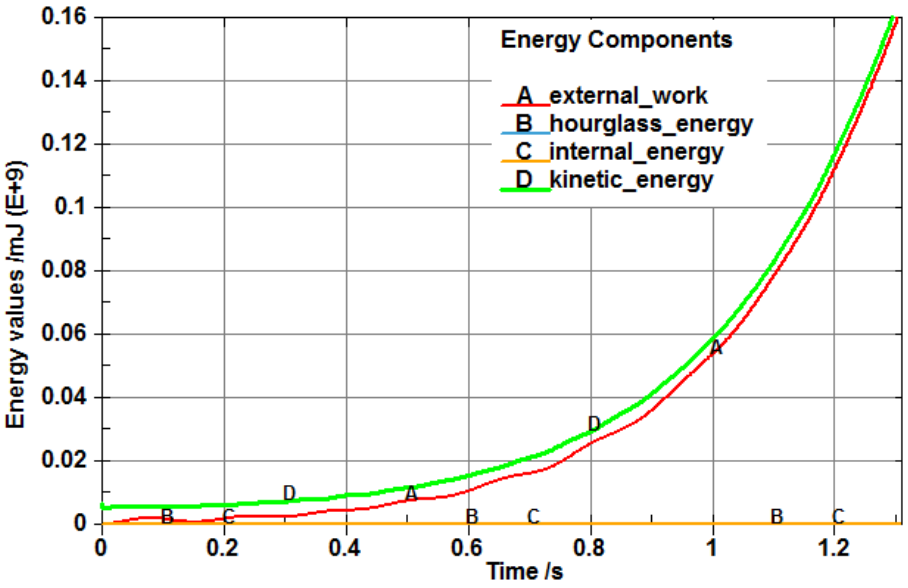

Figure 3-28 Energy time history for free falling simulation

3.6. Impact Simulation and Results

Following the free falling simulation, the impact simulation of the coach rollover starts at the moment of the coach rollover impact, with the applied initial rotational velocity extracted from the free falling process. The initial state of the coach in this simulation is shown in Figure 3-29.

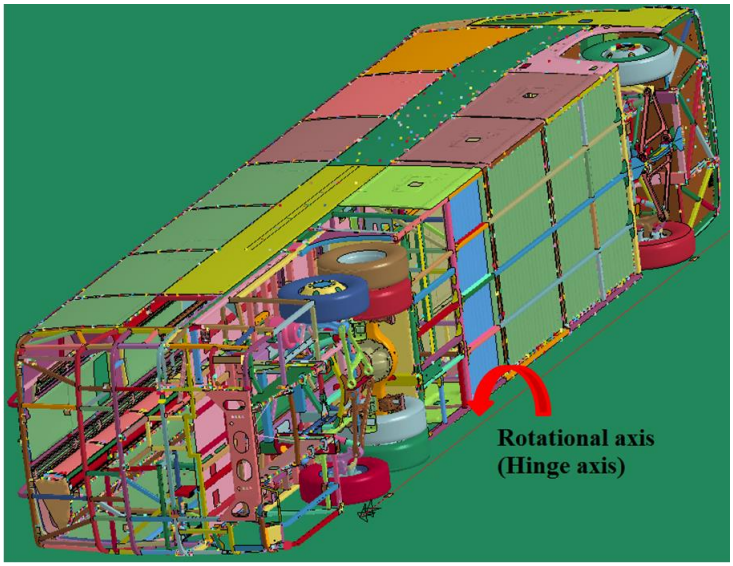

Figure 3-29 Initial state of the coach rollover impact simulation

To validate the model of the complete vehicle with available data, the rollover simulation is performed with no passenger mass, and the results are compared with the results of a physical test completed according to the ECE R66 procedure by NHTSA for a passenger vehicle with very similar structural features [62].

3.6.1. Simulation Results – Deformation

Snapshots of the deformation starting at the moment of impact are shown in Figure 3-30 in comparison with the deformation pattern from the physical test.

PHYSICAL TEST BY NHTSA [62]	SIMULATION
a) Roof corner touches the ground	
	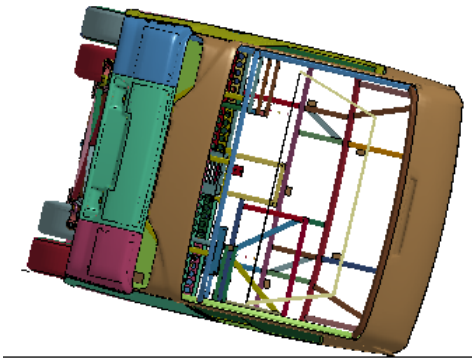
t=0s	t=0.0s
b) Waistrails impact with the ground for 1st time	
	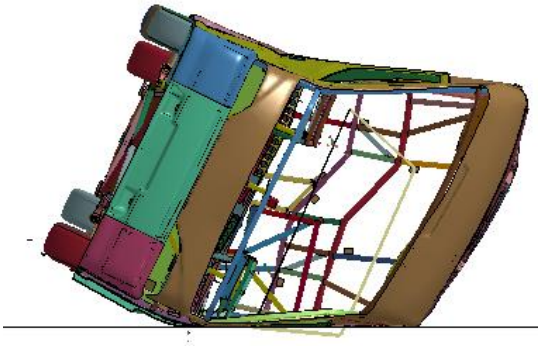
About t=0.16s	t=0.15s

c) Coach bounces up and slides	
	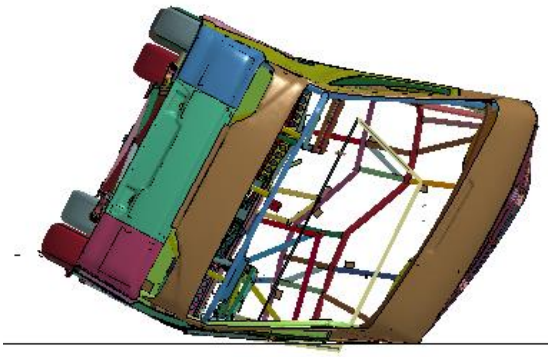
t=0.33s	t=0.375s
d) Waistrails impact with the ground for 2nd time	
	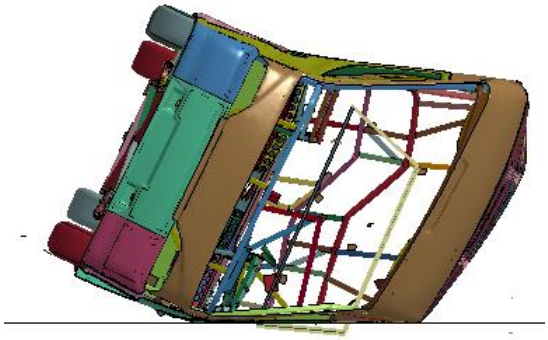
About t=0.55s	t=0.575s
e) Recovered, with residual deformation	
	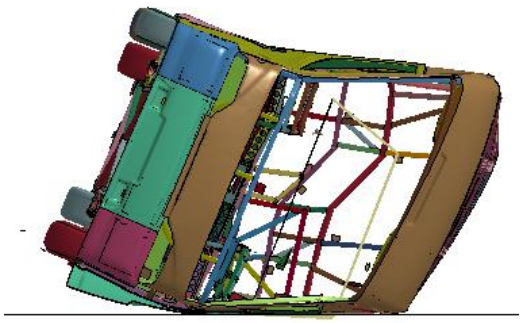
About t=0.78s	t=0.7s

Figure 3-30 Comparison of deformation pattern between NHTSA test and simulation

The comparison shows a good level of qualitative correlation for the deformation pattern in the rollover test. After the roof corner touches the ground at t=0.0s in Figure 3-30 (a), the superstructure starts to deform till around 0.15s when the waistrails impact the ground in Figure 3-30 (b). Then the vehicle bounces up and slides forward along the contact line between the ground and the roof corner in Figure 3-30 (c). It makes the 2nd impact on waistrails in Figure 3-30 (d). The coach rolls back to reach a balanced position in Figure 3-30 (e). The deformed superstructure also restores partially in Figure 3-30 (c) (d) (e).

During the rollover impact simulation, the surviving space is seen to be penetrated by the side frames at the impact side. The maximum penetration is shown in Figure 3-31, as found around 0.3s, during sliding process.

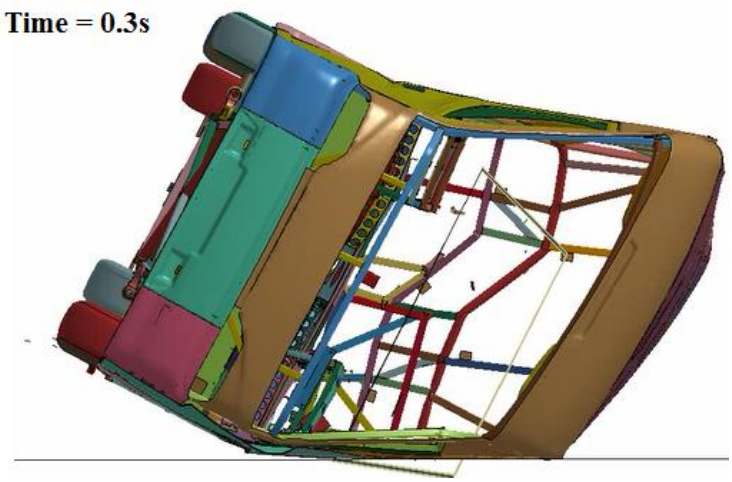

Figure 3-31 Max penetration of the surviving space

3.6.2. Simulation Results – Energy Curves

For verification purposes, the energy curves from the simulation are shown in Figure 3-32.

At the end of the simulation, the majority of the kinetic energy is consumed by the plastic deformation and the ground friction. Internal energy takes up around 86% of the total. Wall

energy due to the friction takes up 5% of the total. Artificial energy terms including hourglass energy and the contact energy only take up 6.6% of the total. Shown in Figure 3-32, the total energy is conserved. The final proportion of each energy term is shown in Table 3-8.

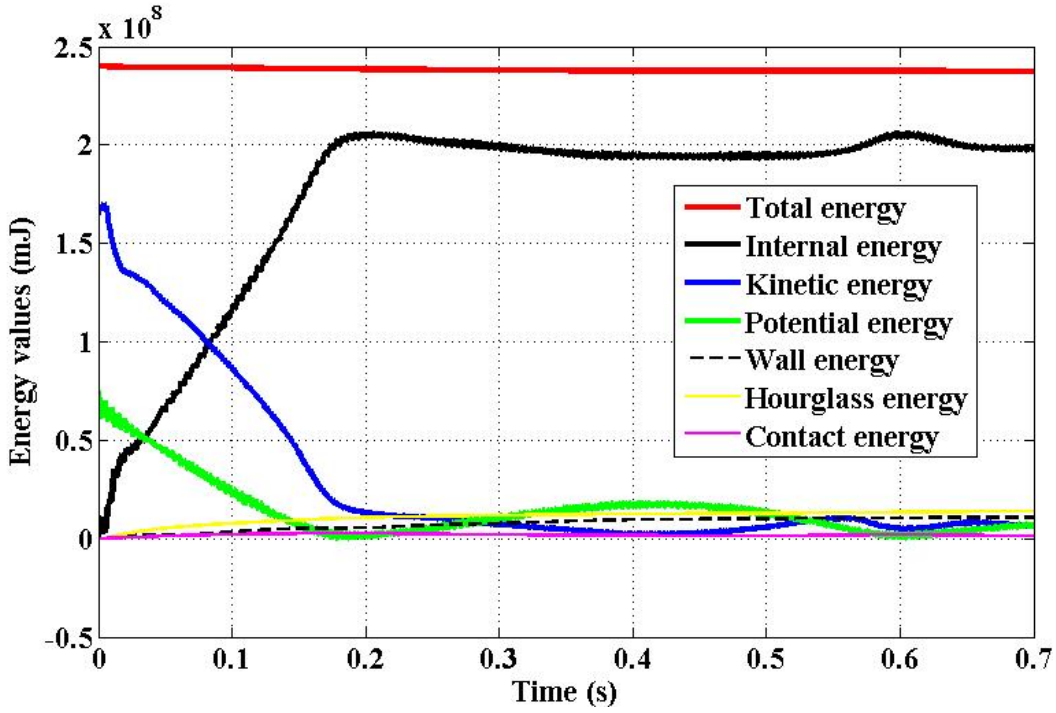

Figure 3-32 Energy time history for impact simulation

Table 3-8 Proportion of energy items for impact simulation

Energy item	Total energy	Internal energy	Kinetic energy	Potential energy	Wall energy	Contact energy	Hourglass energy
Percentage	100%	86%	2.4%	0%	5%	0.6%	6%

The time history of mass increase percentage is shown in Figure 3-33. It is shown the final mass increase is below 5.5%. It is considered acceptable though it is slightly larger than the recommended value of 5% [63]. The mass increase can be reduced by using a smaller time step

in the simulation. Due to the rapidly increased computation cost, it is unnecessary to strictly accomplish in the simulation.

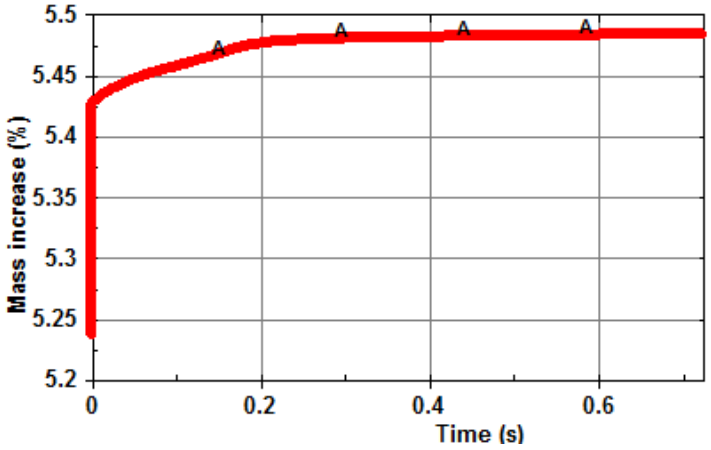

Figure 3-33 Mass increase percentage time history

The verification metrics for the energy results are summarized in Table 3-9.

Table 3-9 Verification metrics for energy results

Criterion	Max value (Absolute value)	Threshold [63]
Deviation of total energy	1.3%	10%
Contact energy /Total energy	0.6%	10%
Hourglass energy /Total energy	6%	10%
Mass increase	5.5%	5%

3.6.3. Simulation Results – Acceleration Curves

To provide the quantitative comparison between the results of test and simulation, the data from the accelerometers placed in the passenger compartment are used [62]. Shown in Figure 3-34, the acceleration is measured on three planes (A, B and C) on the vehicle from the frontal

end to the rear end. All curves are outputted in local coordinates, filtered by SAE J211 filter with Channel Frequency Class of 60Hz, in both the test and the simulation.

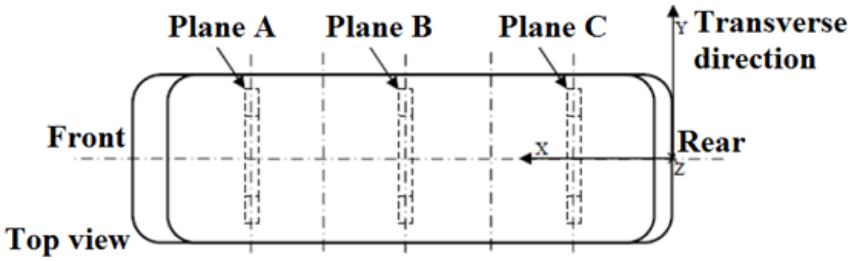

Figure 3-34 Planes in the vehicle to measure the acceleration data

The quantitative assessment of the curve similarity for the acceleration plots is carried out with curve comparison metrics recommended for crashworthiness applications in [63]. Table 3-10 outlines the utilized metrics, together with acceptance criteria. In the table, m_i and c_i denote the measured and computed quantities, respectively; i indicates an instance in time, and n indicates the total number of data samples. The metrics values are calculated using RSVVP software [64].

Table 3-10 Validation metrics

Metrics		Equation	Acceptance criteria, %
Sprague-Geers	Magnitude	$M_{SG} = \sqrt{\frac{\sum c_i^2}{\sum m_i^2}} - 1$	40
	Phase	$P_{SG} = \frac{1}{\pi} \cdot cos^{-1}\left(\frac{\sum c_i m_i}{\sqrt{\sum c_i^2 \sum m_i^2}}\right)$	40
	Comprehensive	$C_{SG} = \sqrt{M_{SG}^2 + P_{SG}^2}$	40
ANOVA	Average residual error	$\bar{e}^r = \frac{\sum(m_i - c_i)}{m_{max}} \cdot \frac{1}{n}$	5
	Standard deviation	$\sigma^r = \sqrt{\frac{1}{n}\sum(m_i - c_i - \bar{e}^r)^2}$	20

Shown in Figure 3-35, acceleration profiles in the transverse direction on 3 planes on the floor are compared. Table 3-11 gives the quantitative metrics comparison for the curves similarity.

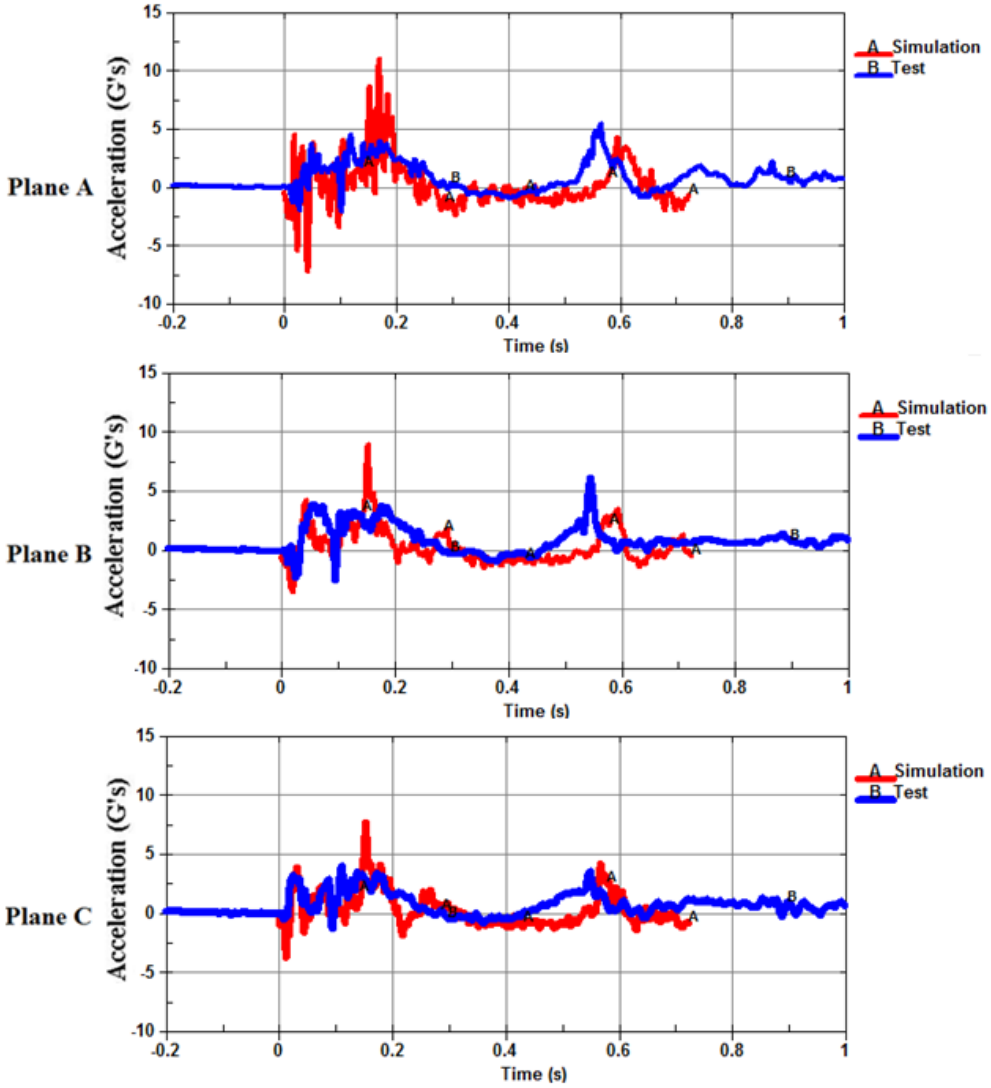

Figure 3-35 Comparison of accelerations on 3 planes on the floor (transverse direction)

Two peaks of the acceleration can be seen from the curves on all 3 planes, corresponding to two impacts on waistrails in Figure 3-30 (b) (d). It is shown that acceleration results are closely correlated in the simulation and the test, as reflected in the low value of the Sprague-Geers metrics. Though the differences exist with regard to the appearance time of the 2nd peak of the curve, the main features of rollover impact are still matched. The values of the ANOVA metrics

violate the recommended thresholds, indicating a presence of the systematic error between the results of the physical test and simulation, which cannot be attributed to a random experimental error. Although the source of the error cannot be easily identified for the model of this scale, it should be noted, that the model of the coaches used in the physical test and simulation are not the same. The differences include the changes in the suspension, frontal and rear parts of the frame. This physical dissimilarities constraint the degree to which the results of the simulation can match the results of the physical test. The rollover simulation of the coach model is therefore considered to be quantitatively validated.

Table 3-11 Curve comparison metrics for acceleration time histories

Metrics	Threshold	Model results		
		Plane A	Plane B	Plane C
S-G Magnitude	0.40	0.20	0.09	0.06
S-G Phase	0.40	0.35	0.34	0.33
S-G Comprehensive	0.40	0.40	0.36	0.33
ANOVA Av. Residual	0.05	0.13	0.11	0.15
ANOVA SD	0.20	0.36	0.27	0.35

3.7. Comparison Results between ECE R66 and Proposed NHTSA Regulation

In contrast to the ECE R66 regulation, the NHTSA's regulation proposal indicates that the full passenger load (each 68kg) must be ballasted for each designated seating to make the test representative of a fully loaded vehicle. In order to investigate the difference the new proposal makes on the rollover resistance of a given vehicle, a new simulation was run based on the

validated model described above. In the new simulation, the coach model is loaded with the full passenger mass for each designated seat.

As the passenger masses are coupled with the structural mass on the seats, compared with the coach model without passenger mass, the coach with full passenger mass has a higher position of the center of gravity. The pre-simulation of the free falling process shows that the full passenger loaded coach has a higher rotational velocity before the impact. For the purpose of the comparison, the mass, position of the center of gravity and the angular velocity at the moment of impact of the two models are shown in Table 3-12.

Table 3-12 Model data comparison

Model 1: without passenger mass; Model 2: with full passenger mass.			
	Model 1	Model 2	Difference
Model mass /kg	17,623.6	21,431.6	21.6%
Centre of gravity position /mm	(0,0,0) if the coordinate is fixed at the C.G.	(-76,1,113) in the same coordinate	/
Initial angular velocity / rad/s	1.92	1.99	3.65%

3.7.1. Deformation Comparison

The comparison of the deformation of two coach models is shown in Figure 3-36. With a raised center of gravity position, the vehicle experiences a larger inertial force. A worse penetration into the surviving space will be produced in the test condition of a full passenger load. At t=0.35 s when the coach starts to slide, the penetration in the model of zero passenger mass is measured to be around 154 mm, while the penetration in the case of full passenger mass is of 2.5 times, to be around 389 mm. The simulation results also show that the coach with the

full passenger mass produces a longer slide distance (S2>S1) during the rollover test, as the additional inertial force from the coupled passenger mass drives the vehicle roll forward.

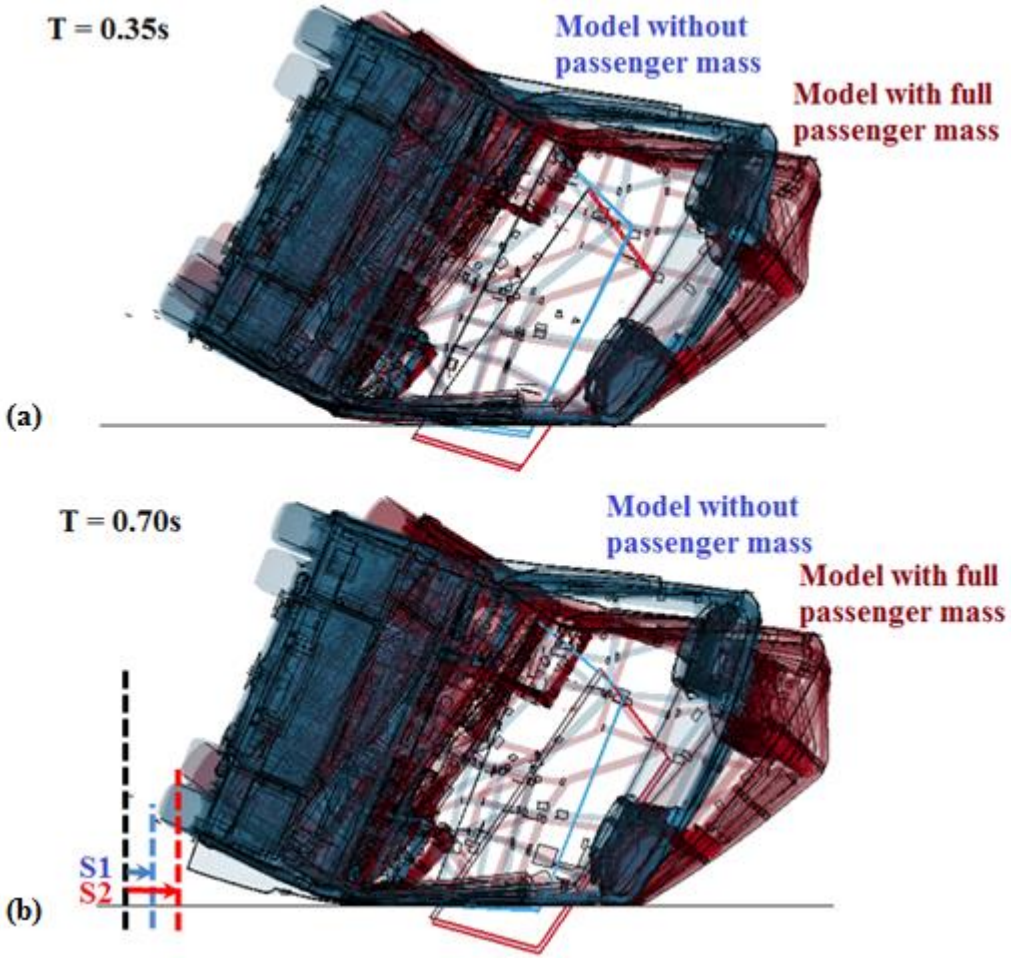

Figure 3-36 Deformation comparison: (a) t =0.35 s when the coach starts to slide; (b) t=0.70 s when the coach finishes sliding

3.7.2. Energy Absorption Comparison

3.7.2.1. Distribution of plastic strain

The extent of the deformation experienced by the coach frame depends on energy absorbing capabilities among structural members [9]. Due to the thin-walled beam construction of the coach structure under consideration, the main mechanism for energy absorption is the formation

of local plastic hinges at the beams' connections. The contours of the effective plastic strain on the deformed structures of the two coach models at the time 0.3s are shown in Figure 3-37 and Figure 3-38. The fringe limit is set to a rather small value 0.01. The locations of red color indicate the area associated with the relatively large plastic strains, which are considered as the plastic hinges.

The simulations show that most of the plastic deformations are localized in the connection joints of beams in the superstructure of the coach in both models, including pillar–roof joints, pillar-waistrail joints, joints of seats, seat-wall joints and welded joints of the rear frame, shown in Figure 3-37. The larger area of plastic hinges can be seen in Figure 3-38 with full passenger mass at joints of seats-wall and pillar-waistrail joints.

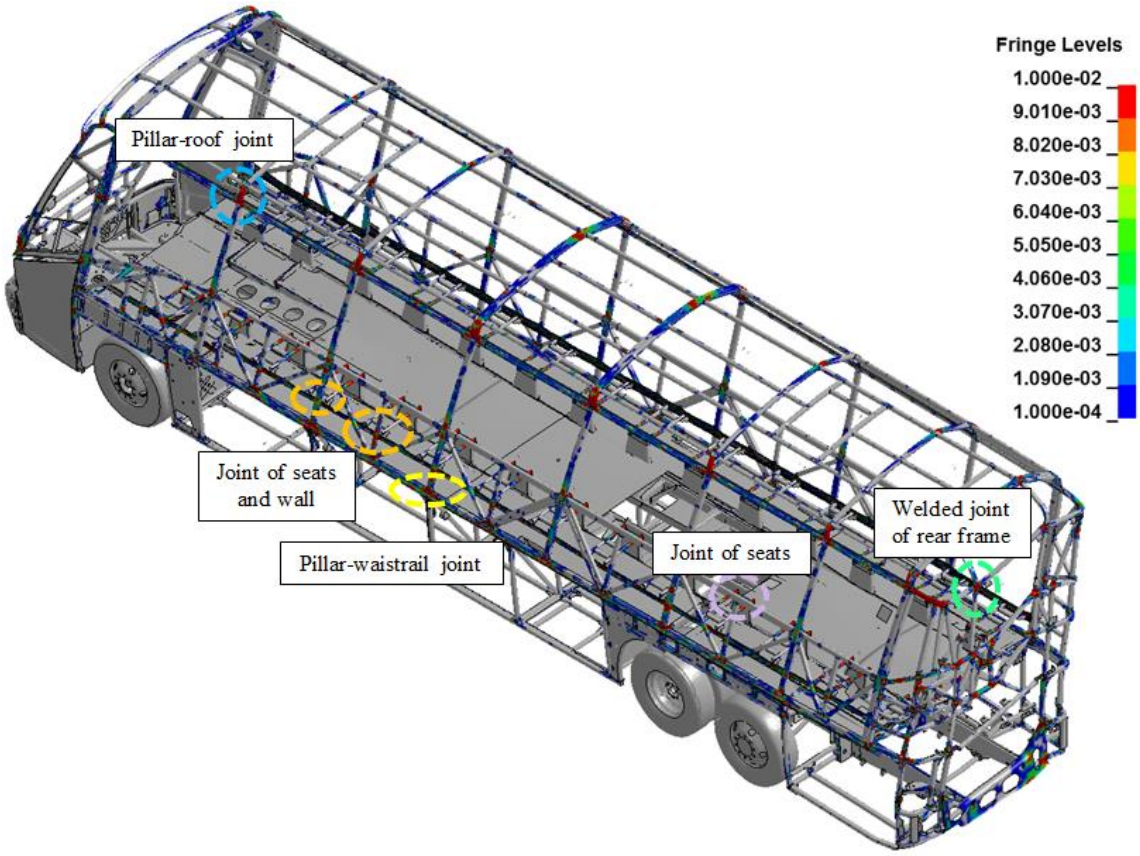

Figure 3-37 Contour of effective plastic strains on the deformed coach (zero passenger mass)

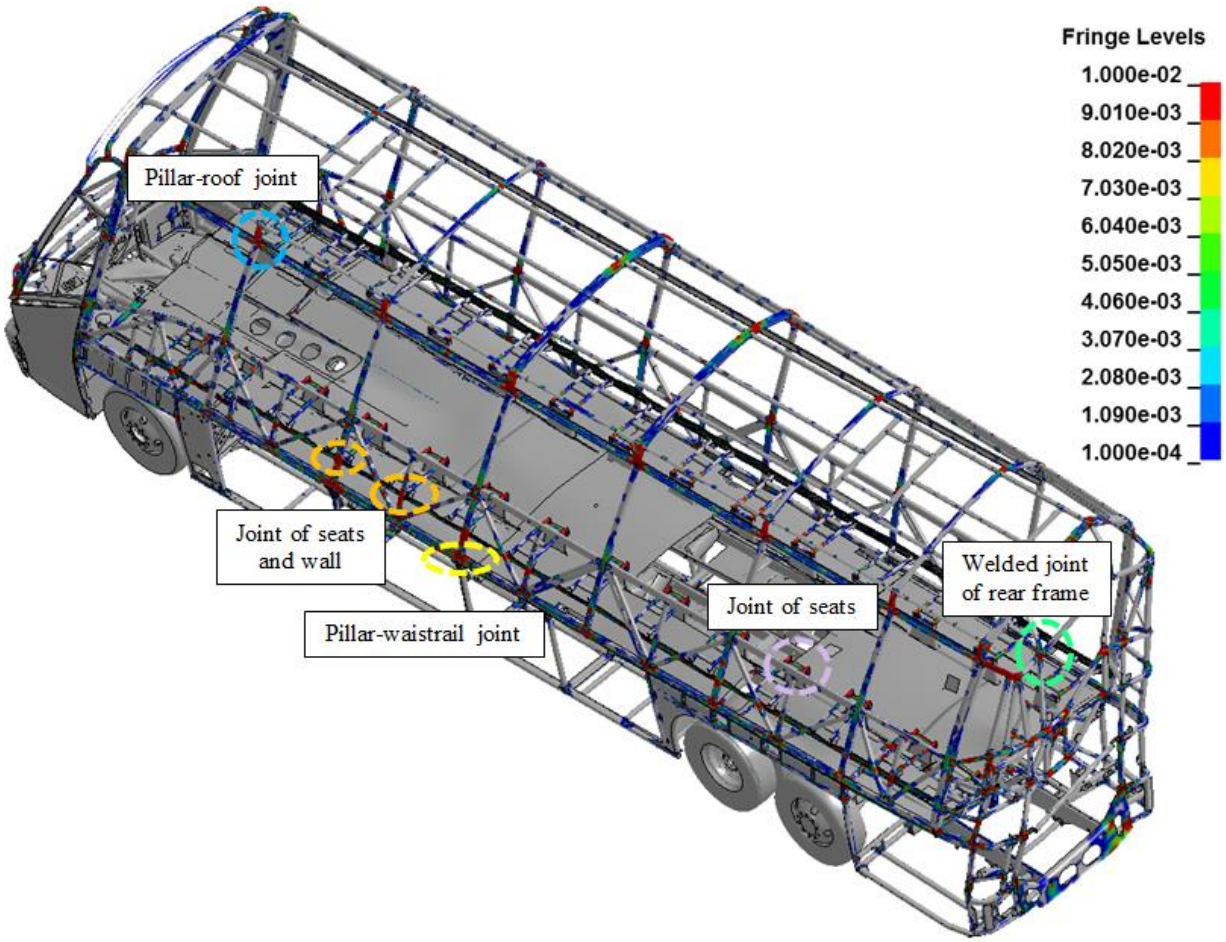

Figure 3-38 Contour of effective plastic strains on the deformed coach (full passenger mass)

3.7.2.2. Distribution of energy absorption

The energy absorption is not evenly distributed among the vehicle frame members, and they also vary during the process of rollover impact. To provide the better understanding of the energy absorbing capabilities of different frame members, a frame model is used in the analysis. Components which are considered much less effective in absorbing energy in rollover, e.g. the glass and skins, parcel rack assembly, are removed from the model. The coach frame is divided into 9 groups, shown in Figure 3-39.

(1) Pillar loops, (2) Rear frame, (3) Seats, (4) Lower frame, (5) Waistrails, (6) Roof longitudinal beams, (7) Wall beams, (8) Floor, and (9) Frontal beams.

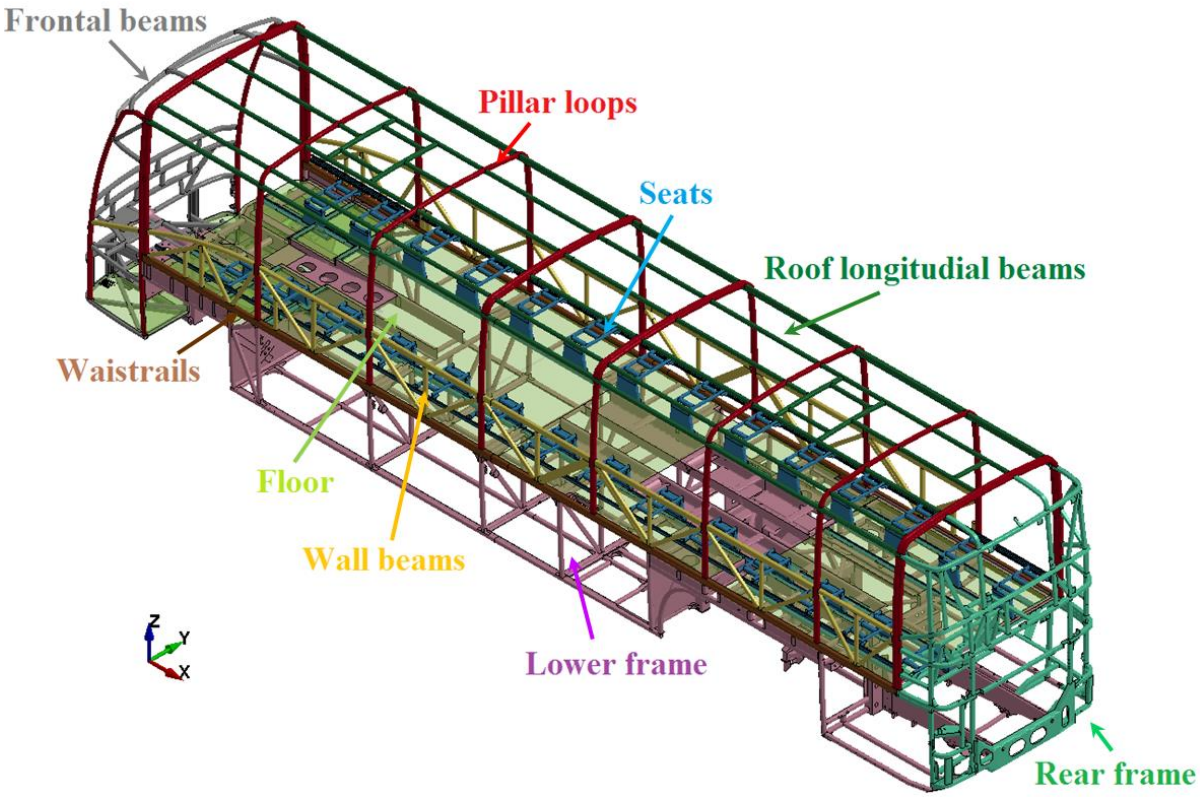

Figure 3-39 Groups of coach frame members

Time histories of the absorbed energy among structural groups during the impact process are shown in Figure 3-40.

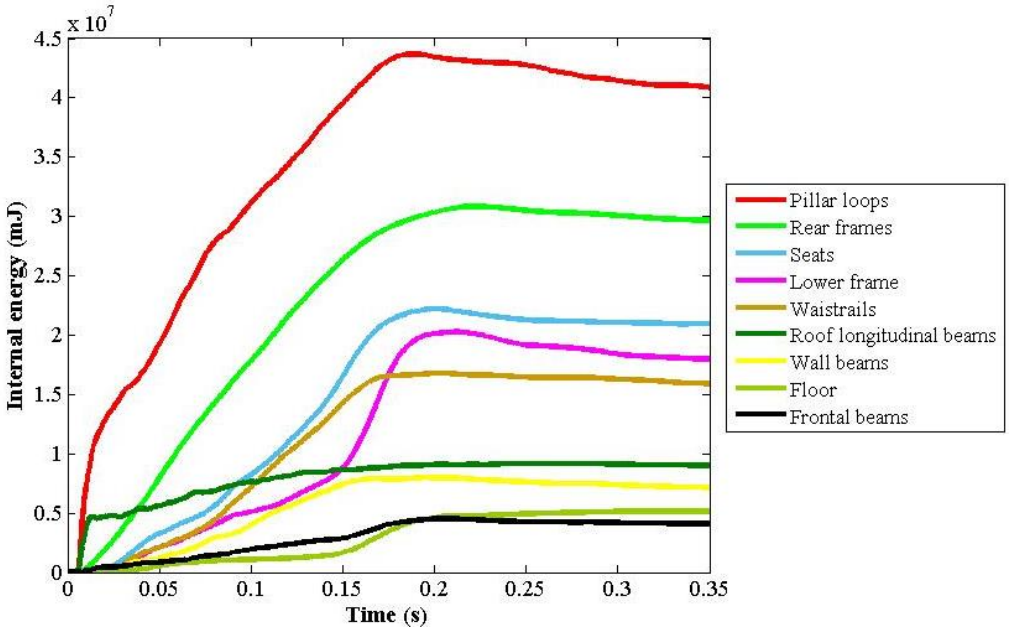

Figure 3-40 Time histories of absorbed energy (model with zero passenger mass)

The internal energy curves in Figure 3-40 show that the pillar loops and roof longitudinal beams absorb the energy firstly from 0 to around 20 ms. This is because of the fact that the pillar-roof joints are the first of all the structural components to impact with the ground. After the first impact moment, the coach frame members deform together. For the pillar loops, around 6.4% of the total absorbed energy is restored after reaching the peak value at around 180 ms, as the elastic deformation recovers after the initial impact.

The energy absorption for all members finishes at around 350ms when the coach starts to bounce and slide, as shown in Figure 3-30 (c).

To clearly quantify the energy absorption portion for each structural group during the impact process, the ratio of the absorbed energy to the total absorbed energy is calculated for each structural group, shown in Figure 3-41.

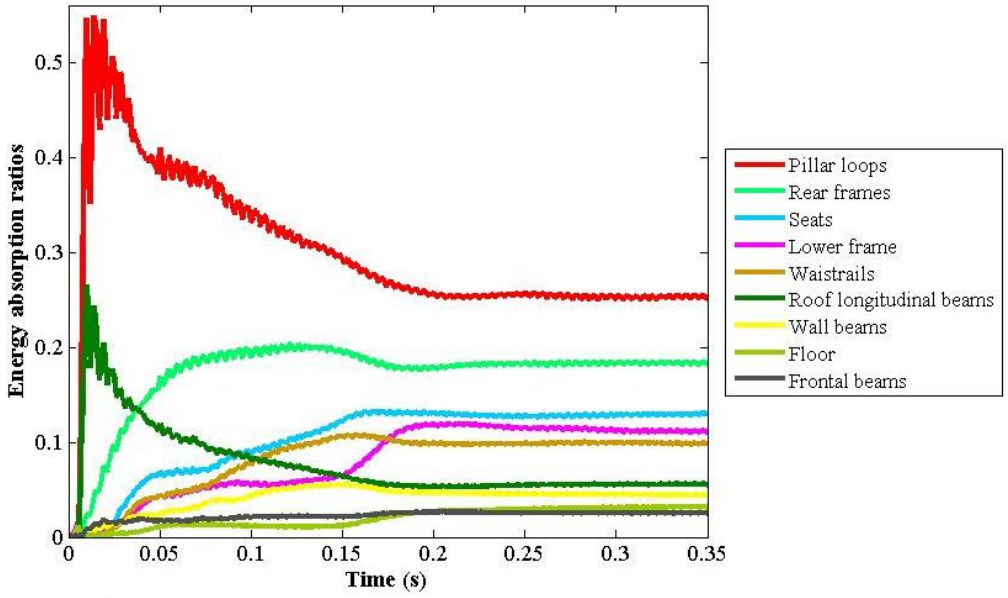

Figure 3-41 Time histories of energy absorption ratios (model with zero passenger mass)

At the first impact moment (20 ms), the pillar loops contribute to around 50% of total absorbed energy, and roof longitudinal beams absorb around 20%. After the first impact moment, though pillar loops and roof longitudinal beams continue deforming, their ratios decrease rapidly, since other structural groups start to deform.

At the end of the energy absorption (350 ms), shown in Figure 3-41, pillar loops still rank first in the energy absorption ratio, and rear frames, seats, lower frames, waistrails, and the roof longitudinal beams following. These groups together take up around 82% in the energy absorption at the end of the impact. Other structural members such as wall beams, the floor, and frontal beams have less prominent energy absorption capabilities.

To better compare the differences of energy absorption between the model with zero passenger mass and that with full passenger mass, rankings of energy absorption among the structural groups at the beginning (t = 20 ms) and at the end of the impact (t = 800 ms) are illustrated in

Figure 3-42 (a) and (b) respectively. In the figure, structural groups are arranged in the decreasing order of energy absorption ratio at the end of impact.

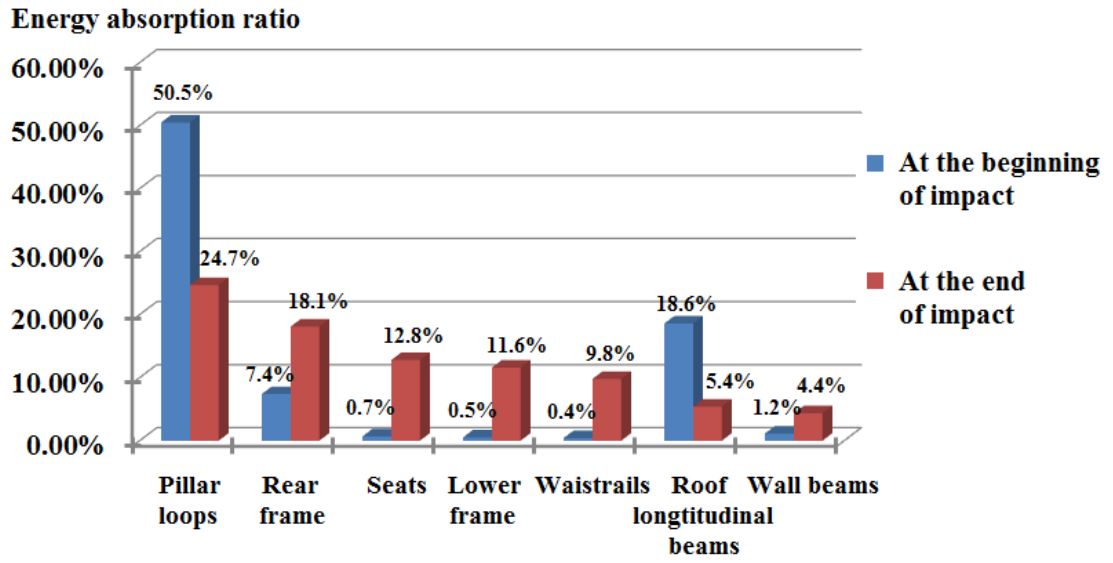

(a)

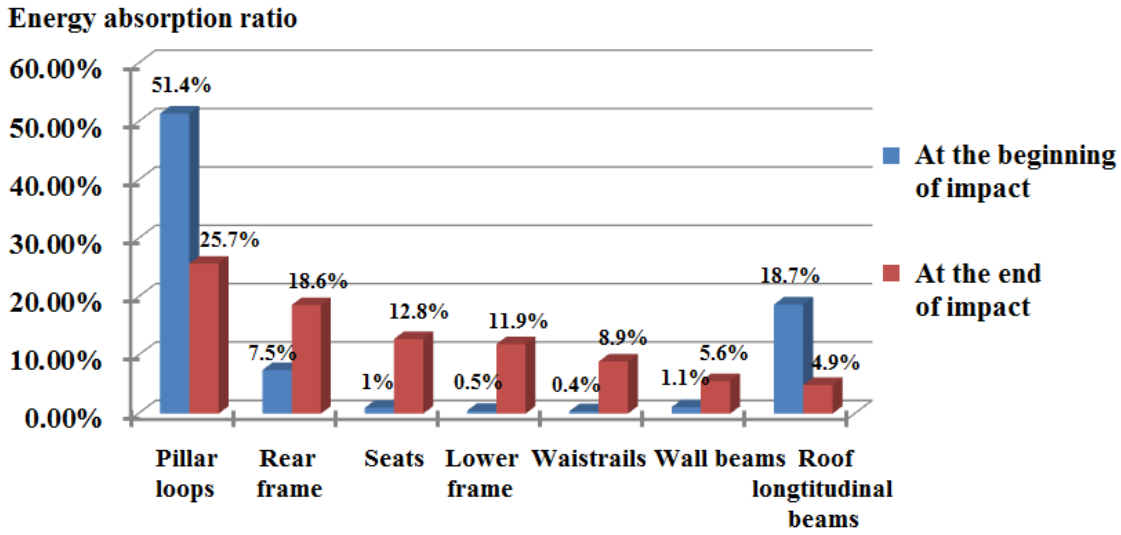

(b)

Figure 3-42 Ranking of energy absorption ratios among structural groups: (a) Model with zero passenger mass; (b) Model with full passenger mass

For the model with full passenger mass, the coach structure needs to absorb much more energy during the rollover, as the simulations show that the initial kinetic energy is around 1.4 times that in the model with zero passenger mass. However, comparing the results in two test conditions in Figure 3-42 (a) and (b), the distribution of energy absorption at the beginning of impact are very alike. The main reason for such similarity is the short duration of the initial impact on the roof corner and the localization of plastic hinges.

The comparison at the end of impact shows that the first five groups have slight changes, but the group of wall beams rises by one spot in the ranking with the energy absorption ratio increasing by 27%. This is because of the effect of the coupled passenger mass on the seats. The inertial force exerted on the seats is transferred through joints between seats and wall, which will lead to a large bending force, in this case experienced by wall beams in the coach superstructure.

From the data shown in Figure 3-42 (a) (b), it can be seen that the pillar loops always absorb the most of energy during the impact process. Thus the pillar-roof joints and pillar-waistrails joints play a significant role for the coach superstructure in the energy absorption of the rollover event. The contribution of welded joints between rear frame beams is also important, as the rear frame group ranks the second in energy absorption at the end of impact.

For the coach with zero passenger mass, joints of seats and joints between seats and wall also contribute to the energy absorption, to a certain amount. In the case of full passenger mass, the contributions of joints between seats and wall will increase largely, and special attention is required to maintain the rollover resistance for the coach superstructure.

3.8. Conclusion

This chapter presents the results of evaluating the rollover structural performance of a typical motorcoach using a full scale coach model. The model is validated at the component level by the roof-pillar joint test and at a system level by complete vehicle rollover test, and a good level of correlation is found. The performance of the coach structure is then evaluated for two loading conditions: with no passenger mass, according to the current ECE R66 regulation, and with full passenger mass of each 68 kg in compliance with a newly proposed NHTSA regulation. Taking advantage of the detailed computational model, energy absorption distribution among structural members is presented. Requirements of the design for a sufficient rollover resistance in accordance with the regulatory changes are studied using the coach frame model. The following conclusions are therefore made.

1) The methodology of the numerical simulation provides an effective tool in assisting vehicle designers to predict and assess the vehicle structural performance for the compliance to the new regulations in the crash event.

2) Simulation results show that a worse penetration into the surviving space is produced for the coach under the newly proposed NHTSA regulation, which is estimated 2.5 times of the penetration distance under ECE R66.

3) Localized plastic deformation can be found at beam joints of the coach in the rollover test, including pillar-roof joints, pillar-waistrail joints, welded joints in rear frame, joints of seats and seats-wall joints. As can be expected, the more severe loading condition of the proposed regulation results in the increased size of the developed plastic joints, especially in the regions of seats-wall joints and pillar-waistrail joints.

4) Simulations under ECE R66 and proposed NHTSA regulation show that pillar loops and roof longitudinal beams absorb the most of energy (70%) at the first impact moment. The absorbed energy of the pillar loops decreases by 6.4% as the elastic deformation recovers. At the end of rollover, pillar loops still rank the 1st in energy absorption ratio, while the rear frame, seats, lower frame, waistrails and roof longitudinal beams also absorb a significant amount of energy. Results exhibit that NHTSA proposed regulation poses higher requirement on the rollover resistance of the wall beams and seats-wall joints than the ECE R66, as their energy absorption ratio at the end of impact increases by 27% due to the coupled passenger mass.

5) The results can be used as the basis for adapting the existing design criteria under ECE R66 test condition to the NHTSA proposed regulation, which poses more stringent requirement on rollover resistance of the vehicle frame. Vehicle manufacturers could benefit from these results through the consideration of reinforcing the key joints in the design stage to achieve a sufficient rollover resistance.

4. LOAD TRANSFER ANALYSIS USING INDEX U* OF VEHICLE STRUCTURE SUBJECTED TO ELASTIC-PLASTIC DEFORMATION

4.1. Review of Theory Preliminaries

As the load transfer index, U* is a non-dimensional value calculated from the strain energy U [34]. It quantifies the strength of connectivity of each point in the structure with the loading point. The calculation of U* is shown as the following [34] [35] [36].

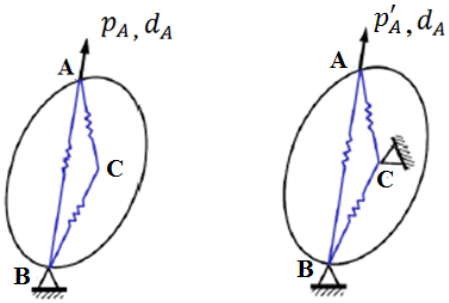

(a) (b)

Figure 4-1 Illustration of conventional U* calculation: (a) Three-spring model; (b) Three-spring model with fixed arbitrary point

Shown in Figure 4-1 (a), a linear elastic body is viewed as a spring system which includes the loading point A, constrained point B and an arbitrary point C. Point A is loaded with a force $\mathbf{p_A}$ and the corresponding displacement is $\mathbf{d_A}$. The total strain energy U is calculated as:

$$U = \frac{1}{2}\mathbf{p_A}\mathbf{d_A} \tag{7}$$

Shown in Figure 4-1 (b), in the load case when a selected arbitrary point C is fixed while the same forced displacement $\mathbf{d_A}$ is imposed on the loading point A, total strain energy U′ is calculated as:

$$U' = \frac{1}{2}\mathbf{p'_A}\mathbf{d_A} \tag{8}$$

where $\mathbf{p'_A}$ is the corresponding force on point A.

The load transfer index U* is defined as:

$$U^* = 1 - \frac{U}{U'} \tag{9}$$

At the constrained point B, U′ equals to U, and the index U* is 0. At the loading point A, U′ tends to infinity, and the index U* is 1. The rest points in the body have the U* between 0 and 1. Equation (9) shows that U* represents the strength of connectivity for any point C and loading point A.

By calculating the U* for each point, the load path can be found as the ridgeline of the U* contour, as this line connects the most strongly coupled points in the structure sequentially from the loading point to the constrained point [35]. Shown in Figure 4-2 as an example, calculated by Equation (9) using the numerical method, the load paths are visualized in a discretized structure of a plate with a central hole under tensile loading. This example also illustrates that the index U* allows the load transfer analysis of structures with geometry irregularities, for example holes.

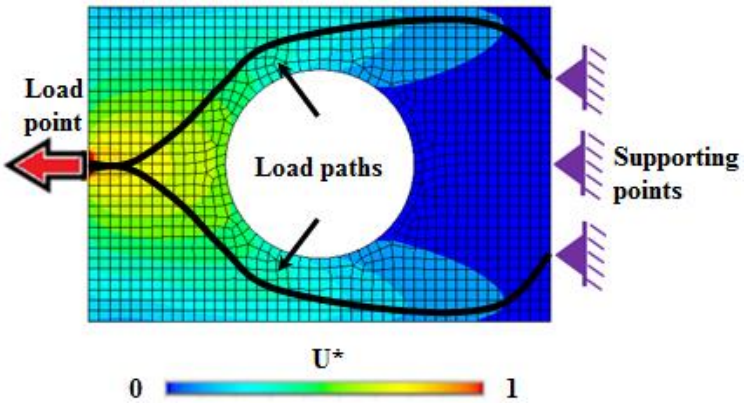

Figure 4-2 Illustration of U* contour and load paths of a plate under tensile loading

The physical meaning of the U* index is presented in [35] [36] [40] [43] [45]. In the model of Figure 4-1, the stiffness constant of each spring within the three-spring model represents the internal stiffness of the structure (i.e., $\mathbf{K_{AB}}$, $\mathbf{K_{AC}}$, and $\mathbf{K_{BC}}$). The relationship between the loading and the displacement can be expressed as:

$$\begin{Bmatrix} \mathbf{p_A} \\ \mathbf{p_B} \\ \mathbf{p_C} \end{Bmatrix} = \begin{bmatrix} \mathbf{K_{AA}} & \mathbf{K_{AB}} & \mathbf{K_{AC}} \\ \mathbf{K_{BA}} & \mathbf{K_{BB}} & \mathbf{K_{BC}} \\ \mathbf{K_{CA}} & \mathbf{K_{CB}} & \mathbf{K_{CC}} \end{bmatrix} \begin{Bmatrix} \mathbf{d_A} \\ \mathbf{d_B} \\ \mathbf{d_C} \end{Bmatrix} \tag{10}$$

where $\mathbf{p_{i(i=A,B,C)}}$ is the force vector at point A,B, and C; $\mathbf{d_{i(i=A,B,C)}}$ is the displacement vector at point A,B, and C; $\mathbf{K_{ij\ (i=A,B,C;j=A,B,C)}}$ represents the internal stiffness tensor between points A,B, and C.

Shown in Figure 4-1(a), since point B is fixed ($\mathbf{d_B} = 0$), then $\mathbf{p_A}$ can be written as:

$$\mathbf{p_A} = \mathbf{K_{AA}}\mathbf{d_A} + \mathbf{K_{AC}}\mathbf{d_C} \tag{11}$$

Shown in Figure 4-1(b), for the case of fixed point C ($\mathbf{d_B} = \mathbf{d_C} = 0$), then $\mathbf{p_A}'$ can be written as:

$$\mathbf{p_A}' = \mathbf{K_{AA}}\mathbf{d_A} \tag{12}$$

Using Equation (7)(8)(11)(12), Equation (9) can be written as:

$$U^* = 1 - \frac{U}{U'} = \left(1 - \frac{2U}{(\mathbf{K_{AC}}\mathbf{d_C})\mathbf{d_A}}\right)^{-1} \quad (13)$$

Equation (13) shows that the U* index is only related to $\mathbf{K_{AC}}$ instead of $\mathbf{K_{AB}}, \mathbf{K_{BC}}$. U* is effective to express the load path as it is related to the internal stiffness between the loading point A and the arbitrary point C. The load path is obtained by connecting the loading point with supporting points along the line which has the smallest gradient of the U* variation, which is regarded as the stiffest path in the structure [35] [43]. The largest portion of loading is transferred on this load path.

The load transfer index here can be noted as U_1^*. Similarly, by tracing the load transfer index of the reaction force, the index to be named as U_2^* can be obtained. The index U_{sum}^* is defined as:

$$U_{sum}^* = U_1^* + U_2^* \quad (14)$$

Shown in Figure 4-3, the contour of U_{sum}^* is plotted on the same plate with Figure 4-2. The index U_{sum}^* was introduced in the design of weight-efficient structure [38] [39]. As it represents the coupling stiffness of each point with both the loading and supporting points [41], the portion associated with a higher U_{sum}^* indicates its more efficient load transfer. The index U_{sum}^*enables the evaluation of the load dispersion state, and statistical methods such as histograms can be used to evaluate the load transfer via the index U_{sum}^*.

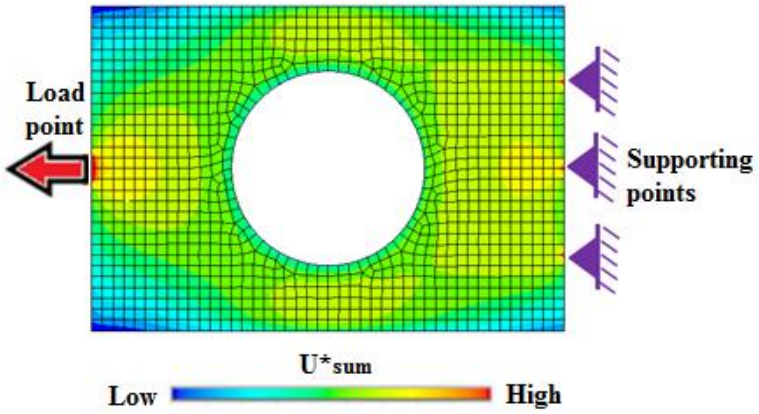

Figure 4-3 Illustration of U^*_{sum}contour of a plate under tensile loading

4.2. Numerical Procedure

As the U* matrix formula of internal stiffness is developed using a linear elastic body, it is not applicable beyond the elastic domain. Nevertheless, the original concept of U* introduced via the Equation (9) does not have limitation to its application to the problems involving the material nonlinearity, considering its physical meaning of expressing the strength of connectivity in a structure.

In the nonlinear U* analysis, the material is modeled as the elastic-plastic piecewise linear function with isotropic hardening. When the load exceeds the material elastic limit, the displacement-force relationship can be modeled by a multilinear curve, where the total strain energy U equals to the area under the curve.

To perform the nonlinear U* analysis, an in-house program was developed using ANSYS APDL [65]. The process is shown in Figure 4-4. Under the elastic-plastic deformation, the strain energy U in the original model is firstly calculated (Figure 4-1(a)). Each node in the model is fixed sequentially, and the strain energy U′ in the modified system (Figure 4-1(b)) is calculated

for each node. U* is calculated using the numerical procedure shown in Figure 4-4 which implements the Equation (9). Then the obtained contour of U* is plotted.

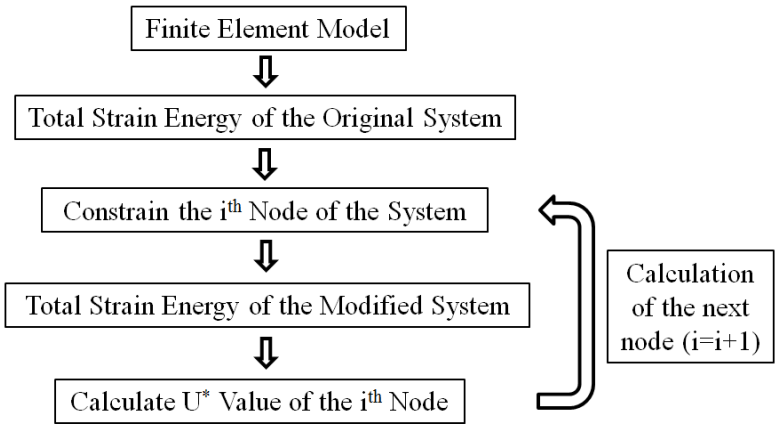

Figure 4-4 U* calculation flowchart

The demonstration of the application of the nonlinear U* approach is shown in the examples as following.

4.3. Load Path Calculation for Case of Non-elastic Deformation

4.3.1. First Example

A finite element model of a plate under tensile loading is used to study the influence of plastic deformation on the load transfer. The plate comprises of two types of material models. Shown in Figure 4-5, the material of the highlighted strip in the middle has the bilinear isotropic hardening plasticity, while the rest are linear elastic. All elements are 4-node SHELL181. The material models have the elastic modulus of 71GPa and Poisson's ratio 0.33.

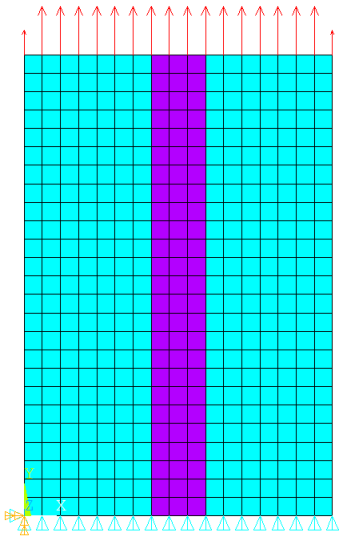

Figure 4-5 Plate model under tensile loading

Two load cases are considered for the model. Under the first loading, the plate experiences only the elastic deformation. In the second case of a larger loading, the plastic strain appears in the middle strip, as shown in Figure 4-6. The index U* is calculated respectively for the two cases and load paths are obtained accordingly.

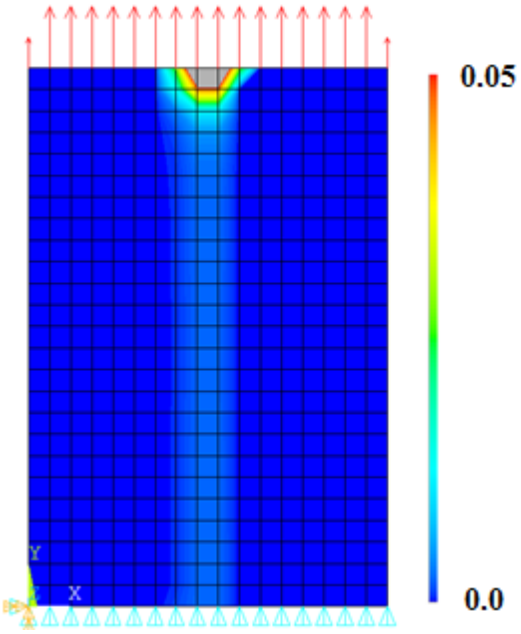

Figure 4-6 Contour of plastic strain of the load case of elastic-plastic deformation

Presented in Figure 4-7(a), the contour of U* is obtained for the load case of elastic deformation. The load path is seen to go from the loading end to the fixed end and to distribute evenly across the width. The diagram of reaction force values of fixed nodes is plotted, and it also shows that the load transfer is equal along the nodes of the fixed boundary in this load case.

The U* contour and load paths for the load case of elastic-plastic deformation are presented in Figure 4-7(b). Load paths mainly go through the linear elastic region in the plate. The diagram of reaction force values of fixed nodes confirms that nodes belonging to the plastic strip transfer much less load than others.

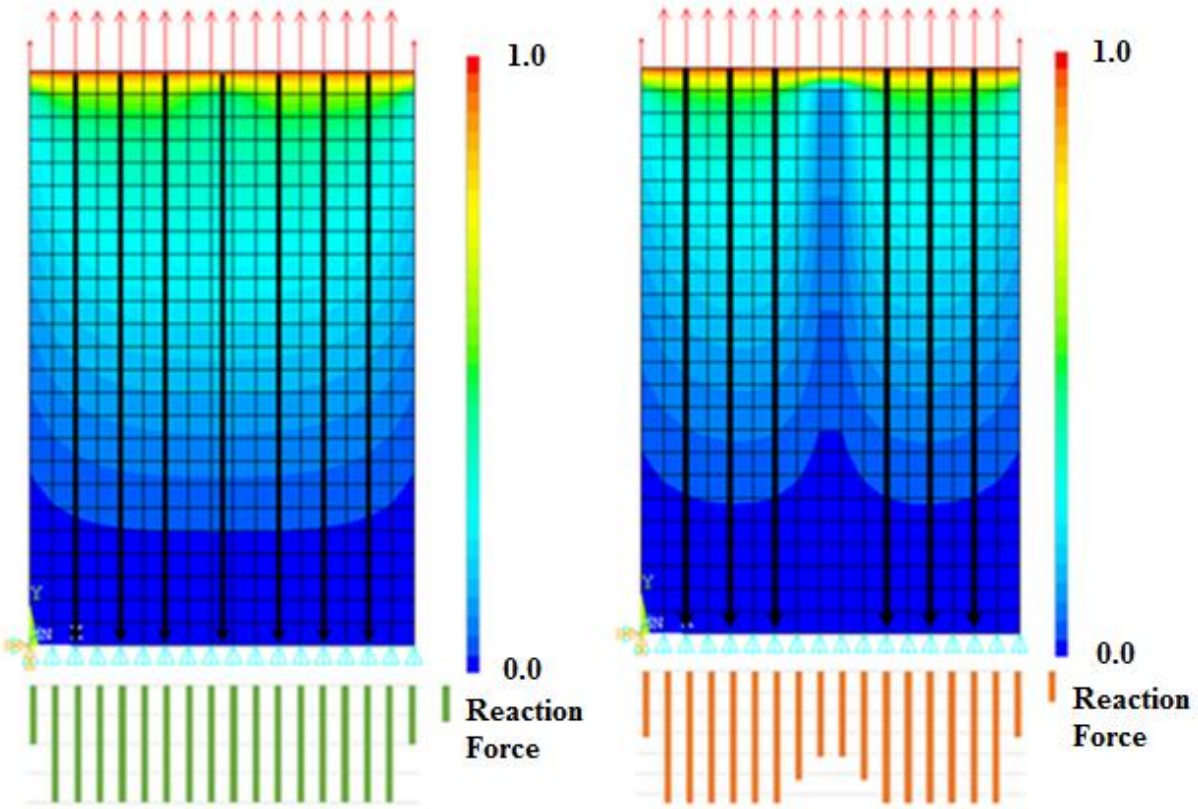

(a) (b)

Figure 4-7 U* contour plots and load paths of the plate with a plastic strip: (a) load case of elastic deformation; (b) load case of elastic-plastic deformation.

4.3.2. Second Example

A finite element model of the plate with a circular hole in the center shown in Figure 4-8 is used as another example. The material model has the elastic modulus 71 GPa, Poisson's ratio 0.33 with the bilinear plasticity. The loading force is applied in the middle of the upper edge, and 3 nodes are fixed on the lower edge. The same ANSYS program is employed for the computation.

In the same manner, the U* is calculated respectively for two load cases where the plate is subjected to the elastic deformation and elastic-plastic deformation. In the load case 1, the structure is still in the domain of elastic deformation. For the load case 2, the plastic strain is produced at edges of the circular hole and around applied boundaries. The contour of plastic strain developed by the loading is shown in Figure 4-8.

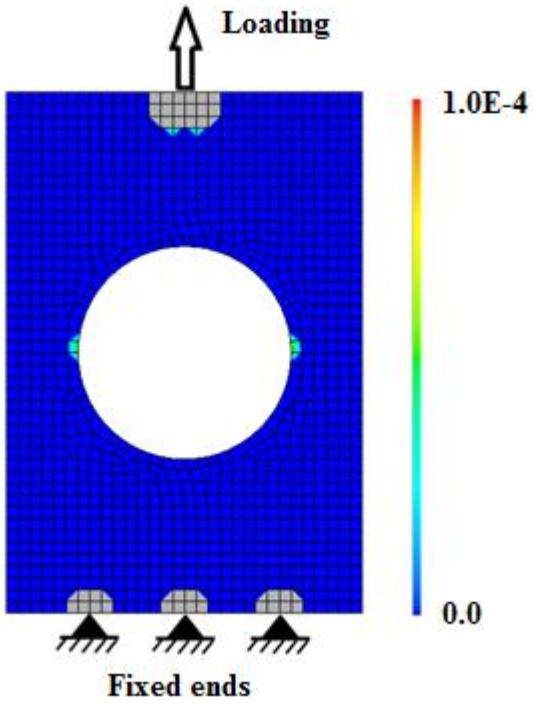

Figure 4-8 Model of plate with a hole with the contour of plastic strain of load case 2

The index U* is calculated for the two load cases and the contours are presented in Figure 4-9 (a) and Figure 4-9 (b) along with the load paths. The diagram of reaction force values of fixed nodes along the loading direction is also plotted. In the first case, shown in Figure 4-9 (a), the load paths go from the loading point to the left and right fixed nodes and they are away from the hole. Reaction force diagram demonstrates that these two fixed nodes transfer most of the loading, 77.6%. In the second case, shown in Figure 4-9 (b), the load paths have included the middle fixed node and they also stay away from the hole. Reaction force diagram illustrates that 3 fixed nodes transfer the equal amount of loads.

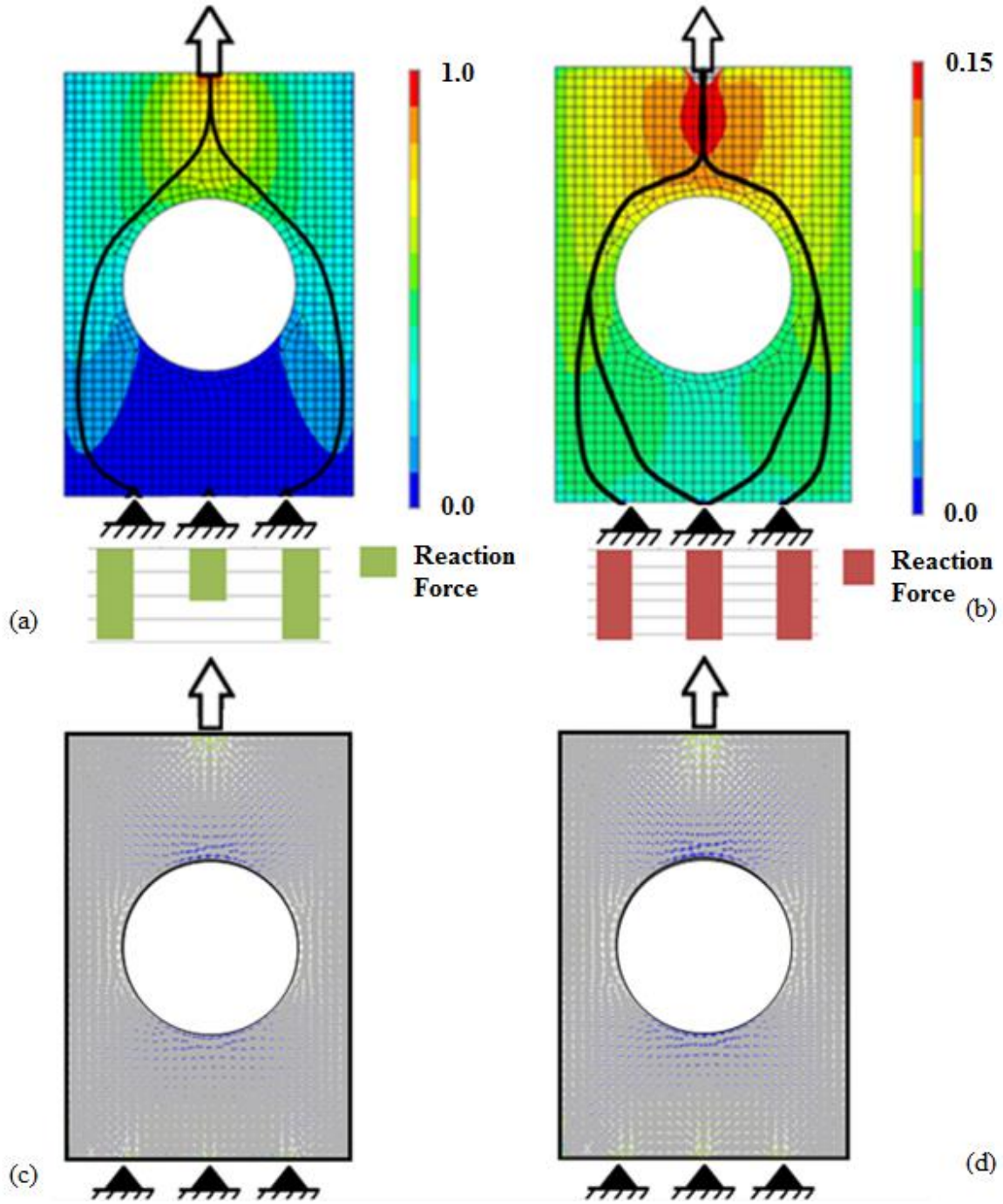

Figure 4-9 Load transfer analysis and stress analysis of the plate with a hole: (a) U* contour plots and load paths of load case of elastic deformation; (b) U* contour plots and load paths of load case of elastic-plastic deformation; (c) Principal stress vector of load case of elastic deformation; (d) Principal stress vector of load case of elastic-plastic deformation

Plots of the principal stress vectors on the plate of the two load cases are presented in Figure 4-9 (c) and (d). Load paths can also be visualized by tracing the trajectories of the vectors. It can be seen in Figure 4-9 (d) that in the second load case the middle fixed node is also included in the load paths. In both load cases, the large principal stresses can be found near the hole due to the stress concentration. In this case, it is not reasonable to obtain load paths by tracing the trajectories of stress vectors since it will lead to the conclusion that the hole is effective to transfer the load.

4.3.3. Discussion of Results

The performed analysis allows concluding that the development of the plastic deformation affects the load transfer in the structure. Figure 4-10 shows the relationship between the magnitude of the reaction force in the left fixed node and the loading force in the second example. A transition phase appears clearly on the curve to indicate the change of load paths. Thus, it demonstrates the applicability of the U* approach for the load transfer analysis in the structure experiencing the elastic-plastic deformation.

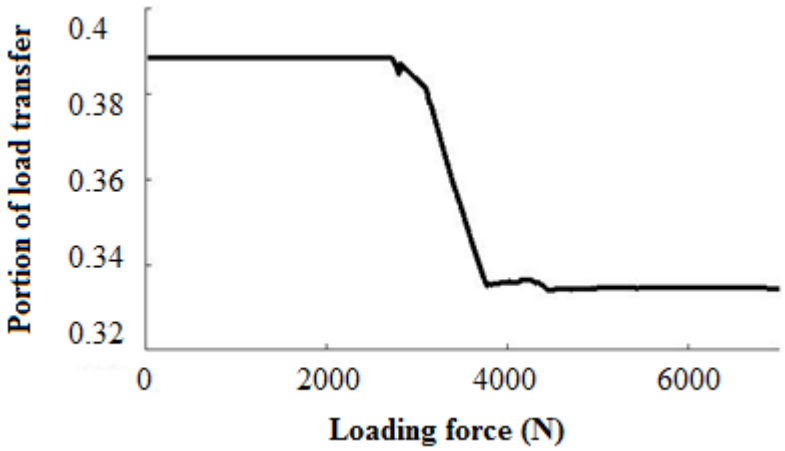

Figure 4-10 Relation between the load transfer portion of left-side fixed node and the loading force

4.4. Load Transfer Analysis of Pillar Structure

As the pillar joint is one of the key components of the superstructure of coach, its load transfer analysis is conducted here as an example. The example of the component is shown in Figure 3-19.

A quasi-static bending test on the pillar joint was conducted to validate the coach modeling in Chapter 3, and the deformation results are shown in Figure 3-21. The bending test result shows that the pillar fails with the buckling and fractures at the beam connection area. The plastic hinge is developed at this connection as the load increases. Thus, material nonlinearity must be considered when analyzing its load transfer capability.

4.4.1. Computational Model

A finite element model for the pillar is built as another example for the application of U* with material nonlinearity. The material model has Young's modulus 210 GPa, Poisson's ratio 0.3 and the multilinear plasticity. The computation model is assumed to have perfect bonding to connect the beams so that the results are independent of the welding quality. In this way, the load transfer performance of the structural design can be studied. The same boundary condition is applied as in the test, shown in Figure 4-11 (a).

Initially, 4 load cases are chosen, as marked in the structure's displacement-force curve, shown in Figure 4-11 (b). By marking elements having the non-zero plastic strain as red, the plastic region is also shown on the pillar structure. Subjected to the first loading 1 kN the pillar deforms elastically. With the loading 8 kN, as shown in red, four corners of the connection area enter the stage of the plastic deformation. As shown in Figure 4-11 (b), 12 kN loading corresponds to the

beginning of the transition on the displacement-force curve. The case of 16 kN loading leads to a larger plastic deformation.

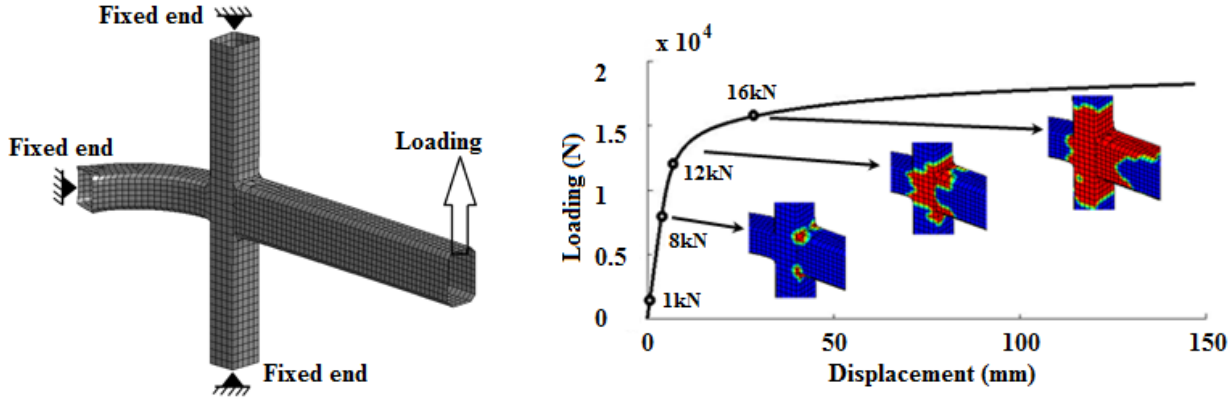

(a) (b)

Figure 4-11 Computational pillar model: (a) Finite element model; (b) D-F curve and load cases

The pillar structure is expected to transfer the load efficiently before it fails. In the case of 16 kN when the pillar undergoes large plastic deformation, the load path would be very different with the other 3 cases. Other types of nonlinearity will also be prominent. In order to examine the load transfer efficiency of the pillar as its deformation goes from the elastic to the elastic-plastic phase, cases of 1 kN, 8 kN and 12 kN are chosen for the U* analysis.

4.4.2. Results and Discussions

The U* contours obtained for 3 load cases are shown in Figure 4-12. The load paths are drawn and it is shown that the four edges of the horizontal beam transfer the most of the load in all cases.

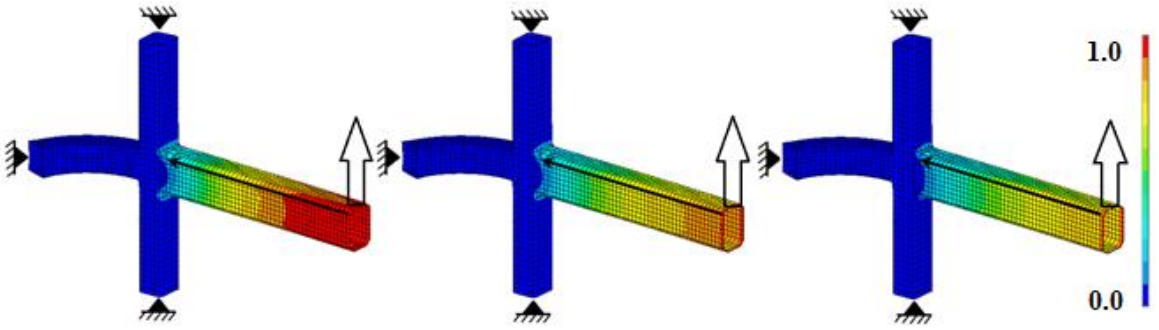

(a) (b) (c)

Figure 4-12 U* contour of the pillar: (a) 1 kN loading; (b) 8 kN loading; (c) 12 kN loading

Variations of U* values along one of the load paths are shown for all three cases in Figure 4-13. It illustrates that due to the material nonlinearity effect, U* has lower values on the horizontal beam.

For all three curves, it is shown that the U*decay rate changes abruptly at the beam connection area. It indicates an ineffective load transfer from the horizontal beam to the vertical beam along this load path. Figure 4-14 illustrates the Von Mises stress contour with the maximum stress along the corner of the beams. This prediction is consistent with the U* based load transfer analysis. The performed analyses indicate that an additional element connecting two parts with different internal stiffness is needed for a better design from the load transfer perspective.

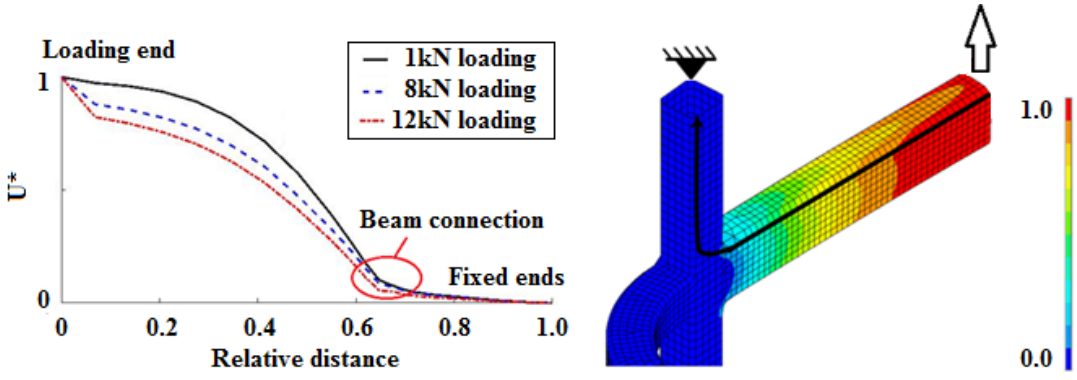

Figure 4-13 Comparison of U* variation along one load path for 3 cases

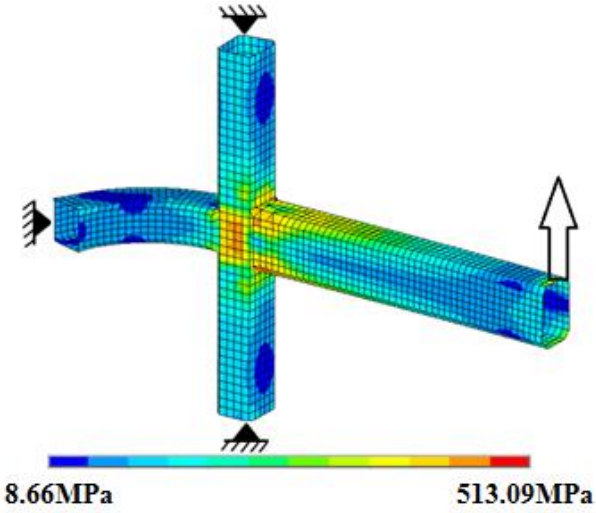

Figure 4-14 Von Mises stress contour of 12kN loading

To proceed with the load transfer analysis let's note the obtained U* here as U_1^*. The U* calculated in the reversed direction (from the 3 fixed ends to the loading end) is labeled as U_2^*. U_{sum}^* is obtained by summing up U_1^* and U_2^*. The U_{sum}^* contours for 3 load cases are presented in Figure 4-15.

As it can be seen on the plane parallel with the shear force, zone with the lower U_{sum}^* in Figure 4-15 tends to move toward the beam connection area. This indicates the significant reduction of the local stiffness there making the zone less effective for the load transfer. In this zone, less load path will pass through.

As shown by the pillar test, the plastic hinge is developed in this location. As the material enters the plastic deformation stage, it has a smaller contribution to the load bearing, so the plastic hinge reduces the local stiffness and interferes with the transfer of the load there. The contour plots of U_{sum}^* distribution in Figure 4-15 capture the re-distribution of the stiffness thus providing the results compliant with the test.

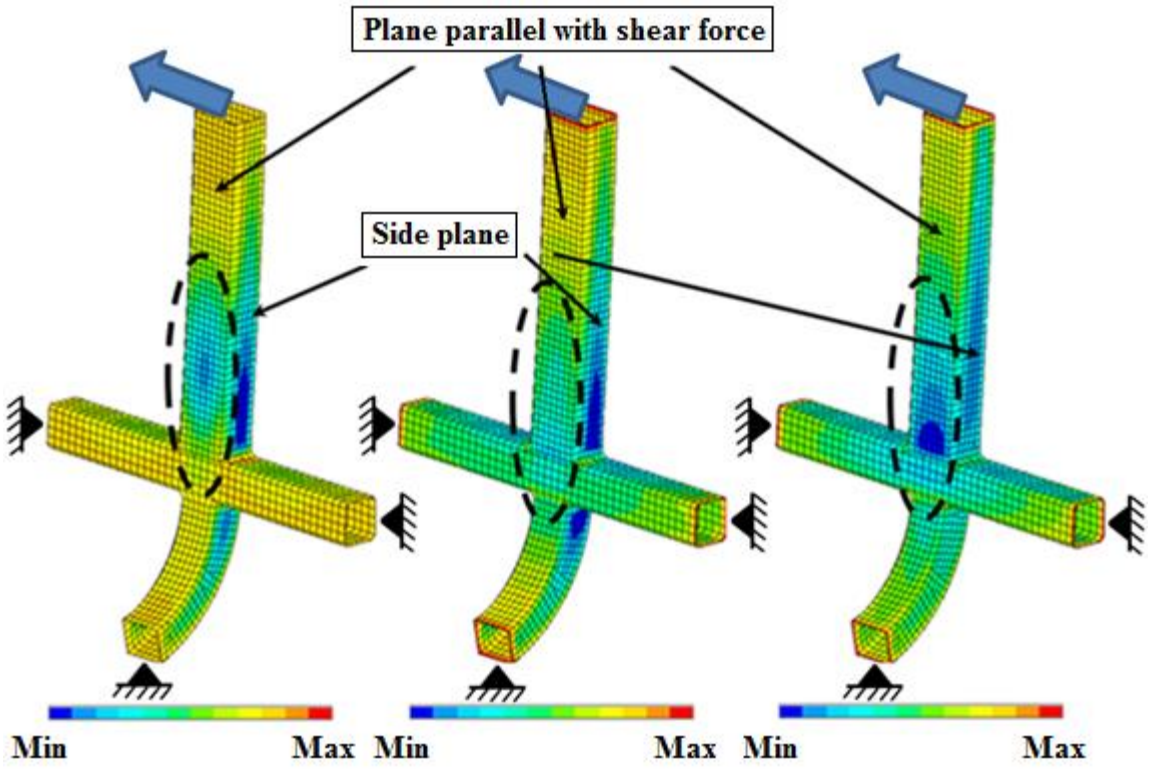

(a) (b) (c)

Figure 4-15 U^*_{sum} contour of pillar under 3 load cases: (a) 1 kN loading; (b) 8 kN loading; (c)12 kN loading

Another observation from U^*_{sum} contours of the pillar in Figure 4-15 is that side plane always has lower U^*_{sum}, thus being less effective to transfer the load. This is reasonable since the side plane is perpendicular to the loading vector [42]. This obtained result shows that an additional structural element in parallel with the loading direction could be added at the connection area to improve the design from the load transfer perspective.

4.5. Conclusions

The present study demonstrates that the application of the U* approach in the non-elastic domain allows to analyze the load transfer in the structure experiencing the elastic-plastic deformation. Performed analyses show that:

(1) The plastic deformation changes load paths. The two examples of the plate show that the load path changes as the plastic deformation develops. The result of the extended U* approach agrees with the observation.

(2) The plastic deformation affects the stiffness distribution of the structure. The example of the vehicle pillar structure shows the index U^*_{sum} of the extended approach is effective to express the load path distribution in a structure experiencing elastic-plastic deformation. This result is confirmed experimentally because the area associated with the least load transfer efficiency predicted by U^*_{sum} is the same location where the plastic deformation develops in the test.

It can be seen that the nonlinear U* approach can be effectively used as the design tool considering the stiffness distribution for the vehicle crashworthiness. The load transfer performance of the vehicle structure under impact can be improved, and a uniform deformation and energy absorption among structure members can be realized.

5. CONCLUSIONS AND FUTURE WORK

5.1. Conclusions and Contributions

In this research work, two numerical approaches are presented for the motorcoach rollover event, i.e., FEA and load transfer analysis using U* approach to evaluate the structural performance and the passenger safety. The following conclusions and contributions are based on this thesis work.

1) The studies demonstrate that the methodology of FEM and U* approach can be effectively used together as tools for solving the problem of vehicle crashworthiness in a rollover event. They are effective in assisting vehicle designers to predict and assess the vehicle structural performance for the compliance to the new regulations in the crash event.

2) In the thesis work, the full coach FE model is modified based on the original Eicher model and validated based on results of a complete vehicle rollover test under ECE R66 conditions and quasi-static component test for a representative member of the vehicle frame. Comparative analyses of rollover resistance and energy absorption distribution features of the coach frame are conducted under the test conditions of both ECE R66 and the NHTSA proposed regulation. Energy absorption ratios among vehicle structural members are presented, and key connections that contribute to the energy absorptions are compared. Results in this study can provide guidance for structural modifications to improve the passenger safety under rollover events.

3) The FEA simulation results can be used as the basis for adapting the existing design criteria under ECE R66 test condition to the NHTSA proposed regulation, which poses more stringent requirement on rollover resistance of the vehicle frame. Vehicle manufacturers could benefit

from these results through the consideration of reinforcing the key joints in the design stage to achieve a sufficient rollover resistance.

4) The load transfer analysis approach studies demonstrate that the U* concept allows to analyze the load transfer in the structure experiencing the elastic-plastic deformation, which is very important for vehicle in crashworthiness problems. Using the U* concept, effects of the material nonlinearity on the load path and the stiffness distribution were analyzed for the representative vehicle component.

5.2. Limitations of This Analysis

The correlation of the full coach model with the NHTSA complete vehicle test is limited by the availability of data of the weight distribution of the coach, the material properties and the component test for all key joints. Due to the time and cost restraints, conducting material tests for all frame beams and component tests for all pillar connections were not feasible.

Based on the available data, however, from the model validation results, it can still be concluded that the full coach model is close to the tested vehicle to a satisfactory extent and the results made are therefore valuable.

5.3. Future Work

The following are recommendations for future work based on this study.

A. The thesis work presents a large scale complete coach rollover model. Work that can improve the quality of model validation and structural performance evaluation include:

1). The validation in the component level can be improved in by refining the mesh of pillar joint model and introducing the material failure criteria.

2). The model validation of rollover deformation with the NHTSA test can be improved by tuning the center of gravity position if data from tilt table test of the tested coach are available.

3). Since the engine has a considerably large mass and it is mounted on the frame using springs and dampers, the deformation of the rear end of the coach is influenced by the inertial force of the engine in the rollover. The mass distribution of the coach can be more accurate by modeling them instead of lumped mass point.

B. The study uses the index U* method to conduct the load transfer analysis on a representative component of the coach. The results allow us to infer that plastic hinges developed on the coach frame in the impact event will change the load path, and they lead to the large deformation and penetration of the surviving space. Engineers are eager to know how impact loads are transferred in the coach superstructure and whether this dynamic load path is the same with the one under a static load.

Thus, it is promising to further explore the application of U* for vehicle crashworthiness problems involving the stiffness distribution, especially for the rollover application. Some future works include:

1). Load transfer analysis using U* method can be applied to a representative bay section of the coach. How the impact load is transferred can be studied efficiently using this simple model which doesn't demand very high computational resources.

2). The applicability and limitations of index U* method can be discussed by results comparison between the U* method and the explicit nonlinear finite element method through tracking the force amplitude in the coach frame in LS-DYNA.

References

[1] Natioanl Highway Traffic Safety Administration, "2014 Motor Vehicle Crashes: Overview," U.S. Department of Trasnportation, Washington, D.C., 2016.

[2] Transport Canada, "Canadian Motor Vehicle Traffic Collision Statistics 2015," Goverment of Canada, Ottawa, 2017.

[3] Department of Transportation, "Motorcoach safety action plan 2012 update," U.S. Department of Transportation, Washington, D.C., 2012.

[4] RONA kinetics and Associates Ltd, "Evaluation of Occupant Protection in Buses," Transport Canada, North Vancouver, BC, 2002.

[5] S. Abrate, "Impact engineering of composite structures," vol. 526, Springer Science & Business Media, 2011, pp. 193-260.

[6] C.-C. Liang and G.-N. Le, "Bus rollover crashworthiness under European standard: an optimal analysis of superstructure strength using successive response surface method," *International Journal of Crashworthiness,* vol. 14, no. 6, pp. 623-639, 2009.

[7] JASIC, ECE, "Regulation No. 66 01-Strength of Superstructure," Economic Commission for Europe, 2006.

[8] C. Bojanowski, "Verification, validation and optimization of finite element model of bus structure for rollover test," THE FLORIDA STATE UNIVERSITY, Tallahassee, Florida, 2009.

[9] S. Hashemi, A. Walton and K. Kayvantash, "Strength of Super-Structure UN-ECE R66 Rollover Approval of Coaches based on Thin-Walled Framework Structures," *International Journal of Vehicle Structures & Systems (IJVSS),* vol. 1, no. 4, pp. 78-84, 2009.

[10] J. Anderson and M. Sadeghi, "Influence of passengers during coach rollover," in *18th International Technical Conference on the Enhanced Safety of Vehicles*, Nagoya, Japan, 2003.

[11] L. Martínez, F. Aparicio, A. García, J. Páez and G. Ferichola, "Improving occupant safety in coach rollover," *International journal of crashworthiness,* vol. 8, no. 2, pp. 121-132, 2003.

[12] M. Guler, K. Elitok, B. Bayram and U. Stelzmann, "The influence of seat structure and passenger weight on the rollover crashworthiness of an intercity coach," *International journal of crashworthiness,* vol. 12, no. 6, pp. 567-580, 2007.

[13] M. Matolcsy, "Body section rollover test as an approval method for required strength of bus superstructures," *Automotive and Transportation Technology Congress and Exposition 2001 Proceedings,* 2001 SAE Technical Paper 2001-01-3209.

[14] R. P. Sergeevich and O. L. Nikolaevich, "Verification of computer simulation results of bus body section rollover," *Journal of Traffic and Transportation Engineering,* vol. 3, pp. 118-127, 2015.

[15] C.-C. Liang and G.-N. Le, "Analysis of bus rollover protection under legislated standards using LS-DYNA software simulation techniques," *International Journal of Automotive Technology,* vol. 11, no. 4, pp. 495-506, 2010.

[16] National Highway Traffic Safety Administration, "Notice of proposed rulemaking (NPRM)," Department of Transportation Vol.79, No.151, Washington, D.C., 2014.

[17] M. Matolcsy, "Unusual statistics about rollover accident of buses," in *85th GRSG Working Party on General Safety Provisions*, 2003.

[18] L. Kwasniewski, H. Li, R. Nimbalkar and J. Wekezer, "Crashworthiness assessment of a paratransit bus," *International Journal of Impact Engineering,* vol. 32, no. 5, pp. 883-888, 2006.

[19] M. Sadeghi and G. Tidbury, "Bus roll over accident simulation," in *3rd International Conference on Vehicle Structural Mechanics*, 1979 SAE Technical Paper No. 790994.

[20] A. Subic and J. He, "Improving bus rollover design through modal analysis," *International journal of crashworthiness,* vol. 2, no. 2, pp. 139-152, 1997.

[21] S. R. Wu and J. Chen, "Advanced development of explicit FEA in automotive applications," *Computer Methods in Applied Mechanics and Engineering,* vol. 149, no. 1-4, pp. 189-199, 1997.

[22] J. Thacker, S. Reagan, J. Pellettiere, W. Pilkey, J. Crandall and E. Sieveka, "Experiences during development of a dynamic crash response automobile model," *Finite Elements in Analysis and Design*, vol. 30, no. 4, pp. 279-295, 1998.

[23] D. Marzougui, M. Zink, A. Zaouk, C. Kan and N. Bedewi, "Development and validation of a vehicle suspension finite element model for use in crash simulations," *International Journal of Crashworthiness,* vol. 9, no. 6, pp. 565-576, 2004.

[24] E. Chirwa, H. Li and Q. Peng, "Modelling a 32-seat bus and virtual testing for R66 compliance," *International journal of crashworthiness,* vol. 20, no. 2, pp. 200-209, 2015.

[25] J. Hutchinson, K. Friedman and D. Mihora, "Finite element modeling comparisons of rollover test devices," in *SAE 2011 World Congress & Exhibition*, 2011 SAE Technical Paper No. 2011-01-0011.

[26] T. Roca, J. Arbiol and S. Ruiz, "Development of rollover-resistant bus structures," in *Automotive Concurrent/Simultaneous Engineering-SP-1233*, 1997 SAE Technical Paper 970581.

[27] N. Indera, R. Zain, S. Mihradi and K. Soe Oo, "Computer modelling of energy absorbing capability of bus superstructure for rollover safety," *Journal of KONES,* vol. 18, pp. 331-338, 2011.

[28] D. Kelly and M. Elsley, "A procedure for determining load paths in elastic continua," *Engineering Computations,* vol. 12, no. 5, pp. 415-424, 1995.

[29] D. Kelly and M. Tosh, "Interpreting load paths and stress trajectories in elasticity," *Engineering Computations,* vol. 17, no. 2, pp. 117-135, 2000.

[30] D. Kelly, P. Hsu and M. Asudullah, "Load paths and load flow in finite element analysis," *Engineering Computations,* vol. 18, no. 1/2, pp. 304-313, 2001.

[31] H. Harasaki and J. Arora, "New concepts of transferred and potential transferred forces in structures," *Computer methods in applied mechanics and engineering,* vol. 191, no. 3, pp. 395-406, 2001.

[32] K. Marhadi and S. Venkataraman, "Comparison of Quantitative and Qualitative Information Provided by Different Structural Load Path Definitions," *International Journal for Simulation and Multidisciplinary Design Optimization,* vol. 3, no. 3, pp. 384-400, 2009.

[33] M. Shinobu, D. Okamoto, S. Ito, H. Kawakami and K. Takahashi, "Transferred Load and Its Course in Passenger Car Bodies," *JSAE Review,* vol. 16, no. 2, pp. 145-150, 1995.

[34] H. Hoshino, T. Sakurai and K. Takahashi, "Vibration Reduction in The Cabin of Heavy-Duty Truck Using The Theory of Load Transfer Paths," *JSAE Review,* vol. 24, no. 2, pp. 165-171, 2003.

[35] K. Takahashi and T. Sakurai, "Expression of load transfer paths in structures," *Transactions of the Japan Society of Mechanical Engineers, Series A,* vol. 71, no. 708, pp. 1097-1102, 2005.

[36] T. Sakurai, K. Takahashi, H. Kawakami and M. Abe, "Reduction of Calculation Time for Load Path U* Analysis of Structures," *Journal of Solid Mechanics and Materials Engineering,* vol. 1, no. 11, pp. 1322-1330, 2007.

[37] K. Pejhan, Q. Wang, C. Wu and I. Telichev, "Experimental Validation of U* index Theory for Load Transfer Analysis," *International Journal of Heavy Vehicle Systems,* vol. 24, no. 3, pp. 288-304, 2017.

[38] H. Koboyashi, T. Naito and Y. Urushiyama, "Study on Similarity of Load Path Distribution in Body Structure," *Honda R&D Technical Review,* vol. 23, no. 1, pp. 80-89, 2011.

[39] T. Naito, H. Kobayashi, Y. Urushiyama and K. Takahashi, "Introduction of new concept U* sum for evaluation of weight-efficient structure," *SAE International Journal of Passenger Cars-Electronic and Electrical Systems,* vol. 12, no. 4(2011-01-0061), pp. 30-41, 2011.

[40] K. Pejhan, C. Wu and I. Telichev, "Comparison of load transfer index (U*) with conventional stress analysis in vehicle structure design evaluation," *International Journal of Vehicle Design,* vol. 68, no. 4, pp. 285-303, 2015.

[41] Q. Wang, K. Pejhan, I. Telichev and C. Wu, "Demonstration of the effectiveness of U*-based design criteria on vehicle structural design," *Proceedings of the Institution of Mechanical Engineers, Part D: Journal of Automobile Engineering,* 2017 Sep 19:0954407017724635.

[42] N. Tadashi, H. Kobayashi and Y. Urushiyama, "Application of load path index U* for evaluation of sheet steel joint with spot welds," in *SAE 2012 World Congress & Exhibition*, 2012 SAE Technical Paper No. 2012-01-0534.

[43] E. Wang, Y. Yoshikuni, Q. Guo, T. Nohara, H. Ishii, H. Hoshino and K. Takahashi, "Load Transfer in Truck Cab Structures under Initial Phase of Frontal Collision," *International Journal of Vehicle Structures & Systems,* vol. 2, no. 2, pp. 60-68, 2010.

[44] S. Akima, M. Omiya and K. Takahashi, "Load Transfer of Passenger Car Compartment for Improvement of Structural Performance in Side Impact," in *24th International Technical Conference on the Enhanced Safety of Vehicles (ESV)*, 2015.

[45] T. Sakurai, M. Tada, H. Ishii, T. Nohara, H. Hoshino and K. Takahashi, "Load path U*

Analysis of structures under multiple loading conditions," *Nippon Kikai Gakkai Ronbunshu A Hen(Transactions of the Japan Society of Mechanical Engineers Part A)(Japan),* vol. 19, no. 2, pp. 195-200, 2007.

[46] Q. Wang, K. Pejhan, I. Telichev and C. Wu, "Extensions of the U* theory for applications on orthotropic composites and nonlinear elastic materials," *International Journal of Mechanics and Materials in Design,* vol. 13, no. 3, pp. 469-480, 2017.

[47] ANSYS, Inc., "ANSYS Explicit Dynamics, Release 17.0," [Online]. Available: https://www.sharcnet.ca/Software/Ansys/17.0/en-us/help/exd_ag/exd_ag_overview.html. [Accessed 15 Jan 2017].

[48] MSC SOFTWARE, "Dytran 2010 Theory Manual," MSC.Software Corporation, Newport Beach, California, 2010.

[49] Livermore Software Technology Corporation, "LS-DYNA Support -What are the differences between implicit and explicit?," [Online]. Available: http://www.dynasupport.com/faq/general/what-are-the-differences-between-implicit-and-explicit.. [Accessed 07 March 2018].

[50] L. Zhu, "Study on Automobile Structural Passive safety Using MSC.Dytran Software," Zhejiang University, Hangzhou, China, 2004.

[51] J. O. Hallquist, "LS-DYNA keyword user's manual," Livermore Software Technology Corporation 970, Livermore, California, 2007.

[52] P. S. Deshmukh, "Rollover and roof crush analysis of low-floor mass transit bus,"

Wichita State University, Wichita, Kansas, 2006.

[53] B. D. Gepner, "Rollover procedures for crashworthiness assessment of paratransit bus structures," Florida State University, Tallahassee, Florida, 2014.

[54] K.-T. Kang, H.-J. Chun, J.-C. Park, W.-J. Na, H.-T. Hong and I.-H. Hwang, "Design of a composite roll bar for the improvement of bus rollover crashworthiness," *Composites Part B: Engineering*, vol. 43, no. 4, pp. 1705-1713, 2012.

[55] Livermore Software Technology Corporation, "LS-PrePost Online Documentation," [Online]. Available: http://www.lstc.com/lspp/. [Accessed 07 March 2018].

[56] S. Golinskikh and R. Iyer, "J Coach Parcel Rack Analysis (Bus Front Impact and Rollover) Report," Eicher Engineering Solutions, Inc, Michigan, 2014.

[57] L. Kotyk and H. Chorney, "Tilt Table Static Rollover Test for Determining the Center of Gravity Height Location on a Production J4500 Coach," Westest, Portage la Prairie, MB, 2016.

[58] J. O. Hallquist, "LS-DYNA Theory Manual," Livermore Software Technology Corporation, Livermore, California, 2006.

[59] L. Zhu, "Development of guidelines for deformable and rigid switch in LS-Dyna simulation," *Mechanical (and Materials) Engineering-- Dissertations, Theses, and Student Research*, vol. 3, 2009.

[60] W. Zhou, A. Kuznetcov, I. Telichev and C. Wu, "Deformable-rigid switch in computational simulation of bus rollover test," in *Proceedings: 24th International Congress*

of Theoretical and Applied Mechanics, Montreal, QC, 2016.

[61] K. Pejhan, A. Kuznetcov, Q. Wang, C. Wu and I. Telichev, "Design assessment of a multiple passenger vehicle component using load transfer index (U*) method," *International Journal of Mechanics and Materials in Design*, pp. 1-17 DOI: 10.1007/s10999-017-9372-7, 2017.

[62] MGA Research Corporation, "Final Report of ECE Regulation 66 Based Research Test of Motorcoach Roof Strength 2000 MCI 102-EL3 Series Motorcoach NHTSA NO.: MY0800," DEPARTMENT OF TRANSPORTATION, Cambridge, MA, 2009.

[63] M. Ray, C. Plaxico and M. Anghileri, "Procedures for Verification and Validation of Computer Simulations Used for Roadside Safety Applications," Washington, DC, 2010.

[64] M. H. Ray and M. Mongiardini, "Roadside Safety Verification and Validation Program (RSVVP)," Worcester Polytechnic Institute, Worcester, Massachusetts, 2008.

[65] ANSYS® Academic Research, Release 15.0, "ANSYS Mechanical APDL Theory Reference," ANSYS, Inc., Canonsburg, Pennsylvania, 2013.

Appendix A Experimental Data of Frame Material Tensile Test

The raw data from the material tensile test include the strain and the load. Thus, stresses are calculated using the measured load divided by the cross section area of the sample. The stress-strain data here is known as the engineering strain and stress.

Using the following equations, the true strain and stress are calculated.

$$\varepsilon_{TRUE} = \ln(1 + \varepsilon_{ENG}) \tag{15}$$

$$\sigma_{TRUE} = \sigma_{ENG} * e^{\varepsilon_{TRUE}} = \sigma_{ENG} * (1 + \varepsilon_{TRUE}) \tag{16}$$

where ε_{TRUE}, σ_{TRUE} are true strain and stress, and ε_{ENG}, σ_{ENG} are engineering strain and stress.

The LS-DYNA plasticity model needs the effective plastic strain, and it is the residual true strains after unloading elastically. Thus, the effective plastic strain is calculated using the formula:

$$\varepsilon_{\text{eff plastic}} = \varepsilon_{TRUE} - \sigma_{TRUE}/E \tag{17}$$

where E is Young's modulus.

The stress and strain data and the calculated results are presented in Table A-1 and Figure A-1.

ro, ton/mm^3	7.85E-09
E, MPa	2.10E+05
Pr	0.3
sigy, MPa	426.74

True Effective		**True**		**Engineering**	
strain	**stress, MPa**	**strain**	**stress, MPa**	**strain**	**stress, MPa**
0.0000	0.0	0	0	0	0
0.0010	426.7	0.00302212	426.7435966	0.003026691	425.4558731
0.0026	480.9	0.004936364	480.9216226	0.004948568	478.5534682
0.0046	497.9	0.007006461	497.9288929	0.007031064	494.4523667
0.0075	506.2	0.009952485	506.1825236	0.010002176	501.1697357
0.0174	516.8	0.019843856	516.7749996	0.020042054	506.6212688
0.0271	524.7	0.029619849	524.685552	0.03006288	509.3723521
0.0463	538.3	0.048835744	538.3212377	0.05004786	512.6635253
0.0926	566.3	0.095298233	566.2809431	0.099986859	514.8070074
0.1370	587.7	0.139758592	587.6783653	0.149996147	511.0263776
				0.199952871	461.5406342

Table A-1 Stress and strain data of frame material tensile test

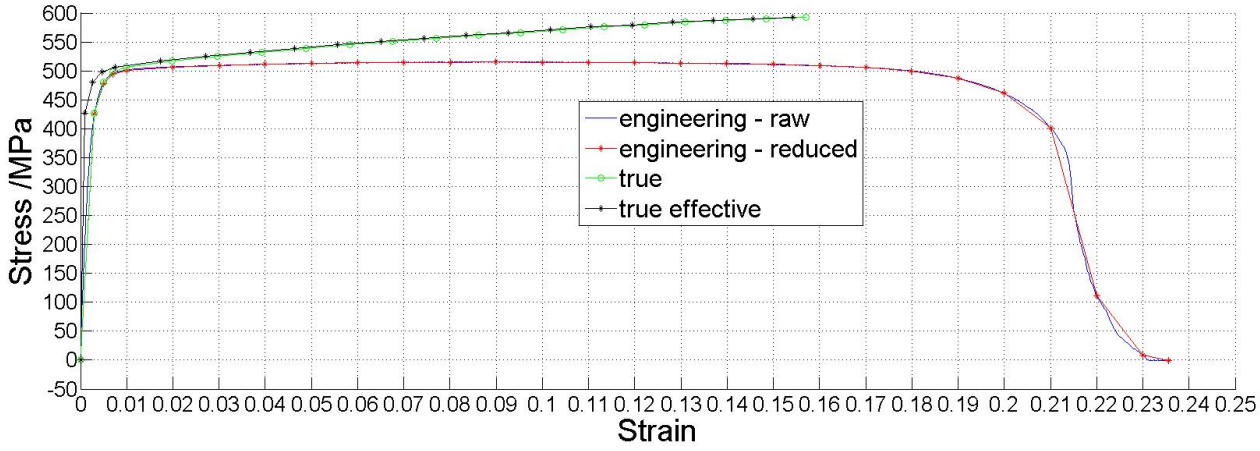

Figure A-1 Different stress and strain curves from material test